Investigation into the behavior of mercury in wet flue gas desulfurization systems

Von der Fakultät für Energie-, Verfahrens- und Biotechnik
der Universität Stuttgart zur Erlangung der Würde einer
Doktorin der Ingenieurwissenschaften (Dr.-Ing.)
genehmigte Abhandlung

vorgelegt von
Ida Masoomi
aus Teheran/Iran

Hauptberichter:	Univ.-Prof. Dr. techn. Günter Scheffknecht
Mitberichter:	Prof. Dr. Ing. Dieter Bathen
	(Universität Duisburg-Essen)

Tag der mündlichen Prüfung: 20. Januar 2022

Institut für Feuerungs- und Kraftwerkstechnik der Universität Stuttgart

2022

Acknowledgment

Table of Contents

Nomenclature

Greek Alphabets

Symbol	Unit	Meaning
Δ	–	difference
ε	$\mathrm{m^2\,mol^{-1}}$	absorption coefficient
η_i	%	removal efficiency of component i
λ	nm	wavelength

Latin Alphabets

Symbol	Unit	Meaning
c_i	$\mathrm{g\,m^{-3}, mol\,m^{-3}}$	concentration of component i
d	m	light's path length through the sample
E_i	V	cell potential
E_i^0	V	standard cell potential
E_λ	-	absorbance of light at a specific wavelength λ
F	$\mathrm{C\,mol^{-1}}$	faraday constant
G	$\mathrm{kJ\,mol^{-1}}$	gibbs free energy
H	J	enthalpy
I	$\mathrm{W\,m^{-2}}$	intensity of light
K	-	formation constant
K_H	$\mathrm{mol\,l^{-1}\,Pa^{-1}}$	Henry-coefficient

Symbol	Unit	Meaning
K_H^0	$\mathrm{mol\,l^{-1}\,Pa^{-1}}$	Henry-coefficient at reference temperature
M_i	kg	mass of component i
p_i	$\mathrm{N\,m^{-2}}$	partial pressure of component i
R	$\mathrm{J\,K^{-1}\,mol^{-1}}$	ideal gas constant
T	°C	temperature
$\dot{V}$	$\mathrm{m^3\,s^{-1}}$	volumetric flow
X	%	mass fraction
x	$\mathrm{\mu g\,kg^{-1}}$	mass fraction
z_e	-	number of transferred electrons

Superscript Indices

Index	Meaning
fil	filtrate
gyp	gypsum
in	inlet of the system
out	outlet of the system
T	total

Subscript Indices

Index	Meaning
air	oxidation air
aq	aqueous
FG	flue gas
fil	filtrate

(Continued on the next page)

Index	Meaning
g	gas
gyp	gypsum
ox	oxidized reactants
p	particulate bound
red	reduced reactants
sol	solution
solid	solid fraction

Chemical Elements and Molecules

Formula	Name
Br	bromine
Br^-	bromide
Ca^{2+}	calcium ion
$CaCO_3$	calcium carbonate, limestone
$Ca(HSO_3)_2$	calcium hydrogen sulfite
$CaSO_3$	calcium sulfite
$CaSO_4 \cdot 2H_2O$	calcium sulfate dihydrate
CH_3Hg^+	methyl mercury
Cl	chlorine
Cl^-	chloride
CO_2	carbon dioxide
F^-	fluoride
Fe	iron
$FeCl_3$	iron chloride
H_2SO_3	sulfurous acid
H_2SO_4	sulfuric acid
HCl	hydrochloric acid
HCO_3^-	hydrogen carbonate
HSO_3^-	hydrogen sulfite

Formula	Name
Hg	mercury
Hg^0	elemental mercury
Hg^+	mercurous
Hg^{2+}	mercuric
$HgBr^+$	bromidomercurate(II)
$HgBr_2$	mercury(II) bromide
$HgBr_3^-$	tri-bromidomercurate(II)
$HgBr_4^{2-}$	tetra-bromidomercurate(II)
$HgCl^+$	chloridomercurate(II)
$HgCl_2$	mercury(II) chloride
$HgCl_3^-$	tri-chloridomercurate(II)
$HgCl_4^{2-}$	tetra-chloridomercurate(II)
HgI^+	iodidomercurate(II)
HgI_2	mercury(II) iodide
HgI_3^-	tri-iodidomercurate(II)
HgI_4^{2-}	tetra-iodidomercurate(II)
$Hg(NH_3)^{2+}$	mercury(II) ammonia
$Hg(NH_3)_2^{2+}$	di-ammoniamercurate(II)
$Hg(NH_3)_3^{2+}$	tri-ammoniamercurate(II)
$Hg(NH_3)_4^{2+}$	tetra-ammoniamercurate(II)
$Hg(NO_3)_2$	mercury(II) nitrate
HgO	mercury oxide
$Hg(OH)_2$	mercury(II) hydroxide
HSO_3^-	hydrogen sulfite
HgS	mercury sulfide
$HgSO_3$	mercury sulfite
$Hg(SO_3)_2^{2-}$	disulfitomercurate(II)
I	iodine
I^-	iodide
IO_3^-	iodate
K^+	potassium ion
Mg^{2+}	magnesium ion

Formula	Name
N_2	nitrogen
Na^+	sodium ion
Na_2S	sodium sulfide
Na_2SO_3	sodium sulfite
$Na_2S_2O_3$	sodium thiosulfate
$Na_3S_3C_3N_3$	2,4,6-trimercaptotiazine, trisodium salt
NH_3	ammonia
NH_4^+	ammonium
$(NH_4)_2SO_4$	ammonium sulfate
NO_3^-	nitrate
NO_x	nitrogen oxides
O_2	oxygen
$S(IV)$	sulfur in oxidation state of 4
$S(VI)$	sulfur in oxidation state of 6
S^{2-}	sulfide
$S_2O_3^{2-}$	thiosulfate
$SnCl_2$	Tin(II) chloride
SO_2	sulfur dioxide
SO_3	sulfur trioxide
SO_3^{2-}	sulfite
SO_4^{2-}	sulfate
SO_x	sulfur oxides

Acronyms

Acronym	Meaning
ABC	activated bituminous coal
ACS	activated coconut shell
AL	activated lignite

Acronym	Meaning
APCDs	air pollution control devices
APH	air pre-heater
aq	aqueous
BET	Brunauer-Emmett-Teller Theory
BJH	Barrett-Joyner-Helenda Theory
BuR	Brennstoff und Rauchgasreinigung
con.	concentration
CVAAS	cold vapor atomic absorption spectroscopy
DO	dissolved oxygen
IFK	Institut für Feuerungs- und Kraftwerkstechnik
Imp.	Impregnation
IUPAC	International Union of Pure and Applied Chemistry
ESP	electrostatic precipitator
FGD	flue gas desulfurization
HD	high dust
HSAB	hard-soft acid base
LCP-BREF	large combustion power plants-best reference document
LD	low dust
L/G	liquid to gas ratio
MATS	Mercury and Air Toxics Standards
MFCs	mass flow controllers
NDIR	nondispersive infrared
Ox	oxidized
PM	particulate matter
ppm	parts per million
ppt	parts per trillion
PID	proportional integral derivative
Red	reduced
Redox	oxidation reduction potential
re-em.	re-emission
SCR	selective catalytic reduction
SHE	standard hydrogen electrode

(Continued on the next page)

Acronym	Meaning
TE	tail end
TMT	trimercaptotiazine, trisodium salt
UBCs	unburned carbons
UV	ultraviolet
VGB	Vereinigung der Großkesselbesitzer
VIS	visible
vol.-%	volume percent
wt.-%	weight percent

Kurzfassung

In Anbetracht der ansteigenden Luftverschmutzung durch industrielle Prozesse ist die Rauchgasreinigung von konventionellen Kraftwerken immer noch ein aktuelles Thema. Die fluktuierende Stromerzeugung durch erneuerbare Energien erfordert eine flexible Betriebsweise der fossilen Kraftwerke, was die Rauchgasreinigung und die Effizienz der emissionsmindernden Komponenten beeinflusst. Da Quecksilber (Hg) als Spurenelement ein Bestandteil von Kohle ist und die Emissionsgrenzwerte immer strenger werden, ist es wichtig, das Verhalten von Quecksilber im Rauchgasweg und den Einfluss von Betriebsänderungen auf die relevanten Reaktionen besser zu verstehen. Die Rauchgasentschwefelungsanlage (REA) ist die wichtigste Senke für Quecksilber im Kraftwerk, da oxidiertes Quecksilber in der Suspension absorbiert werden kann. Unter ungünstigen Bedingungen kann das absorbierte oxidierte Quecksilber jedoch wieder reduziert und in die Gasphase re-emittiert werden. Die komplexe Chemie von Quecksilber erschwert es, sein Verhalten und die Auswirkungen unterschiedlicher Betriebsparameter und Komponenten auf die Reaktionen vorherzusagen, was wesentlich ist um geeignete Maßnahmen zur Quecksilberabscheidung zu finden.

Diese Arbeit wurde an einer Labor-REA mit synthetischer Suspension und Rauchgas durchgeführt, was eine Vielzahl an detaillierten Untersuchungen ermöglicht. Als erstes wurden der Einfluss der Betriebsparameter und verschiedene Zusammensetzungen der Suspension auf die Hg-Partitionierung in der REA getestet. Bei hohen Temperaturen der Suspension stiegen die Hg Re-Emissionen exponentiell an. Obwohl Adsorption eine exotherme Reaktion ist, nahm die Quecksilberkonzentration in Gips bei einer Temperaturerhöhung von 60 °C auf 80 °C zu. Ein höherer pH-Wert führte zu einem Anstieg der Hg-Re-Emission und einer Verbesserung der Schwefeldioxidabscheidung. Wenn jedoch das Hg-Inventar in der Suspension erhöht wurde, konnten auch höhere Re-Emissionswerte beobachtet werden. Des Weiteren konnte gezeigt werden, dass die Adsorption von Hg auf Gips ein isothermes Adsorptionsverhalten aufweist. Der ambivalente Einfluss der S(IV)-Konzentration auf Hg konnte beobachtet werden,

welches entweder eine Reduzierung des oxidierten Hg oder die Bildung von Komplexen hervorrufen kann. Auch Ammoniak (NH_3) kann, abhängig von seiner Konzentration, unterschiedliche Effekte auf SO_2 und Hg haben. Die Anwesenheit von Halogenen hingegen hat eindeutige Auswirkungen und abhängig davon, welches Halogen vorliegt, kann die Hg Re-Emission signifikant gesenkt werden. Die begrenzte Adsorptionskapazität des Gips' konnte in verschiedenen Suspensionen beobachtet werden.

Da die Hg Re-Emission und die S(IV)-Konzentration eng miteinander verknüpft sind, kann eine kontinuierliche S(IV)-Messung dabei helfen, Hg Re-Emissionen vorherzusagen. Abhängig vom pH der Suspension kann S(IV) in den Formen Sulfit (SO_3^{2-}), Schwefelwasserstoff (HSO_3^-) oder als gelöstes SO_2 vorliegen. Durch das Verschieben des pHs in den gewünschten Bereich existiert S(IV) nur als eine der genannten Formen und ermöglicht somit die Messung der gesamten S(IV)-Konzentration. Zwei unterschiedliche Messprinzipien wurden getestet, wovon sich eines selbst in der Anwesenheit von Halogenen als selektiv erwiesen hat. Änderungen der SO_2-Konzentration im Rauchgas sollten plötzliche Anstiege von S(IV) simulieren und den Zusammenhang von der S(IV)-Konzentration und dem Verhalten von Hg in verschiedenen Suspensionen zeigen. Dabei war die Rolle von SO_3^{2-} und HSO_3^- einerseits als Ligand, andererseits als Reduktionsmittel für Hg-Komplexe bei Abwesenheit von Halogenen eindeutig zu beobachten. Die Ergebnisse ermöglichten tiefere Einblicke in die involvierten Reaktionen in der Suspension.

Als zusätzliche Maßnahme um Hg Re-Emissionen aus der Suspension zu verhindern, wurden Additive, wie zum Beispiel Fällungsmittel und Sorbentien, untersucht. Alle Additive verhinderten Hg-Verluste während der Übergangsphase und die meisten zeigten geringere Re-Emissionen im stationären Zustand, da der Großteil des Hg-Inventars im festen Anteil der Suspension vorlag. Halogene verändern die Partitionierung des Hg's in der mit Additiven versetzten Suspension noch weiter und beeinflussen auch die ablaufenden Reaktionen. Für Sorbentien, die auf Aktivkohle basieren, konnte gezeigt werden, dass die Porenverteilung eine wichtige Rolle spielt, da sie das Adsorptionsvermögen der Sorbentien bei verschiedenen Medien beeinflusst.

Abstract

In view of increasing air pollution due to industrial processes, flue gas cleaning of conventional power plants is an ongoing topic. The fluctuating power generation with renewable energies requires a flexible operation of fossil fuel power plants, which influences the flue gas cleaning and the performance of air pollution control devices. The strict emission limits for mercury (Hg) as a toxic and a trace element in coal, emphasizes the need for a better understanding of its behavior in the flue gas path and the influence of changes in the flue gas and operating parameters on the involved reactions. The flue gas desulfurization (FGD) plant is the main sink for Hg from the flue gas, as the oxidized mercury is absorbed in its slurry. However, under unfavorable conditions, the absorbed oxidized mercury can be reduced and re-emitted to the gas phase, which influences its removal efficiency. The complex chemistry of Hg in the slurry makes it difficult to predict its behavior and the effects of different operating parameters and components on its reactions, which is vital for finding adequate measures for the Hg removal from the flue gas.

This work was conducted at a lab-scale FGD with synthetic flue gas and slurry, which provided vast possibilities for detailed studies. At first, the influence of the operating parameters as well as different slurry compositions on the partitioning of Hg in the FGD was investigated. It was found that at high temperatures of the slurry re-emission of Hg increased exponentially. In spite of exothermic characteristic of adsorption, the Hg concentration on gypsum increased at 80 °C compared to 60 °C. Increasing of the pH led to a higher Hg re-emission and a better sulfur dioxide (SO_2) removal efficiency. When the Hg inventory in the slurry was increased, higher Hg re-emission were observed and the adsorption of Hg on the gypsum followed adsorption isotherm behavior. The ambivalent influence of S(IV) concentration on reactions involving Hg was observed, which can either lead to a reduction of oxidized mercury or to the formation of complexes. Ammonia was shown to have different effects on SO_2 and Hg behavior depending on its concentration. The presence of halides induced a significant

decrease in Hg re-emission depending on the type of existing halides. The limited adsorption capacity of gypsum could be observed in various slurries.

As Hg re-emission and S(IV) concentration are closely linked, a continuous S(IV) measurement can help to predict Hg re-emissions. Depending on the pH of the slurry, S(IV) exists in different forms of sulfite (SO_3^{2-}), hydrogen sulfite (HSO_3^-) and dissolved SO_2. By shifting the pH of the slurry to a proper range, only one of the mentioned forms of S(IV) is present in the slurry, which provides the possibility of total measurement of S(IV) concentration. Two different measurement principles for a continuous S(IV) measurement were tested and one was proven to be selective even in presence of different halides. Changing the SO_2 concentration of the flue gas simulated the sudden increase of S(IV) in the slurry and showed the relation of Hg behavior and S(IV) concentration in different slurries. The role of SO_3^{2-} and HSO_3^- as reducing agent and ligand for Hg-complexes was more obvious in the absence of halides. The results gave an insight into the involved reactions in the slurry.

Furthermore, additives, such as precipitating agents and sorbents, were tested as an additional measure to prevent Hg re-emission from the slurry. All of the additives eliminated Hg loss from the slurry during the transition phase and almost all of them showed lower re-emission at the steady state of the system by shifting the Hg inventory mostly to the solid fraction of slurry. The presence of halides changed the partitioning of Hg in the additive containing slurry even further and influenced the involved reactions. For activated carbon based sorbents, the pore distribution was proven to have an important role, which affected the adsorption capacity of sorbents at different media.

Chapter 1

Introduction

1.1 Motivation of the work

The increase in energy consumption is closely linked to modern society and economic growth and is predicted to continue in the future. Providing the required energy is a worldwide challenge. Due to the environmental impact of operating conventional power plants using fossil fuels, installing renewable energy plants has been increased rapidly in the last decades. However, they cannot provide the total energy demand of the world and depending on geological conditions their energy production fluctuates. Thus, conventional power plants will remain necessary to transition from conventional to renewable power generation for the coming years.

One of the most important fossil fuels used worldwide as the source of energy is coal. The main components of coal are carbon, hydrogen, nitrogen, oxygen, sulfur and several trace elements. However, the exact composition depends heavily on the location of the deposit. During combustion, several pollutants such as particulate matters (PMs), sulfur oxides (SO_x), nitrogen oxides (NO_x) and different trace elements are released to the flue gas. Depending on the coal composition and operating mode of combustion, the concentration of these pollutants in the flue gas can vary. Different measures have been used to remove these pollutants and prevent their release to the environment. Power plants are normally equipped with treatment devices such as electrostatic precipitators (ESP) for removal of particulate matters, selective catalytic reduction (SCR) catalysts for NO_x removal and flue gas desulfurization (FGD) systems for controlling SO_x emissions. Mercury (Hg) is one of the trace elements in coal which is released almost completely to the flue gas during combustion processes.

Mercury is widely known as a global pollutant due to its long life and long range of

transport in the atmosphere. Its high vapor pressure is responsible for its evaporation through natural sources or human activities such as combustion of fossil fuels [25]. Hg is highly toxic and has negative effects on human health and on the environment; thus, several regulations have been implemented worldwide to control and reduce Hg emissions from anthropogenic sources. For instance, within the Mercury and Air Toxics Standards (MATS), the limits have been set as a 30-day rolling average on a $lb\,GWh^{-1}$ or $lb\,TBtu^{-1}$ basis, which, for the state-of-the art European power plants, is equivalent to values of < 2.2 µg m^{-3} for hard coal fired plants and < 5.4 µg m^{-3} for lignite fired plants [57]. The new large combustion plant best available techniques reference documents (LCP-BREF), which was finalized in 2017, sets the yearly emission bandwidths for the existing coal fired power plants in the European Union with the capacity > 300 MW$_{el}$ to < 1-4 µg m^{-3} for hard coal and < 1-7 µg m^{-3} for lignite plants [65]. Considering these strict regulations, significant efforts have been undertaken during the last years to reduce Hg emission.

Controlling Hg emissions requires a vast amount of information and suitable course of action. Unlike other pollutants such as NO$_x$ and SO$_x$, which can be removed from flue gas using specific air pollution control devices (APCDs), the fate of Hg depends strongly on the set up and operation of the entire flue gas cleaning system. Hg is mostly released as elemental mercury (Hg^0) during the combustion process. It is partially oxidized to oxidized mercury (Hg^{2+}), mostly as a side reaction occurring in the SCR catalysts. It can be adsorbed on particles and removed using particle removal devices. The oxidized form can be absorbed in wet FGD systems and be removed from flue gas. Composition of the slurry and the operating parameters of the wet FGD play crucial roles in the absorption of Hg. Under unfavorable conditions of the slurry, the already absorbed Hg^{2+} can be reduced to Hg^0 and released again to the flue gas, which is known as Hg re-emission. The latter may decrease the removal efficiency of Hg to high extents. Thus, reaching the adjusted limit values for Hg emission is quite challenging.

Due to the increase in renewable energy production, there is a need for flexible operation of conventional power plants in order to compensate missing amounts of energy and provide a stable base production for industries. It has to be noted that this flexible operation influences the flue gas and the performance of treatment devices. Slurry of the FGD is one of the most important sinks for Hg and changes in its chemistry due to different composition of flue gas or operating parameters may lead to large amounts of Hg re-emission. Thus, by understanding the reactions regarding Hg in the slurry, different options can be implemented to prevent its re-emission back to the flue gas.

1.2   Goal and approach of the work

The goal of this work is to understand the chemical reactions regarding Hg and its phase partitioning in the slurry of FGD to gain required information on the behavior of Hg and the factors responsible for its re-emission. Thus, a suitable measure for preventing Hg re-emission and consequently increasing its removal efficiency can be provided. To reach the mentioned goal, the following approach for this work has been chosen: Chapter 2 provides an overview on mercury and its behavior in flue gas cleaning systems of coal-fired power plants. The role of different air pollution control devices on the fate of Hg and the relevant reactions are described. More detailed explanation is provided regarding reactions taking place in a wet FGD system, as the focus of this work is studying Hg re-emission from the slurry and finding the responsible parameters and components, as well as investigating different measures to prevent Hg re-emission from the slurry. Measurements were carried out in a lab-scale FGD system, using synthetic flue gas and slurry. Thus, the operating parameters and compositions of the slurry could be adjusted as required. Hg phase partitioning in gas, liquid and solid is studied by taking samples from the system and measuring Hg in each phase. The description of experimental equipment and analytical procedure is given in chapter 3.

The results of the study are presented in chapter 4. In order to find the most suitable condition and investigate the effect of each change on the behavior of Hg, a reference measurement point is defined and identified. In chapter 4.1, the influence of each operating parameter and possible condition of the slurry are compared with this reference point. Additionally, the sudden change in the system and its effect on Hg re-emission is studied at different slurry compositions to define the impact of possible changes of the flue gas on the Hg re-emission from the slurry.

Sulfite and hydrogen sulfite are the main reducing agents for Hg^{2+} in the slurry and thus cause its re-emission to the gas phase. Therefore, a continuous measurement of sulfur in the oxidation state of four (S(IV)) is beneficial for a deeper understanding of the reactions involving Hg and S(IV) and the role of S(IV) on Hg^{2+} reduction when sudden changes in the system occur. In chapter 4.2, two measurement principles for continuous measurement of S(IV) were developed and tested in the lab-scale FGD and the possibility of their implementation in the full scale FGD was investigated.

As preventing Hg re-emission is quite challenging and sudden changes of the system may result in a sudden release of Hg inventory of the slurry, utilization of additional additives may be required. Dosing of different additives in the slurry to prevent Hg re-

emission is investigated in chapter 4.3. The effect of these additives in combination with different compositions of the slurry leads to a deeper understanding on their principle and different functional mechanisms. Furthermore, the performance of these additives and their influence in preventing sudden release of Hg from the slurry by sudden change in SO_2 concentration of flue gas was investigated. Chapter 5 summarizes the complete work and provides conclusions of the study.

1.3   Previously published results

This work was carried out with the support of the colleagues in the "Brennstoffe und Rauchgasreinigung" (BuR) department of Institute of Combustion and Power Plant Technology (IFK) and different students, who completed their thesis or student research project under the supervision of the author [11, 78, 82, 95]. The intermediate experiments as well as provided final results in this study were partially presented by the author at conferences [70–73] and journals [77]. In addition, the results of utilization of additives (chapter 4.3) as well as development of an online sulfite measurement (chapter 4.2) have been partially published as reviewed manuscripts in journals [74, 75].

Chapter 2

Mercury and its behavior in the flue gas cleaning of coal-fired power plants

2.1 Mercury and its properties

Mercury is an element of the 12th group of the periodic table with the atomic number of 80 and atomic mass of 200.59 $\mathrm{g\,mol^{-1}}$. It has the unique electron configuration of [Xe] $4f^{14}5d^{10}6s^2$, which explains its high volatility. The filled f shell makes it difficult to remove the s shell electrons. That is why mercury behaves similarly to noble metals with weak bonds formation and thus melts at low temperature. Mercury has seven stable isotopes with ^{202}Hg being the most abundant with 29.6 % [50]. Metallic mercury is the only liquid metal at room temperature with a melting point of -38.84 °C and boiling point of 356.95 °C. It is a heavy metal due to its high density of 13.534 $\mathrm{g\,cm^{-3}}$. It has a high vapor pressure of 0.13 Pa at 20 °C and therefore it can be readily evaporated at room temperature. It has a high surface tension; it is a poor conductor of heat and a fair conductor of electricity.

In the environment, mercury exists in three different oxidation states, namely, metallic mercury (Hg^0), mercurous (Hg^+) and mercuric (Hg^{2+}). However, the monovalent form is unstable and therefore rare [117]. All forms of Hg are toxic and have negative impacts on human health and the environment. The most problematic forms are organic forms such as methyl mercury (CH_3Hg^+). Human exposure to mercury can lead to a permanently damage to the nervous system, with the severity depending on the intake dosage and its type, which in the worst case may result to death. In addition to neurotoxicity, mercury can affect other organs and pose a variety of health risks [17, 84]. High exposure to methyl mercury is known as Minamata disease, due

to the Minamata incident in the 1950s, in which a large number of individuals were poisoned by methyl mercury. Hg was released with the industrial waste water to the water body and accumulated in fish [41].

In the atmosphere, elemental mercury is the predominant form ($> 90 \%$), with the concentration of 1-5 ppt measured above the atmospheric layer [118]. The high vapor pressure of elemental mercury facilitates its long range transport and global disparity in the atmosphere for a lifetime of several months to a year [108]. In the presence of oxidizing agents such as ozone and hydroxyl radicals, elemental mercury can be oxidized in the atmosphere in the oxidized form with high water solubility, which makes it possible to be combined with water vapors and travel back as rain to the Earth's surface. In this way mercury is deposited in soils and bodies of water [87]. In water and soil environments, Hg is pre-dominantly present as different Hg^{2+} inorganic and organic compounds and a small fraction of Hg^0, which can be released back to the atmosphere. Hg^{2+}-compounds have different chemical and physical forms due to the complexing with different ligands. For example, Hg in aqueous environments can be converted to mercury sulfide (HgS), which is insoluble and thus settles in sediments. In addition, it can be converted to methyl mercury by bacteria, which then will be bio-accumulated along the food chain. By progressing its way up the food chain, it can be transferred to humans and other animals by consumption of fish. Mercury can also re-volatilize to the atmosphere and circulate for centuries in the atmosphere-land-water system [109].

Mercury can be released into the environment both naturally and through anthropogenic processes. High vapor pressure of Hg is responsible for its transfer to the atmosphere from different sources. Mercury is released through natural sources commonly as gaseous elemental mercury while anthropogenic emissions are the mixture of both elemental and divalent mercury [26]. Regarding natural sources of Hg emissions geological activities such as volcanic and geothermal emissions and volatilization of Hg in marine environment can be mentioned. Due to the complexity of geological processes and the lack of data, it is difficult to accurately estimate the amount of naturally released Hg to the environment [37, 38]. Anthropogenic sources of mercury can be from point and diffuse sources. Point sources account for more than 95 % of anthropogenic mercury emissions and include combustion, manufacturing and miscellaneous sources [120]. Combustion sources include fossil fuel combustion, waste and sewage incinerations. They can emit both elemental and divalent mercury to the environment, depending on their fuel and flue gas cleaning system. Mercury emission through man-
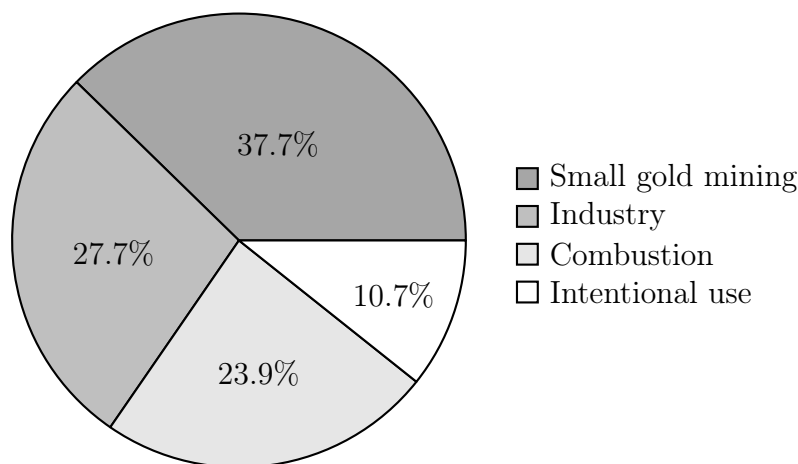
Figure 2.1: Share of Hg emission from different anthropogenic sources in 2015 [119].

ufacturing sources is due to the excessive use of mercury in some industrial processes such as gold mining, chlor-alkali production, and paper and pulp manufacturing. Mercury release from diffuse sources such as landfills, sewage sludge amended fields and mine waste contributes to a small share of anthropogenic Hg emission. Figure 2.1 shows the share of Hg emission from different anthropogenic sources in 2015 [119]. Artisanal and small-scale gold mining contributes to about 38 % of anthropogenic Hg emission. Hg emission produced by industry consists of mostly non-ferrous metal and cement production each contributing to more than 10 %. Iron, steel and large-scale gold production as well as oil refining emit some percentage of Hg and are counted in this section. Among combustion of different fuels for various purposes, coal contributes mostly in Hg emissions with around 21 %. The intentional uses include waste incineration, cremation emissions and other sectors that cannot avoid using Hg in their processes.

2.2   Mercury in coal-fired power plants

HgS is an inorganic mercury compound with negligible water solubility that exists in two different modifications: red cinnabar with a hexagonal structure and black meta-cinnabar with a cubic crystal structure. The more thermal stable form is red cinnabar, which is the most common form found in the environment in the Earth's crust. Mercury exists in association with fossil fuels namely coal, petroleum and natural gas. The concentration of mercury in coal deposits ranges from 0.02 to 1.0 $\mu g\,g^{-1}$, which results in the Hg concentration of 5 to 40 $\mu g\,m^{-3}$ in the flue gas leaving boiler [143]. Hg content

of the coal differs depending on the rank and its origin; for example in low rank coals, including lignite and sub-bituminous coals, the Hg content is lower than in bituminous coal [90]. However, these coals have normally lower halogen content and due to their lower calorific value, greater amount of low-rank coal is required in order to provide the equivalent energy output. Therefore, from the stand point of Hg capture, lower Hg content of low rank coal does not mean lower Hg emissions.

Mercury reduction from coal prior to combustion may occur through coal preparation, selective mining and upgrading low rank coals by drying. In coal preparation, different approaches can be implemented, in which the grain size and mode of Hg occurrence in the coal play an important role. For example removal of pyrite as the main mineralogic host of Hg in bituminous coal using density separation may help to reduce the amount of Hg in the coal. However, this approach is less likely to be effective [63]. Selective mining and coal blending help to have a lower Hg content in the coal entering the combustion, for which analyses of the mining beds and different coals for Hg contents is required. Thermal treatment of low rank coals, which is typically performed to increase the efficiency of the power plant, has the co-benefit of Hg reduction. According to the study from Guffey [36], heating lignite to the temperature of 150 °C to 290 °C can remove Hg up to 80 %. The form of Hg occurrence in coal is mostly important for pre-combustion Hg capture as at high furnace temperatures all the Hg is released as Hg^0.

As the flue gas cools down, released Hg^0 can undergo different reactions such as oxidation with halogen species. Therefore, the halogen content of the coal influences the post combustion Hg capture. Generally, the higher the rank of the coal, the higher the concentration of halogens is, which corresponds to the depth of sedimentary basins [59]. Chlorine (Cl) is the most abundant halogen in coal with an average concentration of around 340 ppm in hard coal, which is three times more than in lignite with 120 ppm [141]. In a study done by Vosteen et al. [127], the native halogen content of coal in several countries was reviewed and the mass ratio of bromine (Br) to Cl has been found to be mostly constant between 0.01 to 0.04, independent of the coal rank. For iodine (I) concentration in coal ranges of 0.15 to 12.8 ppm have been reported by Bettinelli et al. for 158 commercial coal samples [4].

The purpose of coal combustion boilers is to generate steam, which is accomplished by creating a hot gas and transferring the heat from the gas to water or steam. Therefore, the temperature of flue gas drops from the combustion temperature of 900-1500 °C to 340-370 °C. At the air pre-heater (APH), the combustion air is preheated in a

gas to gas heat exchanger, which decreases the flue gas temperature to 135-175 °C. This change in the flue gas temperature affects the Hg chemistry [103]. In flue gas, Hg exists in different forms: gaseous elemental mercury, gaseous oxidized mercury species and particulate bound mercury (Hg_p). Within the group of oxidized mercury species, mercuric (Hg^{2+}) compounds are the most abundant [103]. The speciation of Hg strongly depends on different parameters such as the combustion system, fuel types and the existing APCDs of each plant which affect the choice of methods and degree of difficulty of Hg removal from the flue gas. Figure 2.2 shows a typical flue gas cleaning path of a hard coal combustion plant in Germany, which consists of a SCR catalyst for NO_x reduction, an ESP as a particle removal step and a wet FGD, which has the purpose of SO_x removal from the flue gas. The function of each step and its role in the fate of Hg in the flue gas is explained more in detail in the following chapters.
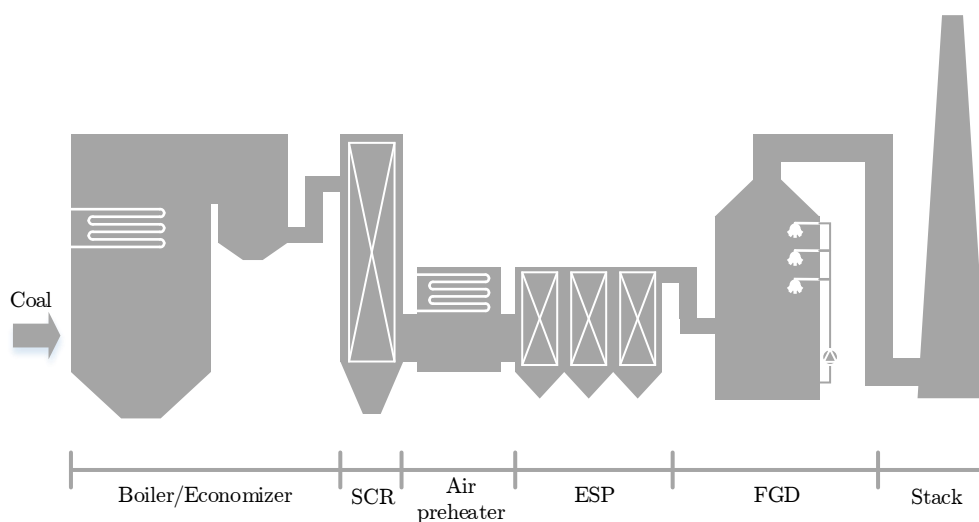
Figure 2.2: Typical flue gas cleaning path of a hard coal combustion plant.

2.2.1 Selective catalytic reduction system

NO_x is mainly produced during combustion of fossil fuels through three different formation mechanisms. Thermal NO_x is formed by reaction between nitrogen and oxygen in air at high flame temperatures, which produces a high share of NO_x concentration of the flue gas [142]. Fuel NO_x is produced by oxidation of nitrogen content of the fuel and prompt NO_x by combination of fuel with molecular nitrogen in the air at high

furnace temperatures [121]. NO_x emissions can be controlled using primary and secondary measures. Primary measures are techniques, which modify the combustion to prevent the formation of NO_x and secondary measures include techniques, which treat the effluent gases. Primary measures achieve almost 50 % reduction in NO_x emissions; however, this is not sufficient to reach limit values. Thus, secondary measures have to be applied. The SCR process is the most commonly used technique to reduce NO_x to water and nitrogen using a reducing agent [10, 29, 86].

SCR deNOx catalysts may consist of different materials such as noble metals, metal oxides and zeolites, which have been extensively researched in the last decades. Metal oxides are the most common and economical in the power plants' applications. Catalyst based on vanadia (V_2O_5), supported on titania (TiO_2) in the anatase crystalline form and promoted with tungsten trioxide (WO_3) or molybdenum trioxide (MoO_3) has shown great NO reduction. It is the most common commercial SCR catalyst due to its high catalyst activity, thermal stability and high resistance to deactivation by SO_2 [14, 55].

SCR catalysts are divided into different categories according to their shapes namely honeycomb, plate and corrugated type catalysts. The honeycomb catalysts consist of channels in cubic form, which are assembled into standard steel cased modules and placed inside the reactor in the form of layers. They have a large active surface due to their structures; however, in high dust applications there is the possibility of blockage of the channels and erosion of the surface. Thus, according to the application the geometric properties such as channel opening and wall thickness have to be adjusted. In comparison to the honeycombs, plate catalysts are less vulnerable to blockage due to their structure. They are made by depositing the catalytic material onto a stainless steel net or a perforated metal plate; therefore, they are more resistant to erosion. These properties make them suitable for high dust and high sulfur applications [86]. The shape and geometry of the catalyst have a significant influence on its efficiency. To optimize the catalyst's performance and increase its lifetime, a suitable geometry has to be considered according to the application.

One important factor for choosing the proper geometry for the catalyst is the flue gas composition, which varies according to the position at which the SCR catalyst is located. There are three different configurations for SCR deNOx catalysts in power plants, in which the location of the catalyst in the flue gas path differs. In the high dust (HD) arrangement, the SCR catalyst is the first step of the flue gas cleaning after the economizer. Due to the high dust content of the flue gas in this arrangement, the

catalyst needs to have larger channel openings. In the low dust (LD) arrangement, the catalyst is located after particle removal step (such as ESP) and up-stream of the air pre-heater. In the tail end (TE) arrangement, the SCR catalyst is used as the last flue gas cleaning step after SO_2 removal unit. As for the TE arrangement, the flue gas temperature drops below 150 °C, which is much lower than the suitable temperature range for SCR catalyst performance, it is necessary to reheat the flue gas. Thus, the first two locations are preferred due to no additional energy requirement for adjusting the flue gas temperature. However, in TE configuration the clean flue gas results in at least 50 % less needed catalyst volume as well as longer catalyst life [14, 86].

The main role of SCR catalyst is the reduction of NO_x, using a reducing agent such as ammonia (NH_3). Due to the small fraction of NO_2 under the coal fired power plant conditions, reaction 2.1 is the most important deNOx reaction, which proceeds rapidly in the presence of excess oxygen in the temperature range of 250-450 °C.

$$4NO + 4NH_3 + O_2 \ \rightarrow \ 4N_2 + 6H_2O \tag{2.1}$$
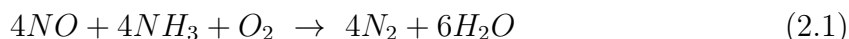
According to this reaction, the stoichiometric ratio of NH_3 to NO is one. However, depending on the reaction's efficiency, some amount of NH_3 is left un-reacted and leaves the catalyst. The un-reacted ammonia is called ammonia-slip and may contribute in reactions downstream of the catalyst.

Oxidation of sulfur dioxide to sulfur trioxide is one of the most important undesired reactions taking place in the SCR catalyst. Sulfur trioxide can react with water to sulfuric acid or ammonium hydrogen sulfate and ammonium sulfate after reacting with un-reacted ammonia. They can cause deactivation of the catalyst, plugging and corrosion of the downstream equipment [14, 86].

$$2SO_2 + O_2 \ \rightarrow \ 2SO_3 \tag{2.2}$$
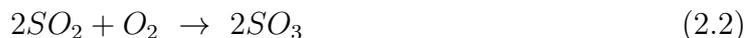
In addition to these reactions, the SCR catalyst can play an important role in the fate of Hg in the flue gas. In the combustion process Hg is released mostly as Hg^0, which is the thermodynamically favored form at high temperatures [93]. As the flue gas temperature drops, Hg can undergo different reactions with other flue gas constituents. It can be oxidized homogenously by halogens' radicals at higher temperatures of around 500-700 °C, as they are more abundant in this temperature range [103]. Even though the concentration of chlorine in coal is much higher than the concentration of bromine, Br radical formation is kinetically more favored. This leads to bromine being more effective than chlorine in homogenous oxidation of Hg [123, 128]. Cl_2 and Br_2, which

are produced through Deacon reaction as shown in reactions 2.3 and 2.4, are the favorable reaction partners for Hg oxidation. According to Griffin reaction, SO_2 may react with Cl_2 or Br_2 and produce HCl and HBr, respectively as shown in reactions 2.5 and 2.6, which influences Hg oxidation negatively. However, in contrast to the chlorine Griffin reaction the bromine Griffin reaction is not thermodynamically favored, which is another proof of the positive influence of bromine in oxidation of Hg [129].

$$4HCl + O_2 \rightleftharpoons 2H_2O + 2Cl_2 \tag{2.3}$$

$$4HBr + O_2 \rightleftharpoons 2H_2O + 2Br_2 \tag{2.4}$$

$$SO_2 + Cl_2 + H_2O \rightleftharpoons SO_3 + 2HCl \tag{2.5}$$

$$SO_2 + Br_2 + H_2O \rightleftharpoons SO_3 + 2HBr \tag{2.6}$$
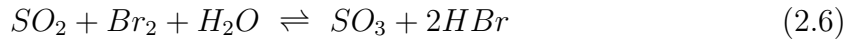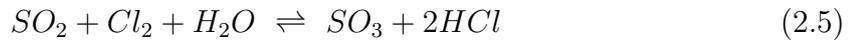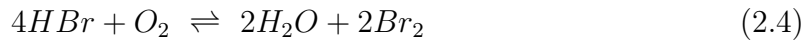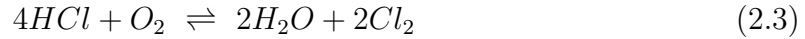
The overall Hg oxidation reaction with hydrogen chloride can be described as below:

$$2Hg^0 + 4HCl + O_2 \rightleftharpoons 2HgCl_2 + 2H_2O \tag{2.7}$$
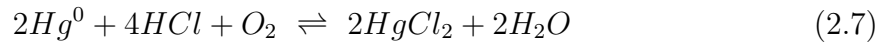
Homogenous oxidation of Hg is kinetically limited and cannot oxidize high amounts of Hg^0. Thus, at typical flue gas temperatures the heterogeneous Hg oxidation is dominant [103, 130, 134]. Heterogeneous oxidation of Hg occurs on the SCR catalyst and fly ash surface at lower temperatures of the flue gas. SCR catalysts have been shown to have significant influence in increasing the share of oxidized mercury in the flue gas. A few mechanisms are proposed for heterogeneous oxidation of Hg; however there is no general agreement on one of these mechanisms. The Langmuir-Hinshelwood mechanism proposes that Hg^0 and HCl are adsorbed to the active sites, and the reaction happens between two bound species [24, 66, 134]. The Eley-Rideal mechanism is proposed by Niksa et al [85], who believe that HCl is adsorbed on the active sites and reacts with gas phase or weakly bound Hg^0. In the Mars Maessen mechanism, proposed by Granite et al. [33], adsorbed Hg^0 on a metal oxide surface reacts with lattice oxidants (O or Cl) and forms a binary mercury oxide, which reacts with O_2 to form HgO. In the next step, HgO reacts with hydrogen halides to form mercury halogenides that are released from the catalyst surface. Several studies have been conducted to prove one of the mechanisms as the main path responsible for Hg oxidation on the SCR catalyst; however, no definitive answer was found and the results are contradictory [24, 44, 85, 92].

Different factors such as flue gas composition and temperature, as well as the age and composition of the catalyst influence Hg oxidation efficiency over the SCR catalyst. One

of the important flue gas compositions, which strongly inhibits Hg oxidation over the SCR catalyst is NH_3. According to Kamata et al., the inhibition is due to competition for active surface sites between NH_3 and HCl or Hg [55, 56]. Thus, two regions have to be considered for SCR catalysts. One is the NH_3-rich zone, in which NO_x reduction is the dominant reaction and the NH_3-poor zone, in which Hg oxidation can take place [85, 134].

Oxidation of Hg is a crucial step for its removal through downstream air pollution control devices. Thus, lots of attention has been given to improve and produce catalysts with high efficiency in Hg oxidation as well as NO_x reduction in the last decades [55, 56, 98–100].

2.2.2   Electrostatic precipitator

During the combustion process, primary and secondary particulate matters are emitted. Primary PM is called fly ash, which is the bulk of non combustible inorganic matters and unburned carbons (UBCs), carried out of the boiler with the flue gas. Secondary PM is produced by condensation of the substances such as sulfuric acid in the stack [101]. Removal of ash and particles from the flue gas is the oldest environmental protection measure that is applied in combustion power plants [65] and can be carried out using different technologies including fabric filters, wet or dry electrostatic precipitators, venture scrubbers and mechanical collectors. Among all techniques, ESPs are the most commonly used in coal combustion power plants in Europe, due to their high removal efficiency.

ESPs can be located after the air pre-heater in the operation temperature of 80-220 °C; these are called cold-side ESPs and are the most commonly used. They can also be located before the air pre-heater and operate in the temperature range of 300-450 °C, which are called hot-side ESPs [65]. ESPs electrically charge the particles with ions and electrons and collect them on plates, due to the electrostatic force. The ions are generated by a corona discharge of central wire electrodes using a 10-80 kV voltage. The collected particles on the plates are removed periodically by mechanical means and collected in a hopper. Collected fly ash can be recycled for utilization in the construction and cement industry [133].

In most of coal power plants a heat exchanger is located downstream of the SCR catalyst before particle control devices. The heat exchanger is used to heat the combustion air to around 300 °C using the hot flue gas. The temperature of the flue gas typically

decreases from 350 °C to 150 °C, which results in condensation and adsorption of Hg on unburned carbon of the fly ash. In addition, the large cold metal surface in the heat exchanger can promote oxidation of Hg across the air pre-heater [51]. A certain fraction of Hg is adsorbed by fly ash particles (Hg_p) and can be removed consequently in electrostatic precipitator located downstream the air pre-heater [132]. In general, Hg can be adsorbed or oxidized on the active surface of UBCs, depending on several factors such as the chlorine content, the amount of unburned carbon in the fly ash and the temperature of the flue gas [51, 102]. It has to be considered that adsorption of Hg on the fly ash may restrict the use of it as a byproduct in construction applications.

2.2.3   Wet flue gas desulfurization system

Sulfur oxides are formed by oxidation of the sulfur contained in the fuel and thus, their concentration in the flue gas is strongly dependent on the fuel composition. Different measures have been applied to control the SO_x emissions from power plants, which are mostly based on absorption or adsorption using alkaline chemicals as a sorbent medium. Thus, as a co-benefit, other acid compounds can be removed during the process. Flue gas desulfurization systems are categorized into two groups: re-generable, in which SO_x is recovered from the sorbents and the sorbents can be reused; and non re-generable, in which the sorbents can only be used once. Among the non re-generable processes, dry, semi-dry and wet processes can be mentioned. The choice of the proper process depends mostly on the SO_x concentration and the required efficiency. For fuels with low sulfur content, a dry process can be sufficient. However, for plants burning fuels with high sulfur content wet processes are favored [12, 28]. Wet flue gas desulfurization (FGD) is the most common technology, which is used in 95 % of power plants in Germany [126]. The advantages of using this technology in addition to its high removal efficiency are its low operating cost and the utilization of its by-product gypsum [124].

In the wet FGD system, SO_x is absorbed in a scrubbing process by circulating an alkaline slurry containing lime, limestone or a sodium based solution. One of the most commonly used processes for removal of SO_x is the wet limestone FGD, in which limestone ($CaCO_3$) is used as a neutralization agent. The process is based on acid-base complex reactions and can take place under forced or natural oxidation. By implementing forced oxidation in the scrubber, gypsum ($CaSO_4 \cdot 2H_2O$) is produced as the final product, which is utilized in the wall-board construction industry [42]. Other soluble gas components such as hydrogen halides (HCl, HBr and HI) and Hg^{2+} can be

captured from the flue gas as a co-benefit of the wet FGD systems. An overview of a wet limestone FGD with forced oxidation is given in figure 2.3. The figure illustrates the reagent preparation, the scrubber in which the absorption occurs and the by-product of de-watering process [6].
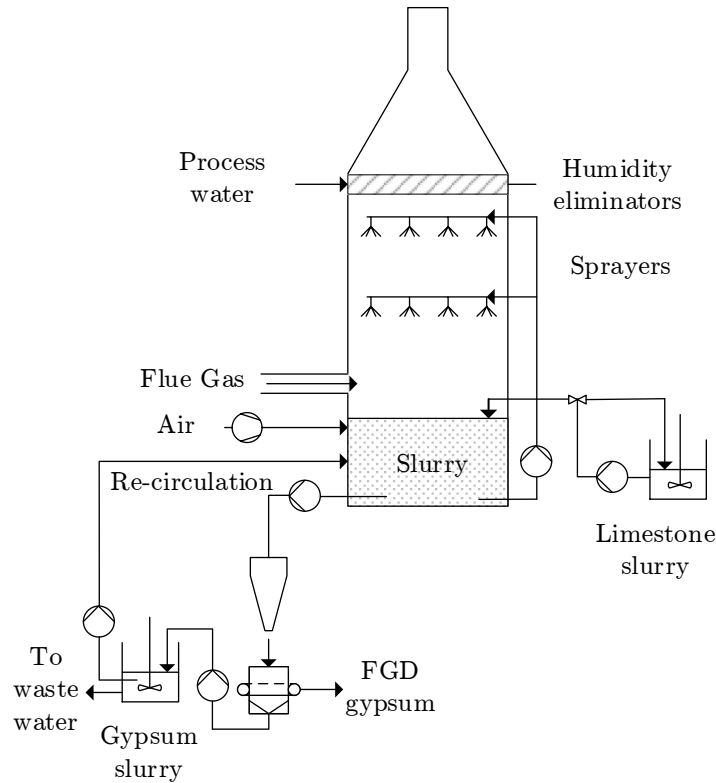
Figure 2.3: Overview of a wet limestone FGD with forced oxidation.

The scrubber has the main role in the absorption process and can be divided into two regions: the gas to liquid contact zone and the reaction tank. In the gas to liquid contact zone, the scrubbing solution is brought into contact with the flue gas counter currently using several spraying levels and the mass transfer takes place. The scrubbing slurry is collected in the reaction tank and in the case of a forced oxidation system, the oxygen is injected in the reaction tank resulting in full oxidation of calcium sulfite to gypsum. The overall reaction occurring in the absorber is shown in reaction 2.8.

$$2SO_2 + 2CaCO_3 + 2H_2O + O_2 \ \rightarrow \ 2CaSO_4 \cdot 2H_2O + 2CO_2 \qquad (2.8)$$

Limestone slurry is prepared and pumped to the slurry in order to control the pH of the scrubber. The optimal pH range of wet limestone FGD systems is between of 5-6. Higher pH is more favorable for SO_2 absorption; however, the limestone dissolution rate

is considerably higher at lower pH [20]. Operating the scrubber at higher pH results in higher SO_2 removal efficiency but it requires higher amounts of limestone, which leads to scrubber scaling [58]. The produced gypsum in the reaction tank is filtrated using a hydro-cyclone and flows to a vacuum filter, where it is washed with fresh water and concentrated to generate the FGD's by-product. The waste water produced in the process is partially recirculated to the scrubber, and the rest is sent to the waste water treatment plant. The FGD's waste water has a complex matrix and contains various water soluble flue gas components such as halides. The treatment consists of different stages, in which alkalization, precipitation and flocculation occur. To remove heavy metals such as Hg that end up in the waste water, sulfidic precipitating agents are added to the water, which results in mercury sulfide formation with low water solubility as mostly suspended solids. Through utilization of flocculation agents such as iron chloride ($FeCl_3$), the suspended solids are coagulated and settled or filtered.

There is a possibility to run the FGD system as a two stage scrubber, in which a pre-scrubber is installed after the particle removal system. In this unit the flue gas is cooled down and the acid gases are removed. The pre-scrubber operates at low pH and thus, it promotes the removal of heavy metals such as mercury. The second scrubber can be used mainly for SO_2 removal by utilization of limestone slurry.

As mentioned before, wet FGD can offer the co-benefit of Hg removal from the flue gas to some extent. In contrast to Hg^0 which has low water solubility, gaseous bivalent mercury halides are more readily water soluble [43]. Thus, Hg^{2+} can be absorbed in the slurry of wet FGD; however, Hg^0 will be released through the stack. Therefore, a high fraction of Hg^{2+} in the flue gas can enhance the removal efficiency [53]. As Hg^{2+} is absorbed in the slurry, it can undergo different reactions. One is complex formation through reacting with different ligands, which is beneficial as complexes cannot be easily desorbed into the gas phase due to their charges [5, 91, 139]. Halides are possible ligands for formation of Hg^{2+} complexes as well as sulfite ($SO_3{}^{2-}$). There is also the possibility of multi-complex formation with different ligands [46, 136]. Beside the complexation reactions, redox reactions play an important role for the fate of mercury in the FGD slurry. As SO_x is readily absorbed in the slurry of wet FGDs, S(IV) is considered as the dominant reducing agent for Hg^{2+} in the slurry. The reaction results in the formation of sulfur in the oxidation state of six (S(VI)) and Hg^0 with a low Henry coefficient, which leads to Hg re-emission [122, 140]. Therefore, even with a high share of Hg^{2+} in the flue gas entering the FGD, depending on the FGD's operating parameters and the composition of the slurry, the overall Hg removal efficiency can be insufficient to reach

the limit values. Thus, additional measures to increase the Hg removal efficiency and reduce its re-emission need to be implemented.

2.3 Reactions in wet limestone flue gas desulfurization system

2.3.1 Absorption of SO$_2$ and its reactions in the slurry of FGD

As mentioned previously wet flue gas desulfurization system is the most common SO$_2$ removal technique used in flue gas cleaning of power plants. It consists of a scrubber, in which the flue gas is brought into contact with the scrubbing solution and the mass transfer takes place. Soluble gas components are absorbed in an aqueous phase with SO$_2$ being the most important one.

$$SO_{2(g)} \; \rightleftharpoons \; SO_{2(aq)} \tag{2.9}$$

Reaction 2.9 shows the absorption equilibrium, which depends on the concentration of SO$_2$ in gas and aqueous phase, contact surface between gas and liquid and the Henry coefficient. Henry's law describes the physical solubility of gas components in diluted aqueous solutions. According to Henry's law the partial pressure of a component in the gas phase above a solution is proportional to its mole fraction in the solution. The proportionality constant is the Henry's law constant K_{H}.

$$K_{\mathrm{H}} = \frac{c_{\mathrm{i(aq)}}}{p_{\mathrm{i(g)}}} \tag{2.10}$$

Henry's constant is temperature dependent and the dependency can be described by van't Hoff equation as shown in 2.11.

$$K_{\mathrm{H}}(T) = K_{\mathrm{H}}^{0} \cdot exp[\frac{-\Delta_{\mathrm{sol}}H}{R} \cdot (\frac{1}{T} - \frac{1}{T_0})] \tag{2.11}$$

K_{H}^{0} is Henry's constant at the reference temperature of T_0 and $\Delta_{\mathrm{sol}}H$ is the enthalpy of dissolution, which is constant for each component. In other words, the equation is only valid for a temperature range in which $\Delta_{\mathrm{sol}}H$ does not change and remains constant. After absorption of SO$_2$ in the aqueous solution, sulfurous acid (H$_2$SO$_3$) is formed by hydrolysis of SO$_2$, which can be dissociated to hydrogen sulfite (HSO$_3$$^-$) and sulfite ion (SO$_3$$^{2-}$).

$$SO_2 + 3H_2O \; \rightleftharpoons \; HSO_3^- + H_3O^+ + H_2O \; \rightleftharpoons \; SO_3^{2-} + 2H_3O^+ \tag{2.12}$$
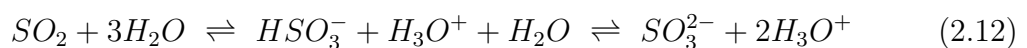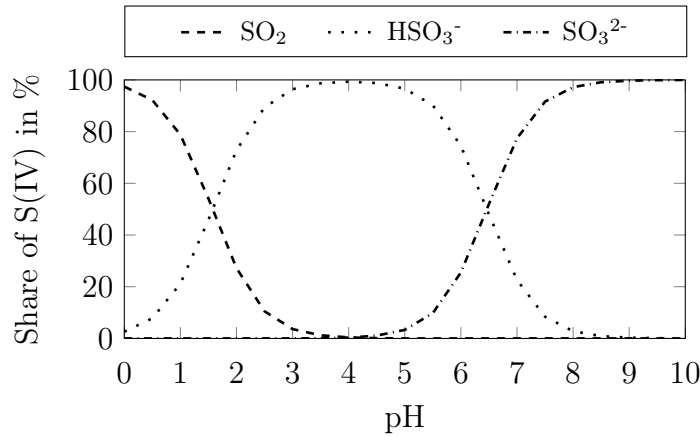
Figure 2.4: Share of S(IV) as a function of pH at 60 °C.

According to the reaction 2.12, the share of S(IV) in an aqueous solution depends on the pH of the solution and it can be calculated using the equilibrium constant of each reaction at a specific temperature. Figure 2.4 shows the share of each species in total S(IV) as a function of pH at a slurry temperature of 60 °C. It can be seen that S(IV) exists mostly as HSO_3^- at typical pH of the FGD's slurry.

SO$_2$ absorption in the slurry leads to a decrease of pH; thus, limestone ($CaCO_3$) needs to be injected to increase pH and SO$_2$ removal subsequently. A controller keeps the pH of the slurry constant by adding the required amount of limestone automatically. Dissolution of limestone results in calcium ions and carbon dioxide, which is released to the gas phase. The speed of dissolution differs between various utilized limestones.

$$CaCO_3 + H_2O \rightleftharpoons Ca^{2+} + CO_3^{2-} + H_2O \rightleftharpoons Ca^{2+} + 2OH^- + CO_2 \qquad (2.13)$$
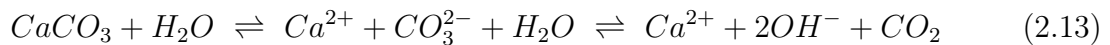
The final by-product of the FGD is gypsum which needs to have high quality by having a high share of calcium sulfate dehydrate ($CaSO_4 \cdot 2H_2O$). Reaching this goal requires the oxidation of low soluble sulfite before crystallization, which means the oxidation of absorbed S(IV) to S(VI) using the dissolved oxygen in the slurry. Flue gas contains oxygen, which can be dissolved in the slurry as well; however, the concentration is not sufficient to fully oxidize existing S(IV) in the slurry. In forced oxidation scrubbers, additional injection of air into the slurry leads to a higher concentration of dissolved oxygen and therefore, full oxidation of S(IV). All S(IV) species can be oxidized to S(VI), with HSO_3^- having the highest reaction rate [39].

$$2HSO_3^- + O_2 + 2H_2O \rightleftharpoons 2SO_4^{2-} + 2H_3O^+ \qquad (2.14)$$
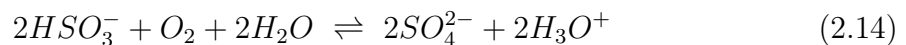
In addition, the oxidation leads to lower concentration of S(IV) in the slurry, which is

a driving force for higher absorption of SO_2. S(IV) concentration plays an important role in reactions involving Hg, which are explained in detail in the following chapters. Reaction 2.15 shows the gypsum production. As soon as the concentration of sulfate reaches its saturation point, crystals are formed. Lower pH (< 5) improves the quality of gypsum due to the decreased concentration of unreacted calcium sulfite in the solid fraction and a higher share of S(IV) as HSO_3^-, which has the highest oxidation rate [126]. On the other hand, the absorption of SO_2 is more favorable at higher pH, which affects the choice of suitable pH for the FGD.

$$SO_4^{2-} + Ca^{2+} + 2H_2O \; \rightleftharpoons \; CaSO_4 \cdot 2H_2O \qquad (2.15)$$

2.3.2 Absorption of bivalent Hg

The flue gas entering the FGD contains different Hg compounds, which are absorbed in the slurry depending on their concentration and their solubility. The important species are Hg^0 and Hg^{2+} compounds as Hg^+ is commonly not present due to its instability. Hg^0 has a very low solubility of 6.1E-05 $g\,l^{-1}$ in aqueous solution at 25 °C. In addition, increasing the temperature leads to lower solubility of gas in aqueous solutions and therefore, the absorption of Hg^0 in the slurry of FGD would be almost zero [18]. The bivalent halogen Hg compounds are the most common in the flue gas with higher solubility in comparison to Hg^0. Mercury chloride ($HgCl_2$) has the highest solubility of 68.1 $g\,l^{-1}$ in water at 25 °C followed by mercury bromide ($HgBr_2$) with 6.1 $g\,l^{-1}$ and mercury iodide (HgI_2) with 5.5E-02 $g\,l^{-1}$ [43]. Higher solubility of especially $HgCl_2$ results in its better absorption in the slurry of FGD.

As already explained in 2.3.1, the physical solubility of gas components in diluted aqueous solutions can be explained by Henry's law. Table 2.1 shows the Henry coefficient of Hg compounds at 25 °C. It must be mentioned that the Henry coefficient of some Hg compounds have not been measured experimentally and some of the values given in the table are calculated values from different references.

Table 2.1: Henry coefficient of Hg^0 and bivalent Hg^{2+} compounds in $mol\,l^{-1}\,Pa^{-1}$.

	Hg^0	$Hg(OH)_2$	HgI_2	$HgBr_2$	$HgCl_2$	HgO
Henry coefficient	1.3E-06	0.1	0.24	7.9	24	32
References	[139]	[68]	[45]	[45]	[139]	[139]

The bivalent Hg compounds are linear molecules with covalent bonds, which are hardly

dissociated in aqueous solutions [81]. They are in the interaction of liquid and gas phase and due to their vapor pressure would readily evaporate. The Henry coefficient is a parameter which shows the solubility or in other words the volatility of different components. It can be seen in table 2.1 that the Henry coefficient of Hg species are quite different and among bivalent halidomercurate compounds, $HgCl_2$ has the highest Henry coefficient and therefore the lowest volatility. In contrast, the low Henry coefficient of HgI_2 shows its high volatility, which leads to higher evaporation from aqueous solutions. The evaporation can lead to release of already absorbed Hg compounds to the gas phase, which influences the removal of Hg from the flue gas. Previous studies have shown the importance of volatility of bivalent Hg compounds from the slurry of FGD and its effect on Hg removal efficiency [45, 75].

2.3.3   Complex formation of Hg in the slurry

After absorption in the slurry, absorbed Hg^{2+} can undergo complexation reactions. The term complex refers to the product of a reaction between a Lewis acid with several Lewis bases. The Lewis acid is normally a cation which acts as the central atom and Lewis bases are known as ligands [50]. A Lewis base is an atom, molecule or ion with at least one pair of valance electron and a Lewis acid has at least one vacant orbital, which can accommodate a pair of electrons. Acids and bases are categorized into two groups of hard and soft based on their characteristics. A soft base has a donor atom with high polarizability and low electronegativity, and it can be oxidized easily. A soft acid has an acceptor atom with low positive charge and large size [31]. As a soft acid, Hg^{2+} can undergo complexation reactions with soft bases according to the hard-soft acid base (HSAB) theory [49]. HSAB is a theory that predicts the stability of complexes qualitatively. Based on the HSAB theory, hard acids prefer to coordinate with hard bases and soft acids with soft bases or in other words the same categories result in more stable complexes [52]. Hg^{2+} is counted as a soft Lewis acid due to its large size and low charge and therefore, the complex formation with soft bases is more favourable. For example, considering halides and S(IV), which are the most common ligands in the slurry and possible reagents for formation of Hg^{2+}-complexes, the softness would increase in the following order $F^- < Cl^- < Br^- < SO_3^{2-} < I^-$. This shows the favorability of Hg^{2+} complex formation in the slurry of FGD [52].

In addition, the formation constant of complexes is another parameter to have a quantitative prediction of the complex existence in the solution. Reaction 2.16 shows the

formation of halidomercurate complexes, in which X represents any of the halogens Cl, Br and I. The numeric value of m depends on the position of the complex formation equilibria and can be between 0 and 4.

$$Hg^{2+} + mX^- \ \rightleftharpoons \ HgX_m^{2-m} \tag{2.16}$$
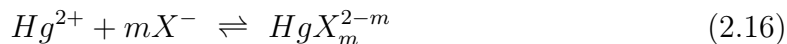
The formation constant of this reaction is shown in equation 2.17, which is the ratio of the product's activity to the activities of the reactants, and is the same as the equilibrium constant of the reaction. For ideal as well as diluted solutions, activities can be replaced with concentrations.

$$K = \frac{c_{\mathrm{HgX_m^{2-m}}}}{c_{\mathrm{Hg^{2+}}} \cdot c_{\mathrm{X^-}}^{\mathrm{m}}} \tag{2.17}$$

Depending on the concentration of relevant ligands and the formation constant of complexes, homoleptic and heteroleptic complexes of Hg^{2+} can be formed [34, 35]. Homoleptic complexes contain only one type of ligands while heteroleptic complexes contain different types of ligands such as reaction 2.18.

$$HgCl_2 + SO_3^{2-} \ \rightleftharpoons \ Cl_2HgSO_3^{2-} \tag{2.18}$$
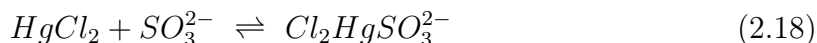
The formation constant of different complexes can also be calculated using models based on empirical data [22, 23], in which the strength of ionic and covalent bonds are considered. This method is explained more in detail in the work from Heidel [45]. The data shown in figure 2.5, are the logarithmic formation constant of Hg^{2+} complexes with various ligands at 25 °C adopted from Heidel [45], which are a collection of the data from [5, 68, 91, 139] and the values for NH_3 are taken from [50, 110].
The distribution of mercury complexes in the slurry depends on the concentration of ligands [94]. According to the formation constant of halidomercurate complexes, the higher the concentration of the individual halide, the higher the coordination number of the complex. As reaching the electron configuration of the next noble gas is the driving force of every reaction, for the haliomercurate complexes with the same halide, the largest formation constant belongs to the tetrahalidomercurate. Among different halides, the formation constant increases in the order of Cl < Br < I [67, 91], which can be explained with the HSAB theory.
It has to be noted that the complex of $Hg(SO_3)_2^{2-}$ has a quite high formation constant, which increases the possibility of its existence at high concentration of sulfite. In addition, SO_3^{2-} is a softer base than Cl^- and Br^-, wherefore it can replace them in a complex when existing in adequate concentrations as shown in reaction 2.19 [68]. This
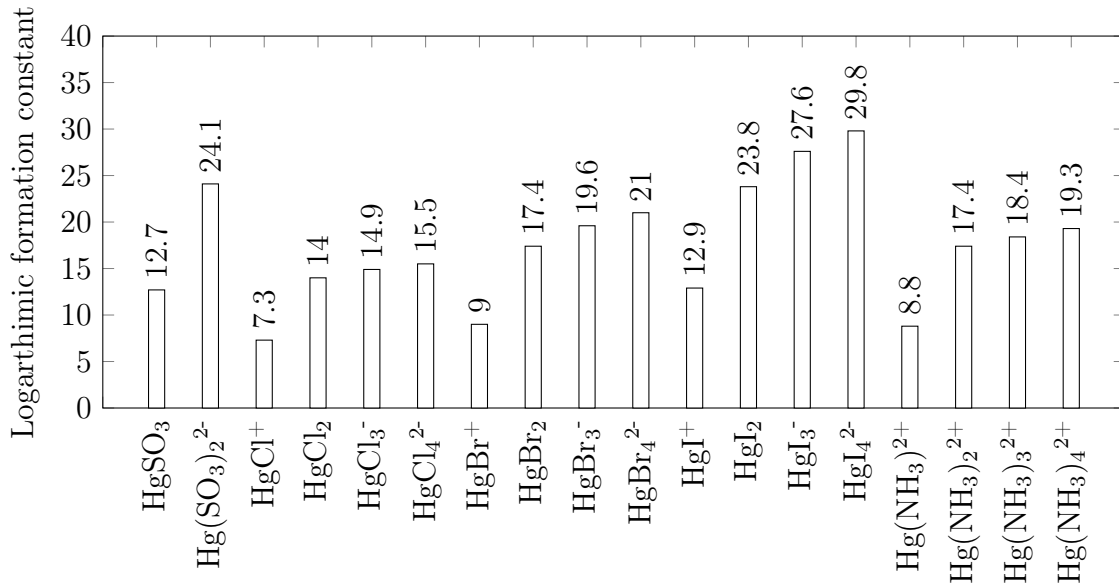
Figure 2.5: Logarithmic formation constant of Hg-complexes at pH=0 and T=25 °C adopted from [45] (a collection of the data from [5, 50, 68, 91, 110, 139]).

means according to the concentration of ligands and their formation constant, they may replace each other in the complex when their concentration in the slurry changes.

$$HgCl_2 + 2SO_3^{2-} \; \rightleftharpoons \; Hg(SO_3)_2^{2-} + 2Cl^- \tag{2.19}$$
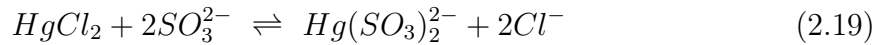
As mentioned in chapter 2.2.1, the un-reacted ammonia from the SCR catalyst may partially end up in the slurry of FGD and influences the reactions regarding Hg. At the relevant pH of the slurry, NH_4^+ is the dominant species [27].

In the presence of high concentration of NH_4X (X can represent i.e. NO_3^-, SO_4^{2-}), $Hg(NH_3)_4^{2+}$ can be formed from $HgCl_2$ with a higher formation constant than $HgCl_4^{2-}$ [50], which affects the fate of Hg in the slurry of FGD. The influence of NH_4^+ presence in the slurry of FGD on reactions involving Hg is discussed in more detail in chapter 4.1.6.

2.3.4   Redox reactions of Hg compounds in the slurry of FGD

Redox reactions are reactions in which electrons are transferred. They consist of reduction and oxidation reactions or half reactions, in which electrons are one of the reactants or products. The spontaneous redox reaction can take place when its Gibbs free energy is negative, or the cell potential of the reaction is positive. The cell potential can be calculated using equation 2.20, in which the Gibbs free energy of a reaction is related to the cell potential by the number of transferred electrons z_e and the Faraday

constant F. In other words, the cell potential is defined in a way that the electric work in an electrochemical cell is equal to $-z_e F E$.

$$\Delta G = -z_e F E \tag{2.20}$$

According to the Gibbs free energy the Nernst equation can be derived, which relates the cell potential to the activities of electron transfer species. As shown in equation 2.21, the cell potential is calculated using the standard cell potential E_i^0, the gas constant R, the constant of Faraday F, the temperature T and the number of transferred electrons z_e. c_{ox} and c_{red} show the concentration of oxidized and reduced reactants, which are equal to their activities in an ideal solution.

$$E_i = E_i^0 + \frac{RT}{z_e F} \cdot ln(\frac{c_{ox}}{c_{red}}) \tag{2.21}$$

The Redox potential of an aqueous system shows the tendency of the system to lose or gain electrons and can be measured using an electrode. The more positive the redox potential of a system, the more oxidizing the environment is and a negative redox potential indicates a reducing environment of the system.

In the slurry of wet FGD, depending on the redox potential and the pH of the slurry, every Hg^{2+}-complex can be reduced to Hg^0, which is then emitted to the gas phase and reduces the removal efficiency of the system [88, 136]. As SO_2 is readily absorbed in the slurry, S(IV) is the most abundant reducing agent for Hg^{2+}-complexes in typical wet FGD units. The redox reaction may occur according to the reactions below:

$$Hg^{2+} + HSO_3^- + 4H_2O \rightleftharpoons Hg^0 + SO_4^{2-} + 3H_3O^+ \tag{2.22}$$

$$Hg^{2+} + SO_3^{2-} + 3H_2O \rightleftharpoons Hg^0 + SO_4^{2-} + 2H_3O^+ \tag{2.23}$$
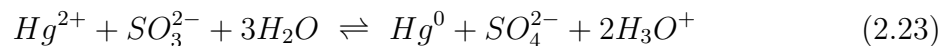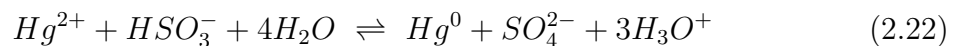
It has been reported that the rate of the reduction reaction with HSO_3^- is smaller than the reduction reaction with SO_3^{2-} by orders of magnitude and are 4.0E-06 1/s and 1.3E-01 1/s, respectively [83, 122]. In addition higher concentration of SO_3^{2-} results in the formation of $Hg(SO_3)_2^{2-}$ with a reduction rate reported to be 5.8E-03 1/s, which is smaller than the one for $HgSO_3$ [122].

Figure 2.6 shows the standard half-cell potentials of the halidomercurate complexes as well as S(IV)/S(VI) at 25 °C and pH of zero [45]. As mentioned before the redox reaction can only take place when the cell potential of the whole reaction is positive. This means that the cell potential of the oxidizing agent has to be larger than the one of the reducing agent. In addition, the driving force of the reaction depends on the
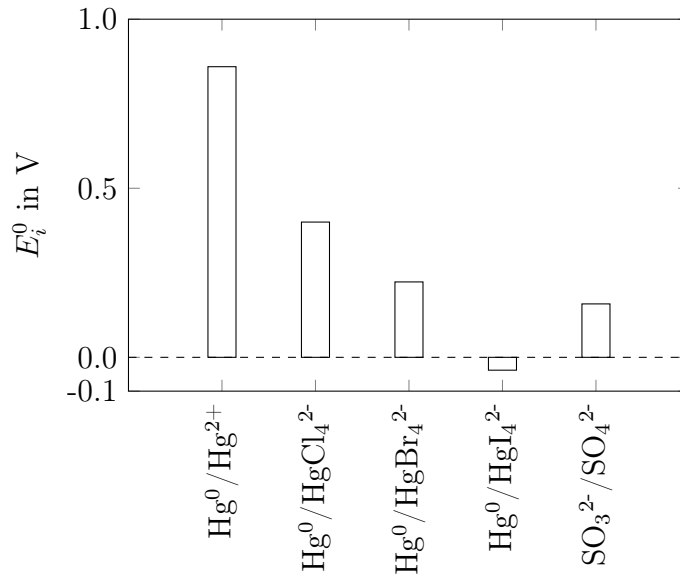
Figure 2.6: Standard half-cell potentials at pH=0 and T=25 °C [50].

difference of the half-cell potentials of the Hg^{2+}-complex and the reducing agent [43]. According to figure 2.6, S(IV) can reduce the halidomercurate complexes except HgI_4^{2-} at pH=0. However, increasing the pH increases the reducing strength of S(IV) and at the typical pH of the FGD, S(IV) can reduce HgI_4^{2-} as well [45].

It has to be noted that the standard electrode potential of individual halidomercurate complexes decreases with increasing values of the formation constant. This means that considering different halides, the driving force of the reduction reaction increases in the order of I < Br < Cl and for a particular halide, the higher the coordination number, the lower the possibility of reduction is [47].

2.3.5   Adsorption of Hg compounds on particles in the slurry

Adsorption can be defined as a process with a complex interplay of convective and diffusive mass transfer coupled with conductive heat transfer [3]. The process can be divided into different steps. First the adsorptive molecule reaches the boundary layer of the sorbent through convective and diffusive mechanisms. After that it is transferred through the boundary layer and into the pores of the sorbent by diffusion. The adsorption takes place by an exothermic attachment of the adsorptive molecules on the sorbent. Finally, the released energy is transferred to the sorbent's surface and into the bulk phase by convection and heat conduction.

Depending on the interaction strength between the sorbent and the adsorbate, ad-

sorption can be categorized as physical and chemical adsorption. Mercury can be adsorbed physically at low temperatures with weak bonds between mercury and the sorbent's surface with binding energies in the range of 10-100 meV [89]. Physisorption involves Van-der-Waals and induced dipole forces upon the mercury atoms. Outer mercurial electrons can be polarized by charges on the sorbent surface and the induced dipole moment leads to dipole attraction of the mercury to the sorbent's surface [137]. Chemisorption involves a stronger bond between mercury and the sorbent surface with binding energies between 1-10 eV [89]. In chemisorptions, mercury forms covalent or ionic bonds with atoms of the sorbent's surface and the strong interaction with the surface may lead to the formation of new sorbent species [137].

In the slurry of the FGD, Hg compounds can be adsorbed on the solid particles existing in the slurry such as gypsum crystals or any other sorbents like activated carbons, which may be injected to the slurry to improve the removal of Hg. Mercury partitioning in the FGD between aqueous and solid phase depends strongly on the operating parameters of the FGD such as pH and temperature as well as composition of the slurry like concentration of chloride, sulfite and metal compounds [8]. Different studies have been conducted to find the correlation between Hg adsorption on gypsum and different parameters. It has been reported that the increase in the share of metallic compounds such as iron (Fe), increases the adsorption of Hg on gypsum particles [112]. Another study shows that in a FGD with a high pH value and low concentration of chloride, Hg is mostly accumulated on gypsum and at a high concentration of halides, high redox potential results in higher Hg concentration in the aqueous phase [6]. In contrast, low redox potential of the slurry leads to higher adsorption of Hg on gypsum [7, 40].

The exact mechanisms of Hg adsorption on gypsum and the involved Hg^{2+} compounds in the reaction are not entirely known. Some researchers have tried to gain an understanding of Hg species associated with FGD gypsum using a temperature decomposition technique [69, 111, 144]. This technique uses the decomposition temperature of each Hg compound to relate the amount of desorbed Hg to the relevant compound. By heating the gypsum sample at a specific heating rate, the released Hg compound at each temperature can be measured. Examining different samples of gypsum from various FGD revealed that the primary Hg species in gypsum of the FGD was HgS. Other Hg compounds such as mercury sulfate and mercury chloride have also been found; however, HgS was the dominant species in all samples. As sulfide ions are not normally present in the slurry, its formation in the slurry has been suggested to be caused by disproportionation of sulfite as shown in reaction 2.24. This reaction can be

catalyzed by metals like mercury [8].

$$4SO_3^{2-} \ \rightarrow \ 3SO_4^{2-} + S^{2-} \tag{2.24}$$

$$Hg^{2+} + S^{2-} \ \rightarrow \ HgS \tag{2.25}$$

The sulfide ion may react with Hg^{2+} in the slurry to form insoluble HgS, which precipitates and results in HgS to be the primary species in the gypsum samples [8]. These reactions can also explain the direct correlation between sulfite concentration in the slurry and accumulation of Hg on gypsum.

2.3.6   Additives in the FGD and their effect on reactions

To reduce the amount of re-emitted Hg from the slurry, it is important to keep Hg^{2+} in a stable form, which decreases the possibility of its reduction. Adjusting the concentration of halides or using additives in the slurry can help to prevent these reduction reactions. Additives are categorized into two groups of precipitating agents, which normally form a more stable Hg compound; and sorbents, which adsorb Hg physically or chemically. In both cases Hg is transformed to a stable form and is more difficult to be re-mobilized. Some studies suggest the utilization of these additives in the slurry of wet FGDs, in order to prevent Hg^{2+} reduction [113, 116, 135] and their utilization in full scale FGDs have also been studied in some power plants [9, 97].

Precipitating agents for Hg are normally organic or inorganic sulfide based components, which react with Hg^{2+} and produce HgS with a small solubility. Thus, Hg is precipitated and stabilized to a high extent. As a side effect of utilizing precipitating agents for Hg, other heavy metals such as cadmium and lead may be removed [79] .

One of the precipitating agents that is commonly used to remove heavy metals from industrial wastewater is 2,4,6-trimercaptotiazine, trisodium salt ($Na_3S_3C_3N_3$) also called TMT. According to the reaction 2.26, 3 moles of Hg^{2+} chemically react with 2 moles of TMT and form weakly water-soluble macromolecular organo-metallic compounds. Therefore, they can be removed as they precipitate as solid substances [61].

$$2Na_3C_3N_3S_3 + 3Hg^{2+} \ \rightarrow \ Hg_3(C_3N_3S_3)_2 + 6Na^+ \tag{2.26}$$

TMT is mostly available as a 15 wt.-% aqueous solution (TMT 15[®]) and has already been widely used in wastewater treatment plants. It is easy to handle due to its non-toxicity and it is environmentally friendly. Using TMT in a wet FGD scrubber may transfer the Hg-TMT compounds to the wastewater treatment plant as well as to the

gypsum. They are chemically and thermodynamically stable, with their thermal decomposition taking place at temperatures higher than 210 °C [61]. The use of different precipitating agents in the slurry of FGD and their influence on reactions involving Hg is investigated and the results are presented in chapter 4.3.1.

Activated carbons are extensively used sorbents for removal of unwanted components from gas and liquid streams in different industries. In coal fired power plants, they are mostly used for removal of Hg^0 and Hg^{2+} from the flue gas. Their utilization in the slurry of FGD is less common as they may end up in the gypsum and thereby, increasing the Hg content of the gypsum affecting its quality. However, proper choice of activated carbon and proper dosing amount may prevent the mentioned problems. Carbon exists in different forms according to the arrangement of its atoms and is characterized as crystalline or amorphous. Materials with a high degree of order and symmetry fall into the crystalline carbons category such as diamond and graphite. Amorphous carbons are materials with less order in their structure and higher irregularities in the carbon structure, which lead to their porous structure. Basically any raw material that can be converted into a carbonaceous form can be activated and processed into activated carbon through different steps. The steps involve dehydration of the raw material, devolatilization of weakly bound organic constitutes, carbonization in a non-oxidizing atmosphere and the activation, which can be achieved either thermally or chemically. In addition, the activated carbon can be chemically impregnated to increase the efficiency of adsorption [137]. For example adding of sulfur to activated carbon improves Hg capture performance due to the formation of stable HgS [60].

The surface area of activated carbons typically ranges from 500 to 1000 $m^2 g^{-1}$ and their properties are defined depending on the shape and size of their pores [19]. According to the International Union of Pure and Applied Chemistry (IUPAC) [105], the pores are classified by their size as micropores with pore diameters of < 2 nm, mesopores from 2-50 nm and macropores with > 50 nm [104].

The different pore sizes fulfill different tasks in the adsorption process. In general large macropores are required to transport pollutants into the sorbent and the smaller micropores with their high adsorptive energies are responsible for adsorbing the pollutants and preventing them from diffusing back to the gas or liquid phase [137]. Utilization of different raw materials can influence the distribution of the pore sizes within an activated carbon. Using coconut shells results in a high concentration of micropores, while wood based activated carbons contain more mesopores and macropores. However, the activation process influences the pore distribution as well.

Chapter 3

Experimental equipment and analytical procedures

The experiments in this study were carried out in a test facility located at the University of Stuttgart, Institute of Combustion and Power Plant Technology. Measurements of the parameters and gas concentrations were conducted by implementing different analytical procedures, which are described in detail in the following chapter.

3.1 Description of the test facility

The experiments were carried out in a lab-scale flue gas desulfurization system, which consisted of two sections: a synthetic flue gas preparation section and a FGD section. The schematic of the test facility is presented in figure 3.1. To minimize the interaction of the surface, the whole reactor was made of glass. The synthetic flue gas was a mixture of 15 vol.-% carbon dioxide (CO_2), 3.5 vol.-% oxygen (O_2) and the remainder being nitrogen (N_2), which simulates the typical flue gas composition of a coal combustion power plant. The dry flue gas was fed with a volume flow of 3 or 4 $l\,min^{-1}$ to the gas preparation section, where the required SO_2 concentration was adjusted by adding SO_2 gas. Hg^0 was dosed directly upstream of the catalyst with a concentration of 50 $\mu g\,m^{-3}$ using N_2 as the carrier gas passing through metallic Hg. Required gas concentrations were adjusted in the flue gas using mass flow controllers (MFCs).

A constant flue gas humidity of 7 vol.-% and hydrogen chloride (HCl) concentration of 10 or 50 $mg\,m^{-3}$ were adjusted using a peristaltic pump by injecting the diluted HCl solution into the reactor. A honeycomb SCR catalyst was used to generate the required share of oxidized mercury in the flue gas. The HCl concentration was adjusted
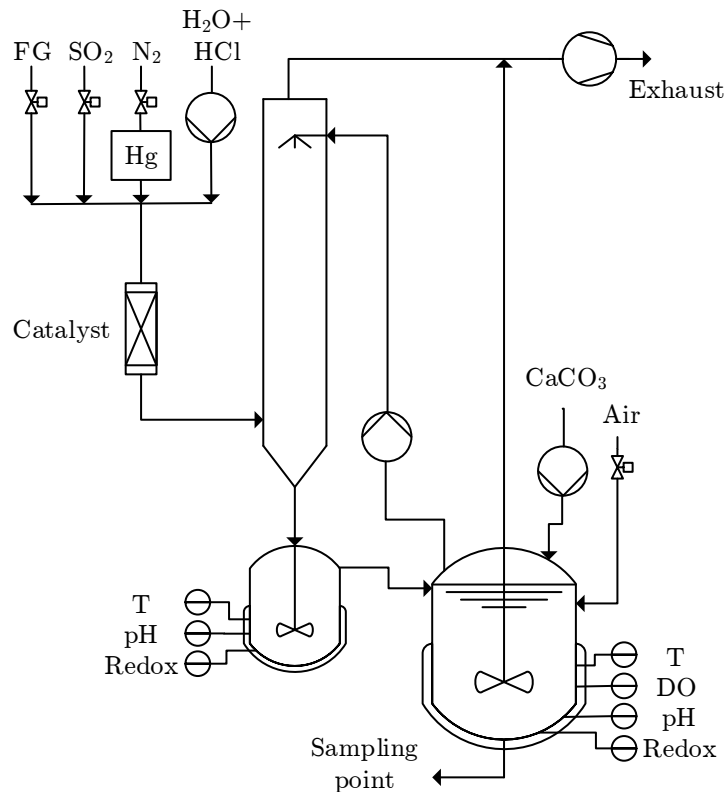
Figure 3.1: The schematic of the test facility.

to generate approximately 50 % oxidized mercury in the SCR catalyst. The mixing zone and the SCR catalyst were heated up using adjustable heating bands, to reach the gas temperature of 300 °C at the inlet of the SCR catalyst and keep the temperature of the gas in the SCR reactor constant. The temperature of the gas entering the FGD was adjusted to around 120 °C.

The FGD section consisted of an absorber and an external sump. The gas mixture entered the bottom of the absorber and was brought into contact counter currently with a limestone slurry, which was pumped to the top of the absorber from the external sump using a peristaltic pump. The liquid-to-gas ratio was set to 20 $\mathrm{l\,m^{-3}}$. The collected slurry at the bottom of the absorber was transferred through a siphon to the external sump; hence, no synthetic flue gas could enter the external sump. The slurry was made of an aqueous 10 wt.-% $CaSO_4 \cdot 2H_2O$ solution, with experiment-specific halide concentrations. To simulate the accumulation of halides in the slurry using flue gases with different halogen contents, appropriate synthetic slurries were prepared.

The runs were conducted using no halides, 10 g l^{-1} chloride (Cl⁻), 1 g l^{-1} bromide (Br⁻) and 0.1 g l^{-1} iodide (I⁻). The concentrations of halides were adjusted using the corresponding sodium (Na⁺), potassium (K⁺) or magnesium (Mg²⁺) salts. The Hg²⁺ concentration in the slurry was set to 300 µg l^{-1} by injection of diluted mercury(II) nitrate ($Hg(NO_3)_2$) solution before starting the measurement.

Redox potential, pH and temperature of the bottom of absorber and external sump were measured. The temperature of the slurry in the external sump was adjusted to 60 °C using a heating plate. Due to heat loss and evaporation, the temperature of the slurry decreases slightly over the height of the absorber from 60 °C at the top to approximately 50 °C at the bottom. The pH of the external sump was set to 5.6 using a PID controller by adding the required amount of fresh $CaCO_3$ solution automatically. Forced oxidation occurred by introduction of dry air with a flow of 2 l min^{-1} into the external sump and the amount of dissolved oxygen was measured continuously. It has to be noted that some experiments were conducted with different operating parameters, which are mentioned specifically in the relevant chapter.

The gas concentration was measured at the inlet and outlet of the catalyst and absorber as well as in the outlet of the external sump. Using the external sump made it possible to differentiate between re-emitted Hg and Hg which was never absorbed in the first place. The system is considered to run in steady state, when operating parameters such as pH, redox potential and dissolved oxygen are constant for at least two hours. For each experiment after reaching steady state, the concentration of Hg^T (sum of elemental and oxidized) and Hg^0 were measured at the inlet and outlet of the absorber and at the exhaust air of the external sump. A slurry sample was taken from the external sump at the end of each run and filtered with a paper filter, with particle retention of 5-13 µm, to separate filtrate and gypsum from each other. Filtrate samples were stabilized by adding diluted HCl and gypsum samples were dried at 40 °C and ground to homogenize the sample. The concentration of Hg in the samples was measured in a laboratory.

3.2   Analytical procedures

All gaseous concentrations in this work are provided as dry in standard temperature and pressure (0 °C, 1.013 bar) and at an oxygen concentration of 3.5 vol.-% O_2. Gas component concentrations were measured using an on-line gas analyzer ABB EL 3020, in which O_2 was measured using a paramagnetic method, SO_2 and CO_2 utilizing the

nondispersive infrared (NDIR) principle. Mercury speciation was determined by measuring the concentration of Hg^T and of Hg^0 with a continuous mercury analyzer Lumex RA 915 AMFG working with cold vapor atomic absorption spectroscopy (CVAAS) with Zeemann-background-correction. As the gas analyzer can only measure Hg^0, a reducing solution of Tin(II) chloride ($SnCl_2$) ensured reduction of oxidized mercury as shown in figure 3.2. The reducing solution is injected to the sampling position and mixed with the gas sample. After providing enough contact time for the reduction reaction, the gas sample containing only Hg^0 is dried in a cooler and sent to the gas analyzer. The measurement of elemental mercury was realized by selectively trapping oxidized mercury using an ion exchange resin. The difference between total and elemental mercury is calculated as Hg^{2+}.

Filtrate and gypsum samples were analyzed for their Hg content with the Hg AAS analyzer DMA-80 MLS Company, using the direct thermal principle.
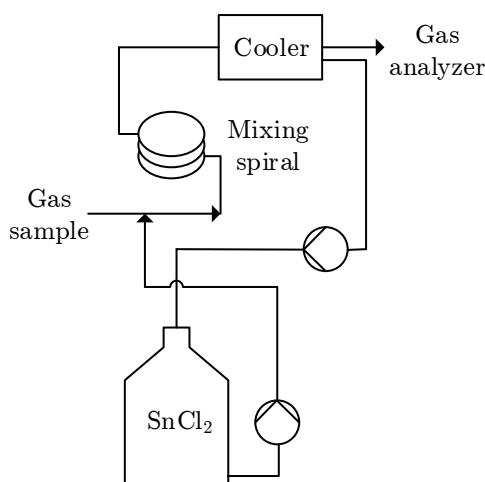

Figure 3.2: Hg reduction unit for Hg^T measurement with $SnCl_2$ as the reducing solution.

Dissolved oxygen measurement was carried out using a VisiFerm DO Sensor from Hamilton® measuring with the luminescence quenching principle. Redox potential was measured in this work, using a silver/silver-chloride electrode. However, the values provided in the result section are corrected by using a specific factor and show the potential difference of the slurry to the standard hydrogen electrode (SHE).

Sulfite concentration can be measured using iodometric titration as the state-of-the-art technology according to VGB [125] . The principle is a back-titration of iodine as the

oxidizing agent with thiosulfate as the reducing agent. Due to the low water solubility of elemental iodine in water, it has to be produced by the reaction of iodide and iodate in an acidic environment by adding HCl in the titration vessel.

$$IO_3^- + 5I^- + 6H^+ \rightarrow 3I_2 + 3H_2O \tag{3.1}$$
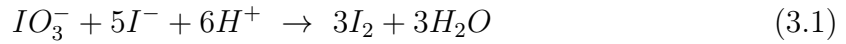
As the reaction only takes place in an acidic environment, the solution of iodide/iodate remains stable as long as there is no addition of acid to the solution. For the experiments in this study, a $0.05\,\mathrm{mol\,l^{-1}}$ iodine solution using potassium iodide and potassium iodate was prepared and for the titration solution, sodium thiosulfate was used. The thiosulfate solution has to be prepared daily, as it is not stable over extended periods. Starch solution serves as a color indicator for the titration. The sample has to be filtrated and titrated immediately after sampling, as sulfite is oxidized continuously by atmospheric oxygen. Thus, long handling times result in the measurement of smaller sulfite concentrations than were initially present in the sample. After preparing the sample, the iodide/iodate solution is added and by addition of HCl, iodine is produced. At this point, the existing sulfite in the solution is oxidized using the produced iodine.

$$I_2 + SO_3^{2-} + H_2O \rightarrow 2I^- + 2H^+ + SO_4^{2-} \tag{3.2}$$
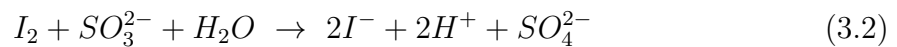
Afterwards, the remaining amount of iodine is titrated using thiosulfate solution as shown in reaction 3.3 and the sulfite concentration can be calculated.

$$2S_2O_3^{2-} + I_2 \rightarrow S_4O_6^{2-} + 2I^- \tag{3.3}$$
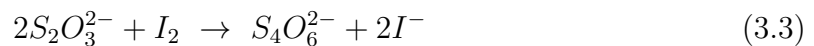
However, continuous measurement of sulfite using this method is impossible. Due to this reason, a continuous measurement principle is developed and implemented in the lab-scale FGD in this study and the calibration was carried out using iodometric titration.

The schematic of the continuous S(IV) measurement using two different methods can be seen in figure 3.3. In both methods, slurry was pumped out of the external sump using filters to retain solid particles from the measurement units. It was then mixed with a suitable reagent according to the chosen method and sent to the measurement device. The measurement principles of both methods are discussed in detail in chapter 4.2.
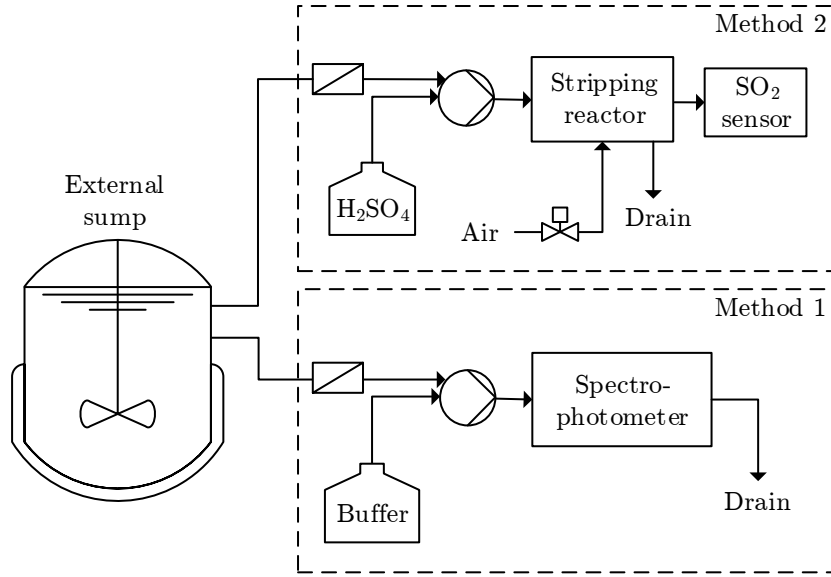
Figure 3.3: Continuous S(IV) measurement using two different methods.

3.3   Evaluation of the results

The presented results in chapter 4 are calculated using measurement values at the
steady state condition of the system. The removal efficiency of gas components can be
calculated using their concentration at the inlet and outlet of the absorber, which is
possible for SO_2 in this system as shown in equation 3.4. Due to the existence of an
external sump and Hg re-emission, the removal efficiency of Hg^T cannot be calculated
using the concentration of Hg at the inlet and outlet of the absorber. At first, Hg
mass flow at the inlet and outlet of the absorber, as well as external sump has to be
calculated related to the volumetric flow of flue gas and oxidation air. The amount of
re-emitted Hg from the external sump has to be counted as a part of Hg, which leaves
the absorber and subsequently, the removal efficiency can be calculated using the Hg
mass flows as shown in equation 3.5.

$$\eta_{SO_2} = \frac{c_{SO_2}^{in} - c_{SO_2}^{out}}{c_{SO_2}^{in}} \cdot 100 \tag{3.4}$$

$$\eta_{Hg^T} = \frac{c_{Hg^T}^{in} \cdot \dot{V}_{FG} - (c_{Hg^T}^{out} \cdot \dot{V}_{FG} + c_{Hg^T}^{sump} \cdot \dot{V}_{air})}{c_{Hg^T}^{in} \cdot \dot{V}_{FG}} \cdot 100 \tag{3.5}$$

Hg partitioning in gypsum and filtrate are presented either in a concentration of Hg or
as a mass fraction, in which the mass of gypsum and filtrate are taken into account.

This way, the distribution of Hg in the slurry can be better visualized, as gypsum has a much lower mass in comparison to the filtrate. Equation 3.6 represents the mass fraction of Hg in the gypsum in %.

$$X_{\text{Hg}}^{\text{gyp}} = \frac{x_{\text{Hg}}^{\text{gyp}} \cdot M_{\text{gyp}}}{x_{\text{Hg}}^{\text{gyp}} \cdot M_{\text{gyp}} + x_{\text{Hg}}^{\text{fil}} \cdot M_{\text{fil}}} \cdot 100 \qquad (3.6)$$

Chapter 4

Experimental investigation and results

4.1 Effect of slurry composition and operating parameters on SO$_2$ removal efficiency and Hg partitioning

The experiments were carried out in the lab-scale FGD at different operating parameters and slurry compositions to gain a deeper understanding regarding complex reactions involving Hg and its partitioning in a wet limestone FGD. The operating parameters were chosen close to the realistic values of wet limestone FGDs with wider ranges to cover all the possibilities in the droplets through the absorber and in the sump and to provide a better overview for understanding the reactions. The studied parameters were adjusted at the beginning of each test and measurements were carried out at steady state of the system for each point. Most of the experiments in this chapter were carried out with a wet flue gas flow of 3.2 l min^{-1}, chloride concentration of 10 g l^{-1} in the slurry and oxidation air flow of 2 l min^{-1}. Any differing conditions are mentioned specifically.

4.1.1 Temperature of slurry

Henry's law constant is a factor that relates the solubility of a gas in a liquid to its partial pressure above the liquid. According to the dependency of the Henry's law coefficient to the temperature, at constant partial pressure the solubility of gases in liquid decreases exponentially by increasing the temperature of the liquid. Figure 4.1 represents the SO$_2$ removal efficiency of the absorber as well as the mass flow of Hg$^{\mathrm{T}}$
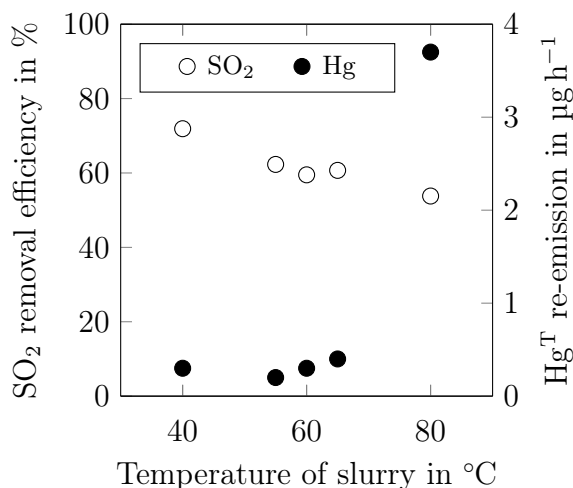
Figure 4.1: Effect of temperature on SO_2 removal efficiency and Hg^T re-emission.
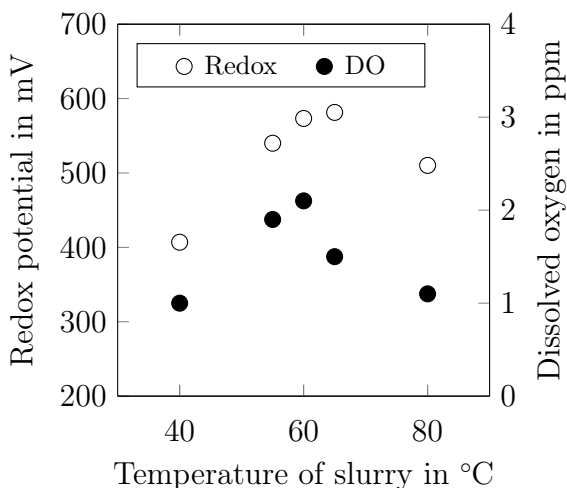
Figure 4.2: Effect of temperature on redox potential and dissolved oxygen.

re-emission from the slurry related to the temperature of the slurry. Results obtained from experiments at different temperatures ranging from 40 °C to 80 °C reveal the temperature dependency of gas solubility. It can be seen that the SO_2 removal efficiency of the absorber at 80 °C was approximately 20 % less than at 40 °C.

By increasing the temperature of the slurry the kinetic of the redox reaction of Hg^{2+}-compounds accelerates (equations 2.22 and 2.23), which results in Hg^0 formation and subsequently its desorption to the gas phase. As shown in figure 4.1, the rise in Hg^T re-emission between 40 °C to 65 °C was not significant, while at 80 °C a drastic increase in Hg^T re-emission took place. The exponential increase in Hg^T re-emission from the slurry by increasing the temperature is firstly due to the lower solubility of bivalent mercury compounds in the slurry and secondly to faster kinetics of redox reactions at higher temperatures. Thus, a higher amount of Hg^0 was desorbed to the gas phase. The exponential increase of reaction rate of reduction reaction with increasing temperature could be the dominant reason for such a drastic increase of Hg re-emission at 80 °C.

The correlation between redox potential of the slurry and the amount of dissolved oxygen in ppm at different temperatures is shown in figure 4.2. Dissolved oxygen is an indicator of the quantitative amount of O_2 present in the slurry. Like any other gas, the dissolution depends on the temperature and the partial pressure of the system. In addition, the reactions taking place in the slurry may consume dissolved oxygen and change the equilibrium. One of these reactions is the oxidation of S(IV) to S(VI). At 40 °C, the solubility of SO_2 was high, which resulted in a higher amount of S(IV)
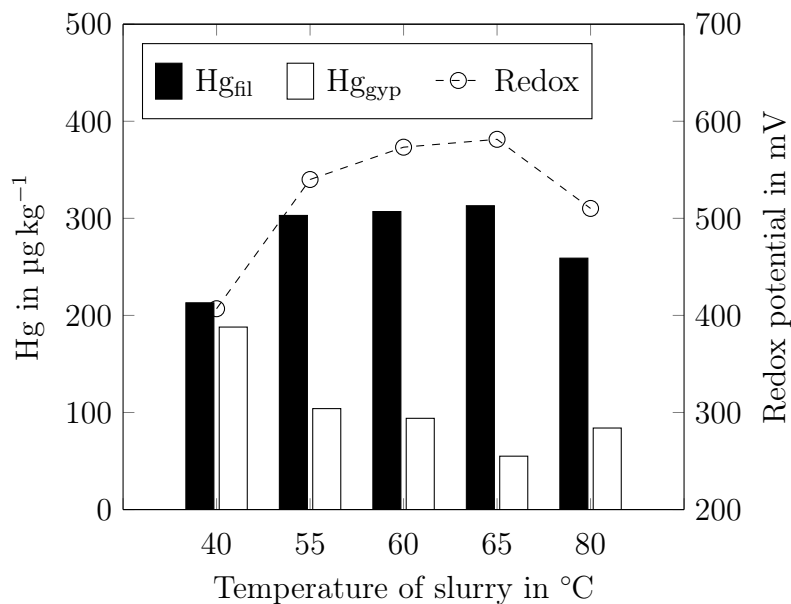
Figure 4.3: Effect of temperature on Hg partitioning in slurry and redox potential.

and therefore, a more reducing environment. By increasing the temperature to 65 °C, the lower solubility of SO_2 resulted in a higher redox potential, but the amount of dissolved oxygen was diminished due to higher temperature. At 80 °C, the decrease in solubility of O_2 affected the redox potential more significantly compared to the lowered dissolution of S(IV) and resulted in a fall of redox potential.

Figure 4.3 demonstrates the partitioning of Hg^{2+} in the slurry and its correlation with the redox potential of the slurry. At 40 °C the concentration of Hg was measured at 213 µg l^{-1} for filtrate and 188 µg kg^{-1} for gypsum. Increasing the temperature to 65 °C, resulted in the Hg concentration of 313 µg l^{-1} and 55 µg kg^{-1} in the filtrate and gypsum, respectively. Adsorption of Hg at the surface of the solid particles is an exothermic reaction, which means by increasing the temperature the adsorption of Hg on the gypsum is diminished. At 80 °C, a Hg concentration decrease of around 50 µg l^{-1} in the filtrate was observed. As the Hg re-emission at 80 °C increased sharply, it can be expected that the Hg inventory of the slurry falls due to high desorption of Hg to the gas phase and results in less Hg in the filtrate. The measurement of Hg concentration in the gypsum at 80 °C, revealed an increase of around 29 µg kg^{-1}, which contradicts the exothermic characteristic of adsorption and the equilibrium between the liquid and solid phase of slurry. Considering this result, it seems possible that the disproportionation of sulfite is kinetically favored at higher temperatures, which opens a new path for Hg in the slurry. According to equation 2.24, sulfide ions can be formed, and due

to the high affinity of Hg^{2+} to S^{2-}, HgS can be produced, whose extremely low water solubility results in its precipitation into the solid fraction. In this cases the increase in concentration of Hg in the gypsum at 80 °C can be explained, despite higher Hg re-emission and adsorption equilibrium.

In addition to the explanations above, figure 4.3 illustrates a direct dependency of Hg share in the filtrate to the redox potential of the slurry in each experiment. As sorption equilibria of Hg-compounds are shifted towards the adsorbed species for reducing conditions, a lower redox of the slurry results in a higher share of Hg in the gypsum [7]. Increasing the temperature influences the solubility of SO_2 as well as O_2 in the slurry, which affects the concentration of dissolved S(IV) and subsequently the redox potential of slurry conversely.

4.1.2 pH of slurry

In order to study the effect of pH on the reactions occurring in the slurry, experiments were carried out at different pH values of 4.2, 5.6, 6.0 and 6.6. At the beginning of each test, the pH was adjusted to the desired value by injecting fresh $CaCO_3$ using a peristaltic pump connected to a PID controller. Each point represents the measurement at steady state and does not include the start-up duration. At higher pH, absorption of SO_2 was improved. According to reaction 2.12, higher pH shifts the equilibrium to the side of SO_3^{2-}, which influences the driving force of absorption due to change in the concentration of $SO_2(aq)$ in a positive manner.

Figure 4.5 illustrates the increase in SO_2 removal efficiency as a result of the increase in pH. Although, increasing the pH of the slurry improves the absorption of SO_2, it diminishes limestone dissolution and additionally results in precipitation of $CaSO_3$ [20], which causes gypsum impurity. The measurement of dissolved oxygen in the slurry shows a decrease of 0.7 ppm while increasing the pH from 5.6 to 6.6. Due to the higher SO_2 removal efficiency at higher pH, the S(IV) concentration in the slurry and the consumption of O_2 for the oxidation reaction increase and result in less dissolved oxygen. The corrected values for redox potential of the slurry, which are shown in figure 4.6 are in agreement with the dissolved oxygen and SO_2 removal efficiency. The higher concentration of S(IV) leads to a more reducing environment and therefore, a lower redox potential.

Measurement of Hg^T re-emission mass flow is shown in figure 4.4. It can be seen that at pH < 5.6, the re-emitted Hg mass flow remained under $1\,\mu g\,h^{-1}$. By increasing the
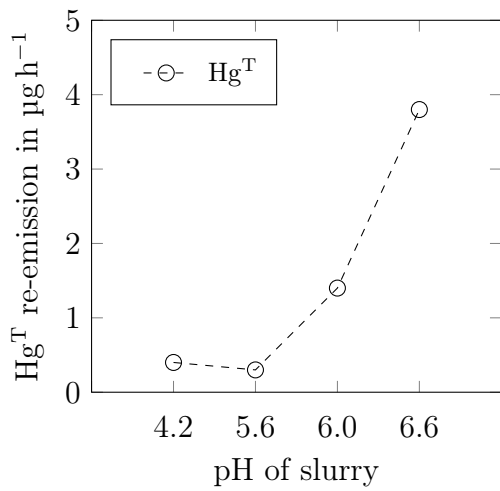
Figure 4.4: Effect of pH on Hg^T re-emission.
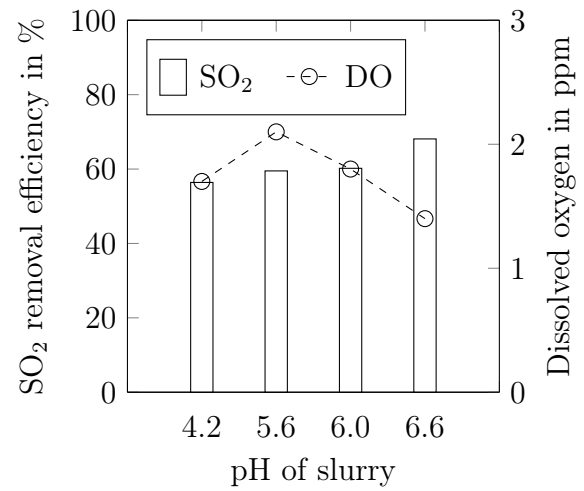
Figure 4.5: Effect of pH on SO_2 removal efficiency and dissolved oxygen.
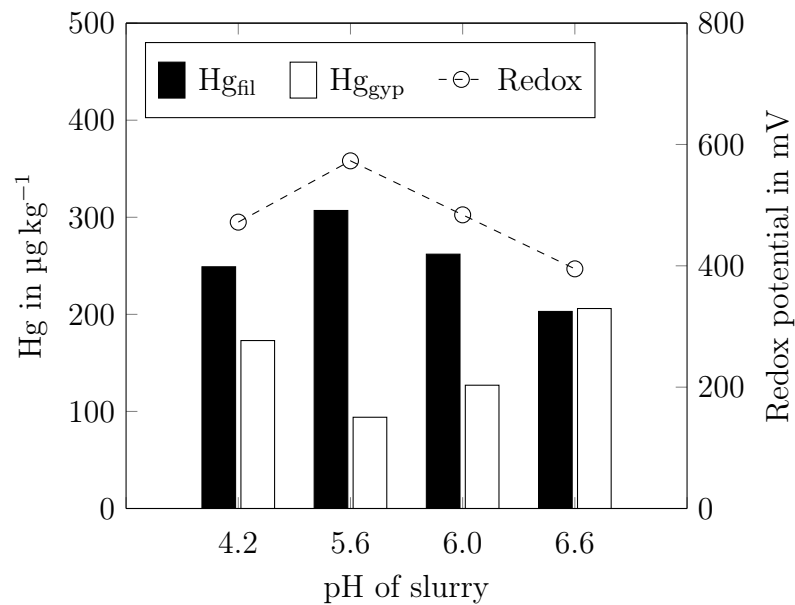
Figure 4.6: Effect of pH on Hg partitioning in slurry and redox potential.

pH to 6.6, Hg re-emission mass flow rose to 3.8 $\mu g\,h^{-1}$. The distribution of S(IV) in the aqueous solution at different pH demonstrates the increase in the share of SO_3^{2-} in the same pH range. The correlation between the increase in share of SO_3^{2-} and reduction of Hg^{2+} leads to the conclusion that SO_3^{2-} is one of the important reducing agents for Hg^{2+} in the slurry, which is in agreement with previous studies [45, 122]. Additionally, it has to be considered that the equilibrium for the Hg^{2+} reduction reaction (reaction 2.23) is shifted towards the products, as pH increases. In other words, the reducing strength of SO_3^{2-} is enhanced and thus, higher Hg^0 desorption to the gas phase is expected.

As shown in figure 2.4, at pH 4.2, the equilibrium of the reaction 2.12 is shifted to HSO_3^- and results in a share of almost 100 % HSO_3^-. Thus, the chemical reaction in the slurry follows another path. At lower pH the product of neutralization by limestone is calcium hydrogen sulfite ($Ca(HSO_3)_2$), which is more soluble than $CaSO_3$ and it is more easily oxidized to SO_4^{2-} [115]. This is also the reason for having lower concentrations of dissolved oxygen at pH of 4.2. In addition due to the higher solubility of $Ca(HSO_3)_2$ than $CaSO_3$, and therefore, higher concentration of dissolved HSO_3^- in the solution, the redox potential was low despite the higher oxidation rate of $Ca(HSO_3)_2$. The correlation between redox potential and the amount of Hg in the filtrate can be seen clearly in figure 4.6. The slurry with pH 6.6, had the lowest redox potential and consequently the lowest concentration of Hg in the filtrate, which indicates the highest concentration of Hg of 206 $\mu g\,kg^{-1}$ in the gypsum. The highest redox potential of the slurry with pH 5.6, resulted in the lowest Hg concentration in the gypsum of 94 $\mu g\,kg^{-1}$ among the carried out experiments.

4.1.3 Hg^{2+} inventory of slurry

Hg inventory of the slurry at each experiment was the result of Hg^{2+} injection to the synthetic slurry at the preparation stage, the absorption of $HgCl_2$ from the gas phase and re-emission of Hg^0 from the slurry during start-up as well as steady state of the facility. Slurries with different primary Hg^{2+} inventory were prepared, and experiments were carried out to study the effect of slurry Hg concentration on Hg partitioning. The total Hg concentration of the slurry at each steady state point was calculated based on the results of the measured Hg concentration in the filtrate and gypsum. Figure 4.7 shows the concentration of Hg in filtrate and gypsum as well as the mass flow of re-emitted Hg in correlation to the total concentration of Hg in the slurry. The re-emission of Hg was the result of the Hg^{2+} reduction reaction with S(IV) as the
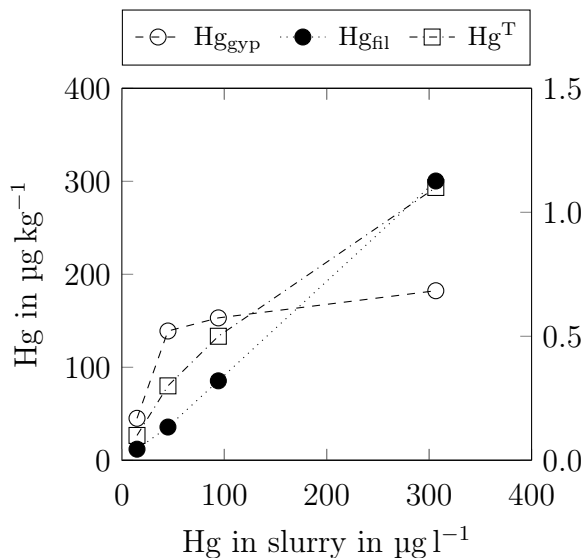
Figure 4.7: Effect of Hg inventory on Hg partitioning in FGD.
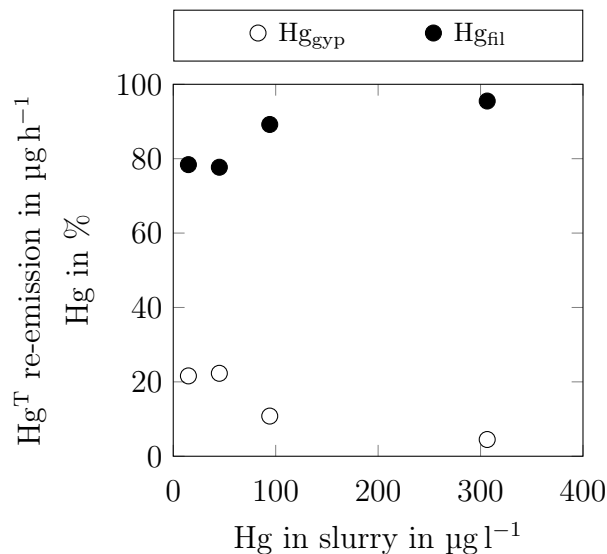
Figure 4.8: Effect of Hg inventory on Hg share in slurry.

dominant reducing agent in the slurry. The increase in mass flow of Hg^T re-emission at a higher concentration of Hg in the slurry, shows the direct correlation between the kinetic of reduction reaction with S(IV) and the Hg^{2+} concentration in the slurry. The results show a linear dependency for the first three investigated Hg inventories, which shows that the kinetic of reduction reaction is a first order reaction regarding the Hg^{2+} concentration. Nevertheless, for the last experimented point a deviation from the linearity can be observed. The same behavior has been discussed in a previous study, having a slurry with different chloride concentrations. According to Heidel [45], at a high Hg^{2+} concentration, the kinetic of the reduction reaction is limited to some other parameters such as concentration of S(IV) as the reducing agent or the kinetic of Hg^0 diffusion to the gas phase.

The concentration of Hg on gypsum particles at steady state condition of the slurry followed the adsorption isotherm behavior. Increasing the Hg concentration of the slurry resulted in an asymptotic maximum value of adsorbed Hg, as there was a limited capacity for adsorption of Hg on the particles. It can be seen clearly in figure 4.7, that the concentration of Hg in gypsum increased rapidly for the first investigated Hg concentrations until it reached a maximum value. Considering the share of Hg in the filtrate and gypsum at each point from figure 4.8, it can be seen that by increasing the total Hg in the slurry, the share of Hg on gypsum particles decreased while the share of Hg in filtrate increased.

4.1.4 SO_2 concentration of the flue gas at steady state

The influence of SO_2 raw gas concentration on Hg behavior at steady state condition of FGD was studied by changing the SO_2 concentration of the flue gas at the start-up of each experiment and carrying out the measurements at steady state of the system. Higher concentration of SO_2 in the flue gas results in a larger concentration difference between gas and aqueous phase, which is the driving force of the mass transfer or absorption of SO_2 to the aqueous phase and results in higher concentration of dissolved S(IV) in the slurry. As the injected mass flow of oxidation air to the external sump was constant, the input of dissolved oxygen did not change. Dissolved oxygen in the slurry was used to oxidize the high amount of S(IV) and thus, its concentration decreased while SO_2 concentration in the flue gas increased. Figure 4.9 represents the measurement of dissolved oxygen in the slurry as well as SO_2 removal efficiency of the absorber. Although increasing the SO_2 concentration of the flue gas increased the absolute amount of absorbed SO_2, the SO_2 removal efficiency decreased. SO_2 removal efficiency is the relative amount of absorbed SO_2 to the concentration of SO_2 entering the absorber; thus, by having a constant absorber length, higher concentration of SO_2 in the flue gas leads to a lower removal efficiency of the absorber.

The partitioning of Hg in the slurry, as well as Hg^T re-emission mass flow is presented in figure 4.11. It has to be mentioned that it was not possible to run the FGD with a constant pH of 5.6 without having any SO_2 in the flue gas. Thus, a low concentration of SO_2 was injected to the system in order to control the pH.
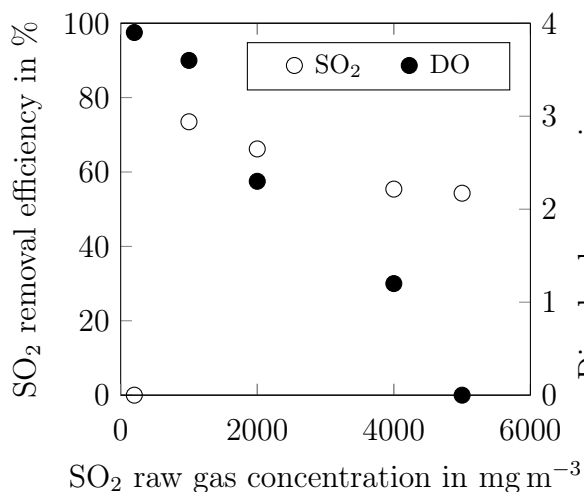

Figure 4.9: Effect of SO_2 concentration on SO_2 removal efficiency and dissolved O_2.
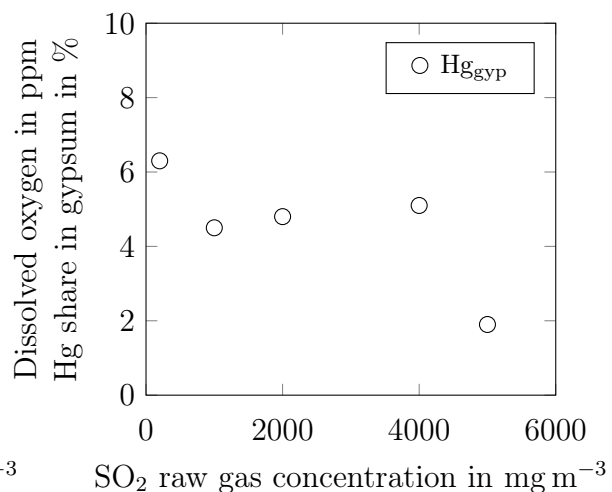
Figure 4.10: Effect of SO_2 concentration on Hg share in gypsum.
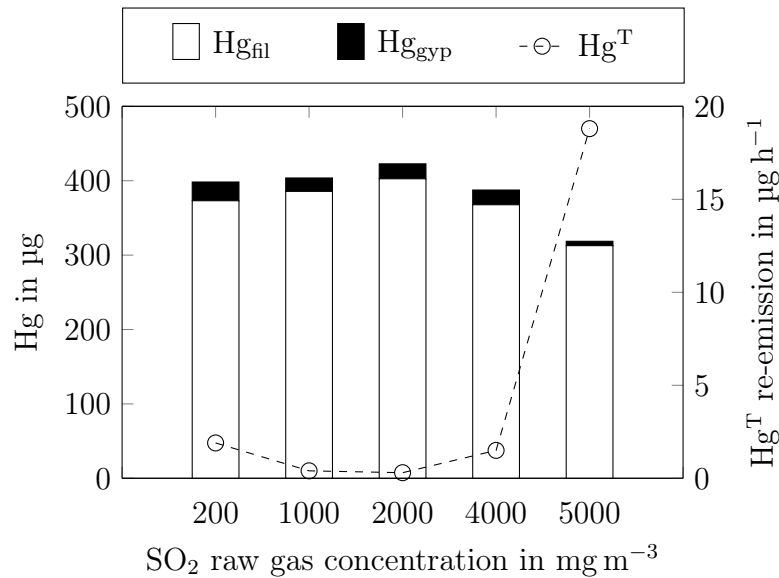
Figure 4.11: Effect of SO_2 raw gas concentration on Hg partitioning.

Checking the Hg^T re-emission reveals the ambivalent influence of S(IV) on Hg^{2+} reduction reaction. Between the SO_2 concentration of 200 and 1000 $mg\,m^{-3}$, there was a decrease in Hg^T re-emission mass flow from 1.9 to 0.4 $\mu g\,h^{-1}$. The reason is the formation of mercury complexes with S(IV) as ligands. By further increasing the SO_2 concentration of the flue gas and subsequently the S(IV) concentration in the slurry, the Hg^T re-emission mass flow increased. At a SO_2 concentration of 5000 $mg\,m^{-3}$, the amount of dissolved oxygen reduced to zero, which resulted in a sharp increase of the S(IV) concentration in the slurry and a significant increase in Hg re-emission mass flow. The Hg^T concentration in the slurry shows a correlation with the re-emitted Hg in the gas phase, as at points with higher Hg re-emission, the amount of Hg in the slurry was smaller. It is important to mention that the Hg concentration in the slurry was calculated from the Hg concentration in the filtrate and gypsum at steady state of the FGD and shows the whole mass transfer during start-up and steady state duration. The results reveal that the Hg re-emission during the start-up phase followed the same trend as the Hg re-emission at steady state and the experiments with high Hg^T re-emission at steady state, showed a lower Hg content in their slurry. The share of Hg between filtrate and gypsum shows a sharp decline in Hg share in gypsum in the experiment with 5000 $mg\,m^{-3}$ SO_2, which is even more obvious in figure 4.10. This could be due to the equilibrium between the aqueous and solid part of the slurry. The significant increase in Hg re-emission at this point, resulted in a high Hg loss in the filtrate and led to desorption of Hg from the gypsum to the aqueous phase. It has to be considered

that the partitioning of Hg in the slurry is due to the equilibrium concentration of Hg between gypsum and filtrate, which can be changed when one of the concentrations is changed. However, this is only valid when Hg is physically adsorbed on the particles. Chemical adsorption of Hg may result in formation of Hg-compounds which cannot be easily desorbed by changing the equilibrium.

4.1.5 Liquid to gas ratio of the absorber

The ratio of liquid to gas (L/G) in the absorber of FGD influences the mass transfer of the gas components to the liquid phase through diffusion. The driving force of the mass transfer is the concentration gradient of the component between the liquid and gas phase. The maximum amount of mass transfer through absorption of the gas component is related to the equilibrium between the gas and liquid phase. At constant partial pressure of SO_2, increasing the L/G led to higher SO_2 removal efficiency due to the higher mass transfer. Furthermore, an improvement of Hg removal efficiency can be observed when L/G is increased as it is shown in figure 4.12. An increase of Hg removal efficiency was the result of two different reactions. Firstly, the absorption of Hg^{2+} in the absorber rose and secondly the reduction of absorbed Hg^{2+} in the slurry and subsequently the amount of Hg^0 re-emission dropped.
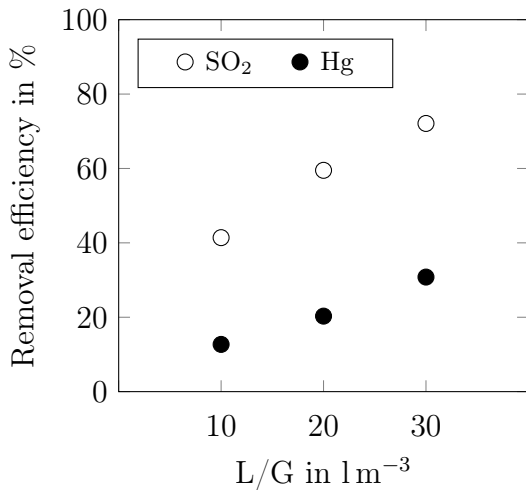
Figure 4.12: Effect of L/G on Hg^T and SO_2 removal efficiency.
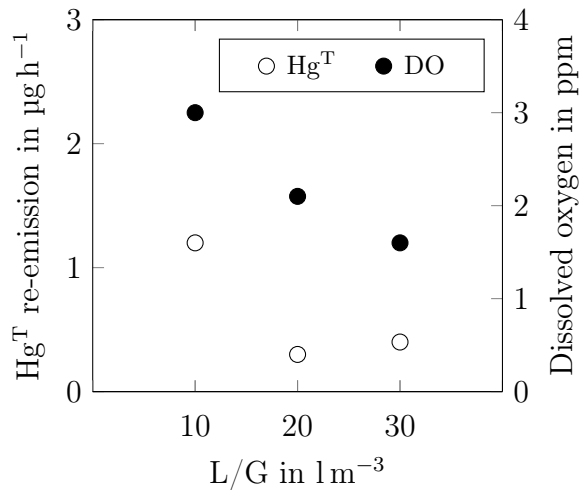
Figure 4.13: Effect of L/G on Hg^T re-emission and dissolved oxygen.

It has to be considered that due to the low concentration of Hg^{2+} in the gas phase compared to the SO_2 concentration and the high equilibrium concentration of Hg^{2+}, the concentration gradient between gas and liquid phase was low. Thus, the increase of

L/G influenced Hg^{2+} absorption and its removal through the absorber insignificantly. Nevertheless, the effect of L/G on the amount of Hg re-emitted from the external sump cannot be ignored. As shown in figure 4.13, the lowest Hg re-emission mass flow belonged to the L/G of $20 \, l \, m^{-3}$ and the highest to $10 \, l \, m^{-3}$.

The obtained results illustrate the ambivalent role of S(IV) on Hg behavior. As previously explained in chapter 4.1.4, on the one hand S(IV) is a suitable ligand for Hg-complexation and on the other hand a reducing agent for Hg^{2+} in reducing conditions of slurry. Thus, it can be concluded that at L/G of $10 \, l \, m^{-3}$, the amount of dissolved S(IV) was low and the formed complexes were not stable enough and easily reduced; however, increasing the concentration of S(IV) by doubling the L/G to $20 \, l \, m^{-3}$, triggered the formation of more stable complexes. It has been shown that above a certain S(IV) concentration, Hg^{2+} reduction was increased, which can be seen at a L/G of $30 \, l \, m^{-3}$. Figure 4.13 shows the decrease in the concentration of dissolved oxygen as well, due to the higher S(IV) concentration by increasing the L/G.

4.1.6   Presence of NH_3

Ammonia-slip from the SCR catalyst influences the downstream equipment and the involved reactions for removal of air pollution components. The un-reacted ammonia and ammonium sulfate $((NH_4)_2SO_4)$, which is the result of a reaction between NH_3 and SO_3, may end up partially in the FGD slurry and affect the reactions involving SO_2 and Hg. In order to study the influence of NH_3-slip on the behavior of Hg and SO_2 removal in the FGD, experiments were carried out using synthetic slurry containing $10 \, g \, l^{-1}$ chloride and wet flue gas volume flow of $4.3 \, l \, min^{-1}$. The remaining operating parameters were adjusted as explained in chapter 3.1. According to the composition curves of ammonia at different pH [27, 114], ammonium (NH_4^+) is the dominant species at the operated pH of the FGD. Thus, to simulate a slurry containing NH_4^+, different concentrations of $(NH_4)_2SO_4$ salt were added to the synthetic slurry. Due to the high solubility of NH_4^+ in water, its concentration in the FGD slurry can reach high values. According to a study, the measurement of NH_4^+ concentration in some power plants in China has shown the maximum concentration of $567.9 \, mg \, l^{-1}$ in the wet FGD slurry [16]. Therefore, the investigated NH_4^+ concentrations were chosen to be in the range of 100 to $600 \, mg \, l^{-1}$.

The influence of NH_4^+ concentration on SO_2 removal efficiency can be seen in figure 4.14. With only 1 % difference in the removal efficiency, no significant effect could be
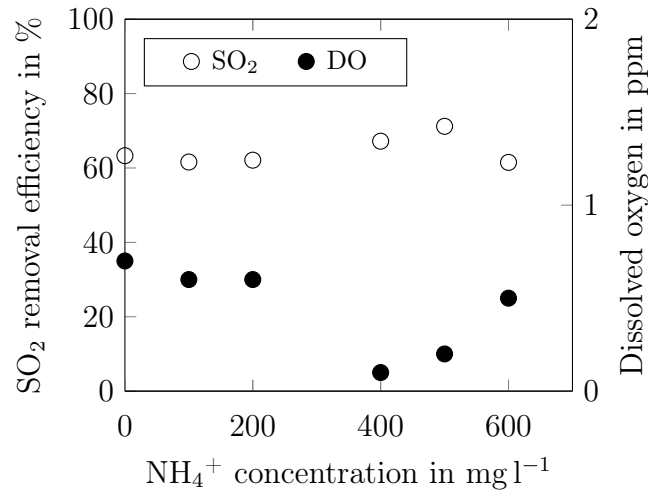
Figure 4.14: Effect of NH_4^+ concentration on SO_2 removal efficiency and DO.

observed for NH_4^+ concentrations up to $200\ \mathrm{mg\,l^{-1}}$. At NH_4^+ concentration of 400 and $500\ \mathrm{mg\,l^{-1}}$, the increase in SO_2 removal efficiency was more pronounced, being 10 % in the case of the $500\ \mathrm{mg\,l^{-1}}\ NH_4^+$.

Improvement of desulfurization using ammonium-based additives has been shown previously [30]. In addition, the experimental study and the results calculated with the absorption model by Takashina et al. [114] suggested a positive effect of ammonium on SO_2 absorption in the wet limestone FGD process. According to the derived model, NH_4^+ accelerates the dissolution rate of limestone and leads to increased formation of HCO_3^- in the bulk area of the liquid phase, which is essential for the reaction of SO_2 to HSO_3^-. Due to the higher concentration gradient between gas and liquid phase more SO_2 could be absorbed. It has to be noted that this study has been done at pH 6 and the pH was controlled by adjusting acid feed and cannot completely simulate the process of FGD. As the pH in the lab-scale FGD was adjusted to 5.6 using limestone dosing, high NH_4^+ concentration led to lower dosage of fresh $CaCO_3$ due to its basic characteristic, which led to drop in desulfurization efficiency. Testing the effect of ammonium in a large scale limestone FGD [138], reveals the negative effect of ammonia-slip on SO_2 removal efficiency and the results obtained in the lab-scale FGD from the experiment using $600\ \mathrm{mg\,l^{-1}}\ NH_4^+$ illustrate the same effect. It can be concluded that the presence of ammonia at low concentrations may improve desulfurization efficiency as long as NH_4^+ concentration does not drastically influence pH and fresh $CaCO_3$ dosing.

The concentration of dissolved oxygen, which is presented in figure 4.14, can be ex-
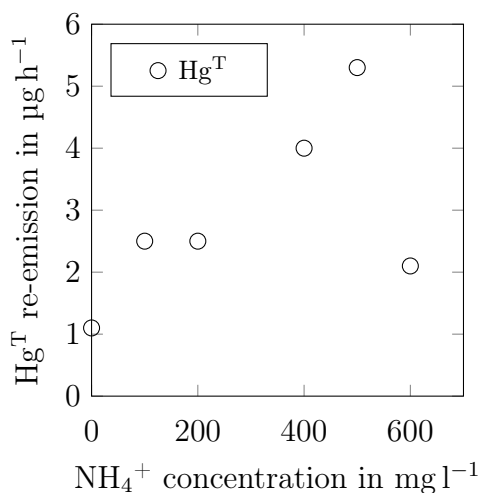
Figure 4.15: Effect of NH_4^+ concentration on Hg^T re-emission.
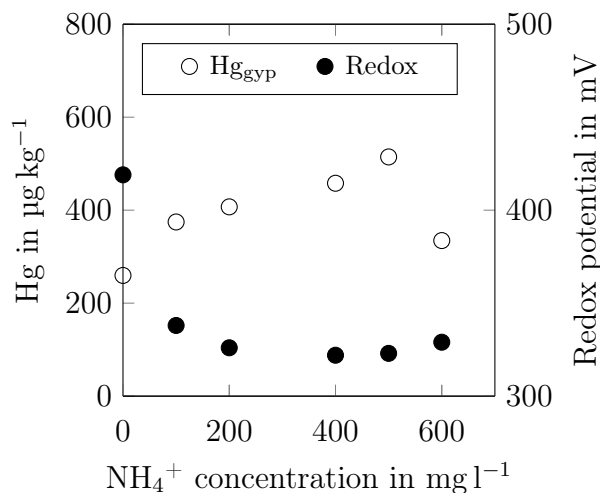
Figure 4.16: Effect of NH_4^+ concentration on Hg concentration in gypsum and redox potential.

plained due to the SO_2 removal efficiency of the absorber. Dissolved oxygen had the opposite trend compared to SO_2 removal efficiency and an increase in SO_2 removal efficiency resulted in a decrease in the amount of dissolved oxygen. For example, at a NH_4^+ concentration of 400 and 500 $mg\,l^{-1}$, higher SO_2 absorption led to more S(IV) in the aqueous phase and consequently more oxygen was utilized to oxidize S(IV) to S(VI); thus, less dissolved oxygen was measured in these slurries.

The mass flow of Hg^T re-emission is shown in figure 4.15. Increasing NH_4^+ up to 500 $mg\,l^{-1}$ resulted in a higher Hg^T re-emission up to 5.3 $\mu g\,h^{-1}$. However, at 600 $mg\,l^{-1}$ NH_4^+, Hg^T re-emission fell back to 2.1 $\mu g\,h^{-1}$. On the one hand, the trend of Hg^T re-emission followed the same trend as S(IV) concentration or in other words SO_2 removal efficiency. As long as NH_4^+ resulted in higher SO_2 removal efficiency and subsequently higher S(IV) concentration, Hg^T re-emission increased and as soon as SO_2 removal efficiency decreased due to higher concentration of NH_4^+, Hg^T re-emission decreased. On the other hand, in the presence of sufficient NH_4^+, reaction with $HgCl_2$ results in the formation of $Hg(NH_3)_4^{2+}$ with a formation constant of 19.1, which is higher than the formation constant of $HgCl_4^{2-}$ [50]. Even though NH_3 is a hard base, soft metals can form metal-ammonia complexes when a sufficient amount of NH_3 is present. Thus, the decrease in Hg^T re-emission at 600 $mg\,l^{-1}$ NH_4^+ could be due to the formation of $Hg(NH_3)_4^{2+}$ complexes. The increase in Hg^0 re-emission from the slurry in the presence of NH_3 in the flue gas has also been observed in a previous study [76], in which the

experiments were carried out using a coal-derived flue gas.

Figure 4.16 illustrates the influence of NH_4^+ concentration on redox potential of the slurry as well as Hg concentration in gypsum. In general, the presence of NH_4^+ led to a decrease of approximately 80 mV in redox potential of the slurry. However, further increase in NH_4^+ concentration did not induce an additional significant change in redox potential. Hg concentration in the gypsum increased around 240 µg kg^{-1}, when NH_4^+ was added from zero to 500 mg l^{-1}; however, at 600 mg l^{-1} NH_4^+, Hg concentration showed a sharp decrease of around 180 µg kg^{-1}. As the 600 mg l^{-1} NH_4^+ resulted in the formation of Hg-ammonia complexes, the solubility of Hg would increase and Hg would not be adsorbed on the solid fraction of the slurry. In the study by Wang et al [131], it has been shown that increasing the concentration of NH_3 leads to higher solubility of Hg in aqueous solutions, as $Hg(NH_3)_3^{2+}$ and $Hg(NH_3)_4^{2+}$ complexes, that are formed at higher NH_3 concentrations, are less adsorbable than $Hg(NH_3)^{2+}$ and $Hg(NH_3)_2^{2+}$ species. It can be concluded that the presence of NH_3 can have two different effects on the behavior of Hg and SO_2 in the FGD, depending on its concentration and in case of lab-scale FGD the limiting concentration is between 500 to 600 mg l^{-1} NH_4^+.

4.1.7   Different halides in the slurry

In order to investigate the influence of existing halides in the slurry on reactions involving Hg and SO_2, different synthetic slurries were prepared. The measurements were carried out using a synthetic flue gas wet volume flow of 4.3 l min^{-1} and with keeping the other operating parameters constant. The first experiment was conducted using a slurry without halides, to check the behavior of Hg in the absence of halides and to obtain baseline results for comparison. The results of this slurry are shown with the lable of 0, representing the presence of no halides. The following concentrations were determined for the tested halides: 10 g l^{-1} of chloride, 1 g l^{-1} of bromide and 0.1 g l^{-1} of iodide. These concentrations were chosen in a way to follow the same order of halogen content in coal. In addition, as the results of this chapter are used for comparison in the rest of the study, they had to be chosen in a way to not prevent Hg re-emission completely and provide a base for investigating the influence of sudden changes and addition of other additives.

Figure 4.17 illustrates the SO_2 removal efficiency of the absorber for all experiments. The SO_2 removal efficiency was around 60 % for all runs. The presence of halides for the concentrations investigated showed no significant impact on SO_2 removal efficiency.
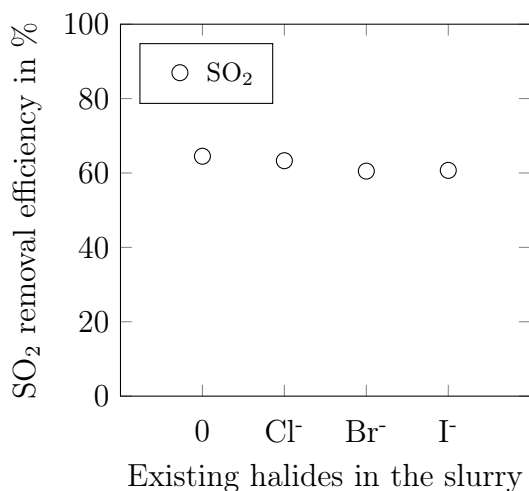
Figure 4.17: Effect of different halides on SO$_2$ removal efficiency.
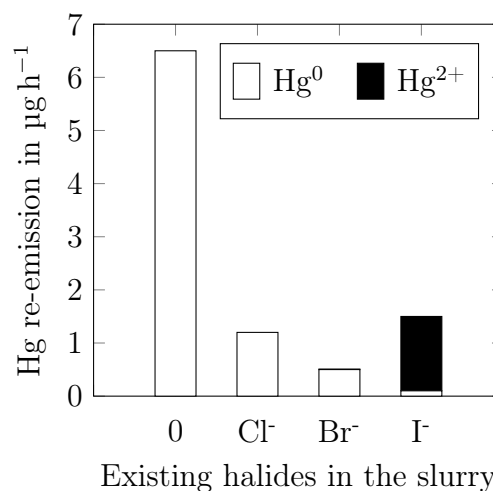
Figure 4.18: Effect of different halides on Hg^0 and Hg^{2+} re-emission.

It could be speculated that the increase in ionic strength and corresponding change in diffusion rate in the presence of halides could have a positive effect on SO$_2$ removal efficiency. However, the actual removal efficiency of the scrubber depends not only on chemical parameters, but also on thermodynamic properties of the phases such as surface tension, which could be affected by addition of halides adversely.

After reaching steady state, the concentration of Hg^T and Hg^0 were measured at the external sump, which represents re-emitted Hg exclusively. Figure 4.18 shows the distribution between Hg^0 and Hg^{2+} of the corresponding Hg re-emission mass flow, as well as the mass flow of total re-emitted Hg in all the studied cases. The presence of halides led to a decrease in Hg re-emission. It can be concluded that the highest Hg^0 re-emission belonged to the slurry containing no halides at all and the lowest to the slurry containing 0.1 g l^{-1} iodide. The results are in agreement with previous studies [5, 47], as the presence of halides plays an important role in the formation of Hg complexes. The individual half-cell standard electrode potentials of the various halidomercurate-complexes correspond with different reaction rates of the chemical reduction of the Lewis acid Hg^{2+}. Thus, the re-emission of Hg^0 was in the order of Cl > Br > I. Comparing the Hg^T re-emission, the slurry containing iodide showed higher re-emission than the slurry with bromide. However, by analyzing the distribution of Hg^0 and Hg^{2+}, it can be seen that in the presence of iodide more than 90 % of the total mercury re-emitted consisted of Hg^{2+} species. The corresponding emitted volatile Hg^{2+} compound was likely to be HgI$_2$. This compound has the highest vapor pressure
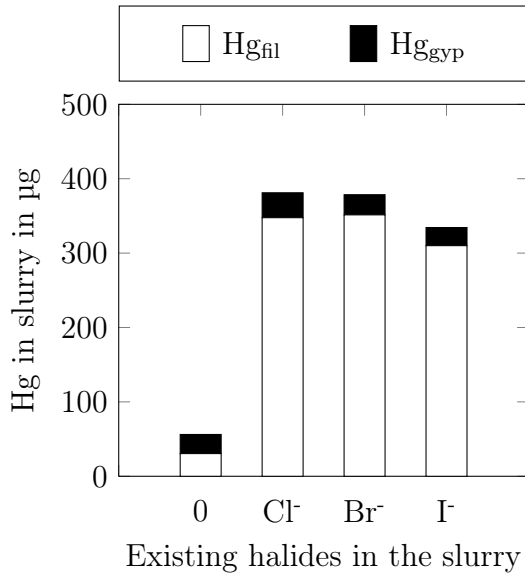
Figure 4.19: Total distribution of Hg content of slurry between gypsum and filtrate.
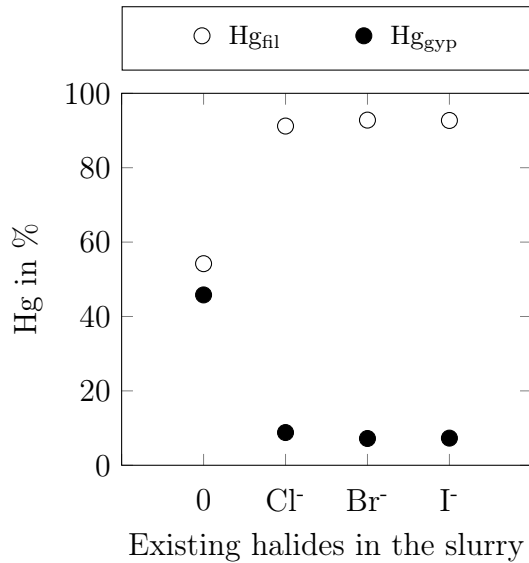
Figure 4.20: Effect of different halides on Hg partitioning in slurry.

when compared to the other bivalent Hg^{2+} species as discussed earlier. For the halide free baseline case and chloride containing slurry, the re-emitted Hg mass flow consisted of Hg^0 exclusively, and for the bromide containing slurry, only 2 % of the total re-emitted Hg consisted of Hg^{2+} in the form of $HgBr_2$. These findings are in agreement with previous studies regarding Hg re-emission from FGD slurries [5, 45].

Figure 4.19 shows the total Hg content of the slurry and its distribution between gypsum and filtrate for steady state operation of the system. Low Hg content of the slurry indicates high transient Hg re-emission from the slurry in the whole process until reaching steady state. As Hg re-emission measurements evaluated previously were carried out after the FGD reached steady state, the data in figure 4.18 cannot be compared directly with the Hg content of slurry in figure 4.19. In the absence of halides, the slurry contained around 50 µg Hg which amounts to about 10 % of the initial Hg^{2+} inventory of the synthetic slurry. The corresponding re-emission of 90 % of the initial Hg^{2+} content of the slurry underlines the high rate of re-emissions in the absence of halides. When comparing halide containing slurries, the one containing 0.1 g l^{-1} iodide had the lowest Hg content of the slurries due to high re-emission of Hg^{2+}; even though the re-emission of Hg^0 was comparably low for this case, as evaluated previously.

The share of Hg in the gypsum and filtrate is depicted in figure 4.20. The values represent the relative share of Hg associated with the gypsum or filtrate to the total Hg content of the slurry. The absolute quantity of Hg in the gypsum for all slurries

investigated was approximately 25 µg, which amounts to 50 % of the total Hg content of the slurry without halides. For the slurries with halides, the same absolute quantity of Hg was analyzed in the gypsum, resulting in a share of less than 10 % due to higher total Hg content of the slurry. From this observation it could be concluded, that the adsorption capacity of the solid particle content of the slurry was the limiting parameter for the slurries investigated. Hence increasing total Hg content of the slurry would not result in elevated Hg content of the solid phase, since the maximum adsorption capacity of the gypsum particle inventory was already exceeded for a Hg^{2+} concentration in the aqueous phase as low as 20.8 µg l^{-1}. The latter has already been discussed in detail in chapter 4.1.3 , when investigating Hg adsorption on gypsum at different Hg^{2+} inventory of the slurry.

4.1.8 Dynamic change of SO$_2$ concentration at different slurry compositions

As previously discussed in this chapter, each operating parameter and flue gas composition has an influence on Hg re-emission from the slurry. All of the discussed results up to this point were steady state results of the system, which were taken after giving the system enough time to reach equilibrium of all reactions. Due to the flexible operation of power plants and utilization of different fuels, it is important to experiment and understand reactions involving Hg inventory of the slurry when sudden changes are occurring, which may result in a sharp emission peak of released Hg from the stack. As S(IV) is the main reducing agent for Hg^{2+} in the slurry, which results in re-emission of Hg^0, the effect of a sudden change of its concentration and subsequently its influence on Hg re-emission has to be investigated. Changing the SO$_2$ concentration in the flue gas entering FGD would be the best way to trigger the change in S(IV) concentration. Thus, in this chapter, the dynamic behavior of Hg re-emission at sudden change in the concentration of SO$_2$ entering the FGD is studied. It must be considered that the results of this chapter represent the behavior of FGD during the change and are not directly comparable with the steady state results of the system. Specially, for Hg re-emission the concentration was measured continuously in µg m^{-3}, however, the steady state results of Hg re-emission were presented in mass flow in µg h^{-1}.

At first, a synthetic slurry containing no halides was chosen to define and understand the direct relationship between Hg and S(IV) in the slurry without having other halidomercurate complexes interfering with the reactions involving mercury. After-

wards, the influence of each halide in the slurry on Hg re-emission by sudden change in SO_2 concentration was investigated separately to show the role of halides on preventing Hg re-emission. All the measurements were carried out with 4.3 $l\,min^{-1}$ of synthetic flue gas. The volume flow of oxidation air in the external sump was 2 $l\,min^{-1}$ and was kept constant in all tests. Thus, the ratio of oxidation air to synthetic flue gas was lower in comparison to the previous tests and the increase in SO_2 concentration could result faster in deficiency of dissolved oxygen in the slurry.

In each graph, the horizontal axis represents the duration of the measurement. The change in SO_2 concentration was carried out by changing the volume flow of SO_2 injected to the gas entering the FGD using a mass flow controller and is shown corresponding to the time of measurement. The continuous measurement of Hg^T re-emission from the external sump as well as relevant parameters in particular redox potential and the amount of dissolved oxygen in the slurry are shown in each plot. In all experiments, the starting concentration of SO_2 was adjusted to 3 $g\,m^{-3}$. After giving enough time for the system to reach steady state conditions, the first change was implemented by increasing the concentration of SO_2 to 4 $g\,m^{-3}$, and the second change by increasing SO_2 concentration to 5 $g\,m^{-3}$. The parameters were kept this way for a certain time until the Hg re-emission reached a constant value. Afterwards, the SO_2 concentration was readjusted back to 3 $g\,m^{-3}$ to check the influence of reverse change on Hg behavior.

Figure 4.21 (a) illustrates the online measurement results of the slurry containing no halides. At the beginning of the experiment redox potential had the value of 360 mV, dissolved oxygen was at around 1 ppm and Hg^T re-emission above the external sump showed a concentration of around 45 $\mu g\,m^{-3}$, which corresponded to the concentration of around 21 $\mu g\,m^{-3}$ or the mass flow of 8 $\mu g\,h^{-1}$ in the clean gas leaving the absorber. A change of SO_2 concentration to 4 $g\,m^{-3}$, resulted in a drop of dissolved oxygen to 0.4 ppm, and an increase in Hg^T re-emission to 65 $\mu g\,m^{-3}$. It has to be noted that no change in redox potential was observed in this step. The decrease of dissolved oxygen represents the slight increase in S(IV) concentration, which led to reduction of Hg^{2+} and increase in Hg^T re-emission; however, the rise in S(IV) concentration was not significant enough to influence the redox potential of the slurry.

When all parameters were steady, a second change of SO_2 concentration to 5 $g\,m^{-3}$ was carried out. It could be seen that some minutes after the change, the system reacted and all parameters changed. The dissolved oxygen and redox potential declined and Hg^T re-emission rose sharply. It has to be noted, that the changes were not simultaneous. The change in dissolved oxygen and Hg^T re-emission started first. After several minutes,

dissolved oxygen showed the value of zero, and at this moment redox potential started to fall. Having no dissolved oxygen in the slurry revealed the fact that the amount of dissolved oxygen was no longer sufficient to oxidize the S(IV) entering the slurry. Thus, the concentration of S(IV) increased rapidly, which resulted in extreme Hg re-emission from the slurry. 15 minutes after the change in SO_2, the concentration of Hg^T re-emission reached the maximum value of around $250\,\mu g\,m^{-3}$, followed by a decrease. The Hg re-emission peak in the external sump was equivalent to $114\,\mu g\,m^{-3}$ or the mass flow of $43\,\mu g\,h^{-1}$ in the clean gas leaving the absorber. As the system stabilized by keeping the same conditions, Hg^T re-emission dropped slowly to even lower values than the initial concentration. These results can lead to the conclusion of the ambivalent influence of S(IV) in reactions involving Hg. As there were no halides present in this experiment, S(IV) played an import role as a ligand for Hg complex formation in addition to its role as a reducing agent. The increase of SO_2 and subsequently S(IV) resulted in a sharp increase in Hg^{2+} reduction; however, by further increasing the S(IV) concentration Hg^T re-emission decreased due to the formation of Hg-S(IV) complexes.

It can be concluded that in the absence of halides, a higher concentration of S(IV) resulted in a higher share of Hg^{2+} as the mercury disulfite complex, which has a slower decomposition rate to Hg^0 than a monosulfite complex. This conclusion is in accordance to the results obtained in another study [8], which suggested the positive effect of higher S(IV) concentration on the stability of Hg complexes in the absence of halides. The reverse change of SO_2 concentration from 5 to 3 $g\,m^{-3}$ triggered the Hg^{2+} reduction reaction and Hg^T re-emission concentration increased slowly. It could be observed that as soon as dissolved oxygen concentration reached values above zero, the redox potential steadied and Hg^T re-emission decreased sharply. A time difference of around 35 minutes was observed between the change in SO_2 concentration and the increase of dissolved oxygen in the slurry and subsequently reaching steady state. During this time all dissolved S(IV) in the slurry had to be oxidized and dissolved oxygen increased as soon as there was more than the required amount for the oxidation of the existing S(IV) in the slurry. It could be seen that the decrease of S(IV) concentration at this step resulted in an increase in Hg^{2+} reduction before reaching equilibrium. The latter can be due to the decomposition of $Hg(SO_3)_2{}^{2-}$ to $HgSO_3$, which has a higher decomposition rate and formation of Hg^0. A study by Chang [15] revealed the same trend for Hg re-emission; however, the experiments were carried out in a bench system without including Ca^{2+} in the slurry. The results of the experiment revealed that in the absence of halides there is a range of S(IV) concentration, which prevents Hg^{2+}

reduction and its re-emission due to the low rate of reduction reaction of $Hg(SO_3)_2^{2-}$ complex.

The same procedure was repeated for slurries containing $10 \, g \, l^{-1}$ chloride, $1 \, g \, l^{-1}$ bromide and $0.1 \, g \, l^{-1}$ iodide and figures 4.21 (b) to (d) represent the online measurement results, respectively. The concentration of measured Hg^T re-emission at SO_2 concentration of $3 \, g \, m^{-3}$ in all of the cases was lower than the Hg^T re-emission in the absence of halides, which shows the positive influence of the halides' presence on preventing Hg re-emission and has been already discussed in chapter 4.1.7. The dissolved oxygen concentration in all three cases was around 1 ppm; however, the redox potential was different for each halide due to the presence of the different salts and ions in the slurry. When the SO_2 concentration in the flue gas entering the FGD was increased, all parameters showed the same trend as with the slurry without any halides. In all the slurries, as soon as the amount of dissolved oxygen reached zero, the redox potential started to fall and Hg re-emission increased. The maximum amount of Hg^T re-mission at a SO_2 concentration of $5 \, g \, m^{-3}$, depends on the type of halide that was used in the slurry. By comparing all the graphs, it can be seen that the highest peak in Hg^T re-emission concentration belongs to the slurry containing no halides with around $250 \, \mu g \, m^{-3}$, followed by the slurries containing chloride, bromide and iodide with 89, 55 and $50 \, \mu g \, m^{-3}$, respectively. Even though slurries containing bromide and iodide showed lower redox potential representing a reducing environment, the peak of re-emitted Hg by increasing S(IV) concentration was lower due to the presence of more stable Hg-complexes. It could be seen that in the case of the iodide containing slurry, the change in redox potential during the whole measurement was not significant.

By adjusting the SO_2 concentration back to $3 \, g \, m^{-3}$, the redox potential started to rise and reached a steady value as soon as dissolved oxygen reached values above zero. Exactly at this point, Hg^T re-emission decreased towards its original low values. The Hg^T re-emission measurement in figure 4.21 (b), when the slurry contained chloride was quite similar to the one in figure 4.21 (a), when no halides existed. In both cases, two peaks occurred, once at the point that dissolved oxygen reached zero and once when the amount of dissolved oxygen rose from zero. The only difference was in the maximum of peak which was higher in case of the slurry without halides. The peaks occurred at a specific S(IV) concentration, in which the formation of monosulfite complexes are favored. The second peaks were observed for the tests, in which Hg^T re-emission concentration decreased already before the change of SO_2 concentration back to $3 \, g \, m^{-3}$ and could be seen in the absence of halides and for the slurry containing
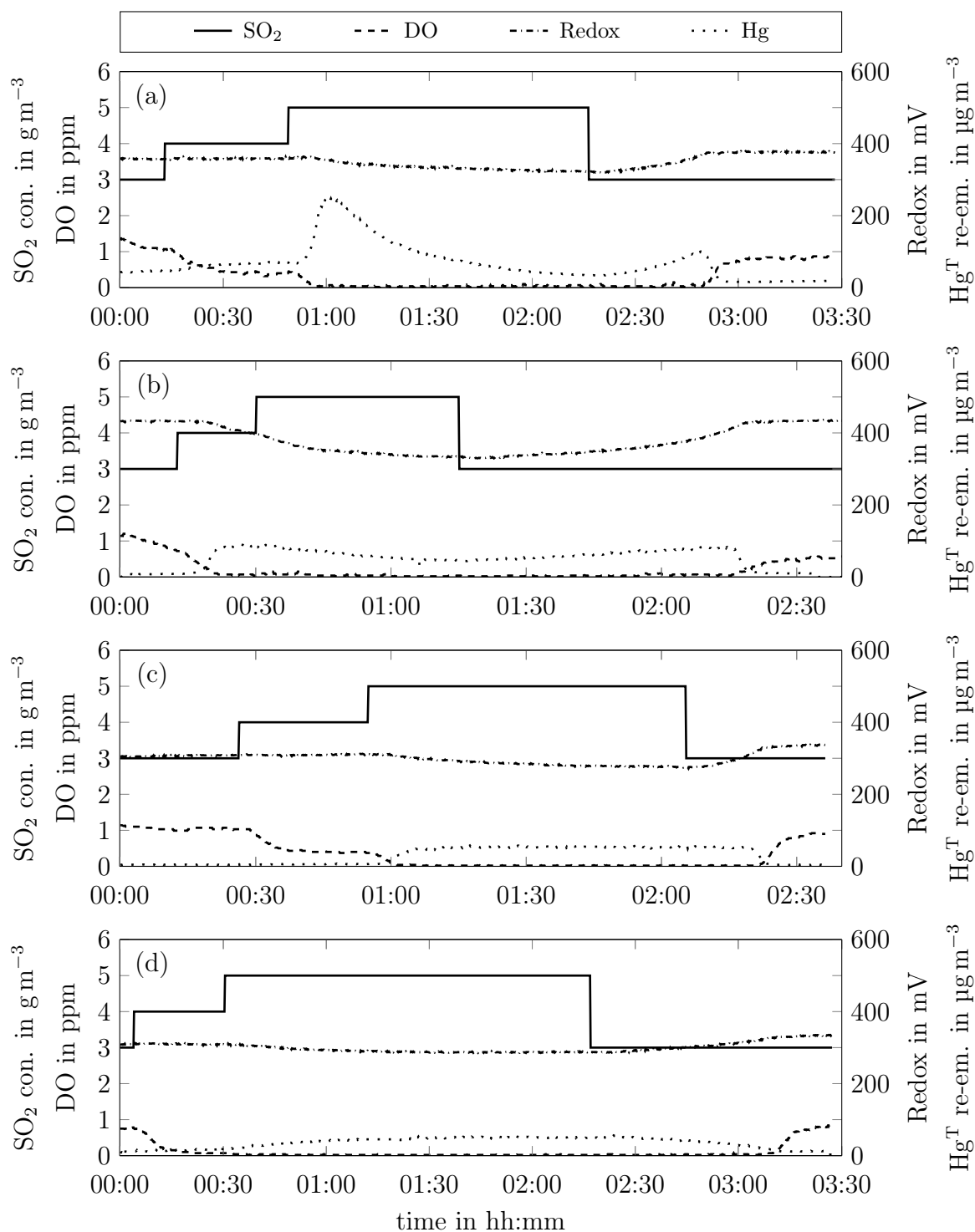
Figure 4.21: Online measurement results of slurries containing (a) no halides (b) $10\,\mathrm{g\,l^{-1}}$ chloride (c) $1\,\mathrm{g\,l^{-1}}$ bromide and (d) $0.1\,\mathrm{g\,l^{-1}}$ iodide when changing the SO_2 concentration of flue gas.
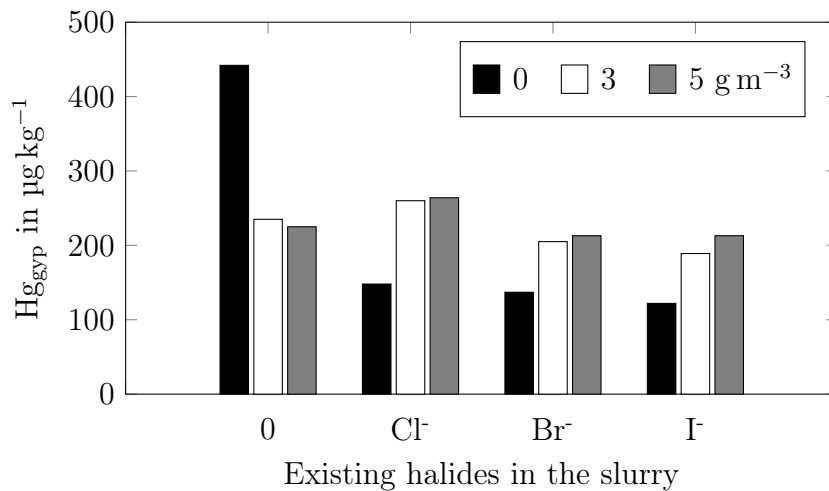
Figure 4.22: Concentration of Hg in gypsum of different slurries at different SO_2 concentration of flue gas.

chloride. In the case of slurries containing bromide and iodide, no second peak could be observed. It can be concluded that in these slurries either a higher concentration of S(IV) is required in order for S(IV) to be counted as a ligand for Hg and resulted in a decrease in the amount of Hg^{2+} reduction or due to the high formation constant of bromo- and iodomercurate-complexes this point would have never been reached.

To study the effect of SO_2 concentration on the partitioning of Hg in slurries containing various halides, samples were taken from each slurry at three different times. The first sample was taken before start-up of the absorber, when the synthetic slurry reached 60 °C. At this point, S(IV) concentration in the slurry was zero and the loss of Hg inventory was due to the increase in temperature. The second sample was taken at the steady state of the system, when the SO_2 concentration was $3 \, g \, m^{-3}$ and the last sample when the SO_2 concentration was $5 \, g \, m^{-3}$. Hg concentrations in the gypsum of all mentioned samples are depicted in figure 4.22.

It can be seen that increasing the S(IV) concentration resulted in higher Hg concentration in the gypsum in the presence of halides, which can be explained using reaction 2.24. According to this reaction, at a higher concentration of S(IV), sulfide ions are formed, which results in the formation of insoluble HgS and its precipitation. Thus, the concentration of Hg in gypsum increases. It has to be noted, that in the presence of halides, the total Hg loss of the slurry is quite low due to the existence of halidomercurate complexes. However, in the slurry without halides, the addition of S(IV) to the slurry results in high Hg re-emission and thus, a lower concentration of total Hg in the

slurry in general. The latter explains the decrease of Hg concentration in the gypsum by increasing the S(IV) concentration in the slurry containing no halides due to the high amount of Hg re-emission and thus, a lower Hg inventory.

It cannot be denied that S(IV) concentration in the slurry has a critical effect on the behavior of Hg and the amount of re-emitted Hg from the slurry. That emphasizes the importance of S(IV) measurement in the slurry, in order to reveal its role and investigate the possibility of predicting Hg re-emission. Chapter 4.2 focuses on possible measurement principles to obtain a suitable method for continuous S(IV) measurement.

4.2 Predicting Hg re-emission using S(IV) measurement

The critical influence of S(IV) on the behavior of Hg in the slurry of FGD has already been discussed in chapter 4.1.8. The state-of-the-art sulfite measurement method is iodometric titration. Unfortunately, this measurement method has some disadvantages. Firstly, samples can only be tested consecutively and not continuously. Secondly, samples must be taken from the slurry, filtrated and titrated, which gives the dissolved sulfite in the filtrate enough time to be partially oxidized and results in a lower estimation of the real values. The preparation of the reagents has to be done meticulously and requires a laboratory. In addition, the process is not selective and counts all the reducing agents in the solution as sulfite [80].

Besides titration, sulfite concentration can be measured using other methods. A very accurate measurement principle is the ion chromatography. In this process, due to the time required between extracting the sample and measurement, specific chemicals have to be used to stabilize the sample and prevent oxidation [21]. This method requires an equipped laboratory and cannot be carried out continuously. Another measuring method is using a sensor that sends a series of voltages into the slurry via two electrodes and evaluates the response currents. With this data the correlating sulfite concentration can be calculated [62].

The approach of reducing Hg emission by measuring and regulating sulfite concentration has already been suggested in some other works [2, 64]. However, they have not shown the direct relationship between sulfite concentration and Hg re-emission. In the following chapter, two different continuous measurement principles using a spectrophotometer and a gas sensor are introduced and tested in combination with the lab-scale

FGD. The feasibility of their implementation in a working system is proven and the correlation of sulfite concentration and Hg behavior in the slurry is investigated.

4.2.1   Dissolved sulfite measurement using a spectrophotometer

Sulfite measurement using a spectrophotometer has been already investigated by adding different additives to make colorful complexes with sulfite and thereby enabling a measurement of the concentration in the visible light spectrum [1, 106]. Measuring the light intensity of sulfite directly, using a UV spectrophotometer has also been investigated in some studies [32, 48]. The implementation of this method in the lab-scale FGD and the possibility of the continuous operation is examined in this chapter.

The measurement principle of the UV/VIS spectrophotometer is based on light absorption by molecules at a specific wavelength. By measuring the absorbed light at a characteristic wavelength, the concentration of the specific molecule can be calculated. The relationship between the light intensity and the concentration of the desired compounds is defined by the Beer-Lambert law, in which the intensity of light passing through a substance depends on the substance's concentration and the light's path length through the substance as shown in the following equation:

$$E_\lambda = log_{10}(I_0/I_1) = \varepsilon_\lambda c d \tag{4.1}$$

E_λ is the absorbance of light at a specific wavelength λ, I_0 is the initial intensity of light, I_1 is the intensity of transmitted light, ε_λ is the absorption coefficient at a specific wavelength, c is the sample's concentration and d the light's path length through the sample. As the absorption coefficient for a specific molecule is constant, the higher the concentration or the longer the light's path, the more light is absorbed. The Beer-Lambert law is only applicable for homogenous solutions with low concentrations of the desired substance.

To measure sulfite concentration in the slurry, a sample has to be extracted continuously and passed through a filter to remove the solid fraction of the slurry. Afterwards, it is fed to the UV/VIS spectrophotometer. This way, the concentration of sulfite can be calculated using the Beer-Lambert law. As the pH of the slurry in the FGD is 5.6, the dissolved S(IV) exists mostly as HSO_3^- and a small fraction of SO_3^{2-} according to figure 2.4. To measure the total S(IV) concentration in the slurry at one specific wavelenght, S(IV) must be present in only one form. Thus, the pH of the slurry has to be shifted to a basic range using a buffer solution. The choice of a suitable buffer solution and the proper mixing ratio has been determined in a previous study [48], which showed the

dependency of the absorbance maximum of different sulfite samples on the pH of the solution. The suitable buffer solution has been found to be one with pH of 10 and the proper mixing ratio was one to one. Under this condition the absorbance maximum was at the same wavelength for all tested sulfite samples. The measurements were carried out using a quartz glass cuvette with a path length of 10 mm.

To measure the sulfite concentration using this method, the absorption coefficient must be found using a standard solution with a known concentration. Therefore, a standard solution with a specific concentration was prepared using sodium sulfite (Na_2SO_3) and water. To prevent the rapid oxidation of sulfite, ethanol was used as a stabilizer. As the Na_2SO_3 salt may be partially oxidized, the sample was titrated at first to determine the exact concentration of S(IV). A dilution series of the standard sample was prepared and mixed with the buffer solution at the ratio of 1:1 and the measurements were carried out. The maximum absorbance wavelength of sulfite was measured at 205 nm. The correlation of the absorbance maximum and the concentration of the titrated sample was used to calculate the unknown concentration of sulfite in the following tests.

In addition to the calibration of the spectrophotometer, the spectrum of the components present in the slurry must be checked individually for possible spectral interference with the sulfite measurement. For this reason, three samples were prepared, each containing one of the following components: sulfite, chloride or mercury with the concentrations of 130 $mg\,l^{-1}$, 10 $g\,l^{-1}$ and 100 $\mu g\,l^{-1}$, respectively. Each sample was measured in combination with the buffer solution at a 1:1 ratio. Figure 4.23 represents the spectra of these samples between 190 to 250 nm. It can be seen that the maximum wavelength for sulfite, chloride and mercury are at 205, 204 and 207 nm, respectively. To enable the measurement of sulfite in the presence of these components, the same slurry matrix without sulfite was used as the baseline measurement for the spectrophotometer. This way, only sulfite ought to be measured.

To measure sulfite continuously in the lab-scale FGD, a constant flow was extracted from the external sump using a peristaltic pump. Figure 3.3 shows the schematic of the set-up. A filter was installed into the extraction hose with a mesh size of 0.5 μm to remove the solid fraction of the slurry. The filtrate was mixed with the buffer solution at the ratio of 1:1 and continuously fed to the flow-through cuvette of the UV/VIS spectrophotometer. The delay time of the sample reaching the spectrophotometer was measured to be 2 minutes. A baseline measurement was conducted each day using filtrated slurry before starting the measurement. This means that the baseline contained the exact composition of all components of the slurry without sulfite.
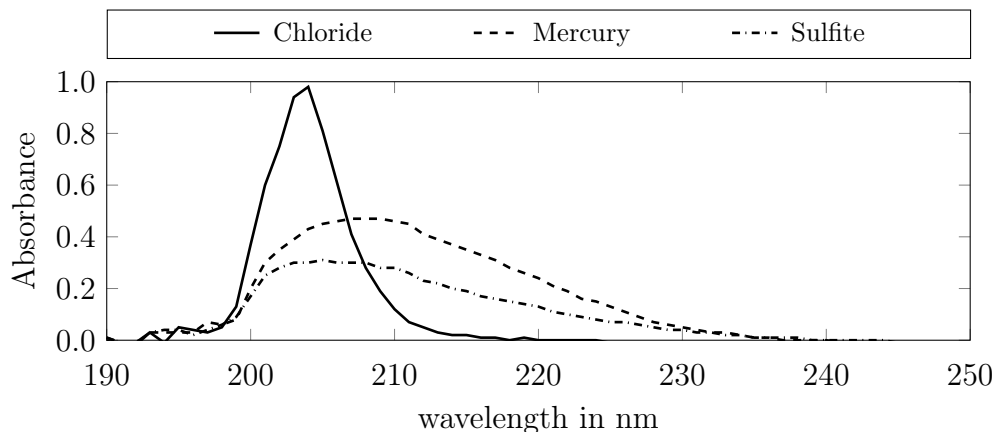
Figure 4.23: Spectrum of standard solutions containing 10 g l^{-1} chloride, 100 µg l^{-1} mercury or 130 mg l^{-1} sulfite.

To compensate the extracted amount of slurry from the external sump, the same amount of a new slurry was dosed back into the sump. This is important to ensure that the solid-liquid-ratio and thus the concentration of the slurry does not change and the volume of the external sump stays constant. However, long time experiments showed some minor changes in the state of the system using this dosing principle.

The synthetic slurry used in this chapter contained 3.5 wt.-% CaSO$_4$·2H$_2$O and 50 µg l^{-1} Hg^{2+} as the baseline and in the case of chloride containing slurry the concentration of 15 g l^{-1} chloride was added to the slurry. The synthetic flue gas had a flow rate of 3.21 l min^{-1} containing 7 vol.-% humidity. The test conditions in this chapter are slightly different than in the rest of the study. Hence, the results cannot be compared directly with each other. However, the concept and principle of the measurement can be discussed independently from the exact conditions.

The procedure of the tests is similar as described in chapter 4.1.8. After reaching the steady state conditions of the system by keeping all the operating parameters constant, the SO$_2$ concentration in the flue gas entering the absorber was changed to trigger a change in S(IV) concentration. The influence of this change on the redox potential, dissolved oxygen and Hg re-emission has already been discussed in detail in chapter 4.1.8. The values cannot be compared directly due to different conditions of the system; however, a similar trend is observed for all the mentioned parameters. The goal is to measure the concentration of S(IV) continuously and explain the behavior of the system accordingly. For this reason, the measurement was carried out first in the absence of chloride, to decrease the number of disturbing factors for the spectrophotometric measurement.
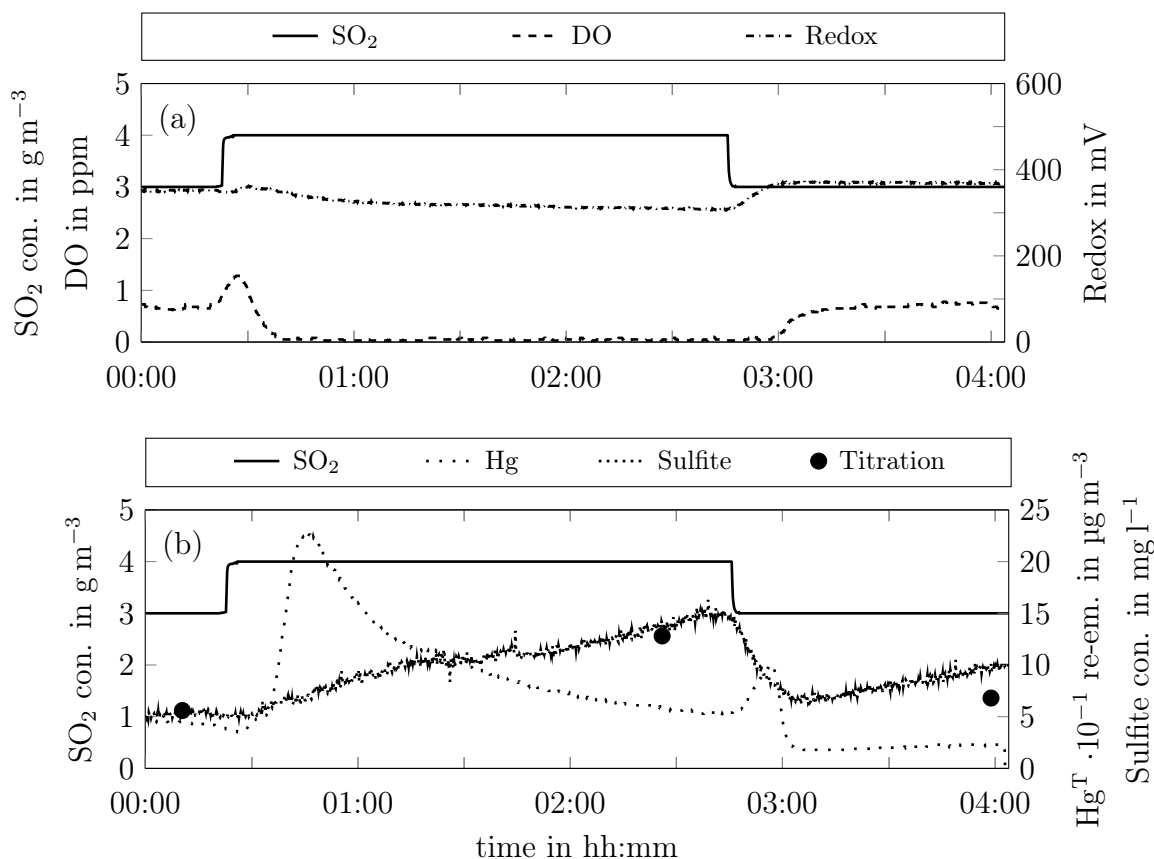
Figure 4.24: Online measurement results of the slurry containing no halides when changing the SO_2 concentration of flue gas (a) operating parameters (b) Hg^T re-emission and sulfite concentration.

Figures 4.24 (a) and (b) represent the dynamic measurement of the relevant parameters and the effect of change in SO_2 concentration for each parameter individually. When the SO_2 concentration of the flue gas was changed from 3 to 4 $g\,m^{-3}$, a decrease in redox potential and dissolved oxygen was measured. Hg re-emission showed a sharp increase to 220 $\mu g\,m^{-3}$ as soon as the dissolved oxygen reached zero. Continuous sulfite measurement revealed the concentration of around 5 $mg\,l^{-1}$ at the steady state condition and the change in SO_2 concentration resulted in a slow increase of sulfite concentration in the slurry.

When Hg re-emission reached its maximum, the concentration of measured dissolved sulfite was not very high. This shows that at first the excess amount of sulfite participated in the reaction of Hg^{2+} reduction according to the reactions 2.22 and 2.23, which resulted in the formation of sulfate and Hg^0. Thus, the excess amount of sulfite was oxidized and no sharp increase in sulfite concentration could be detected. It has

already been observed in chapter 4.1.8, that by keeping constant conditions, Hg re-emission started to decline slowly as the sulfite concentration rose. The measurement of sulfite showed a continuous increase in sulfite concentration, which caused a higher share of Hg^{2+} as $Hg(SO_3)_2^{2-}$ complex. $Hg(SO_3)_2^{2-}$ has a slower decomposition rate to Hg^0 than a $HgSO_3$ complex and therefore, resulted in a decrease of Hg re-emission.

By changing the SO_2 concentration back to $3\,\mathrm{g\,m^{-3}}$, the sulfite concentration decreased. This triggered a short peak of Hg re-emission due to the decomposition of $Hg(SO_3)_2^{2-}$ complexes. However, the system was back to the initial state as soon as there was excess dissolved oxygen in the slurry. It has to be mentioned that the increase in continuous sulfite concentration during the last hour of measurement was due to the signal drifting of the spectrophotometer and did not represent the increase in the concentration. Filtrate samples were taken from the external sump and titrated using iodometric titration before each change in order to re-check the continuous measurement of the spectrophotometer and the results showed the same range of sulfite concentration in all cases. Thus, in the absence of chloride, sulfite can be measured continuously using a spectrophotometer.

In the second step a slurry containing $15\,\mathrm{g\,l^{-1}}$ chloride was tested in order to study the influence of disturbing factors on the spectrophotometric measurement of sulfite. The peak in Hg re-emission of $22\,\mathrm{\mu g\,m^{-3}}$ due to the change in SO_2 concentration in the flue gas and the subsequent change in sulfite concentration can be seen in figure 4.25 (b). However, the sulfite measurement with the spectrophotometer did not show a significant change. In addition, changing the SO_2 concentration back to $3\,\mathrm{g\,m^{-3}}$, did not show any change in sulfite concentration, despite the decrease of Hg re-emission after a while. Iodometric titration of the slurry samples revealed a completely different trend for sulfite concentration, which can be explained considering the results of Hg re-emission as well as the previous measurement with the slurry without halides.

The results obtained from this study reveal the detrimental effect of chloride on the measurement of sulfite using a spectrophotometer. As mentioned before the maximum wavelengths for sulfite, mercury and chloride are close to each other and despite using the same slurry as the baseline to neglect the light absorption of chloride and mercury, the measurement of sulfite in the slurry containing chloride was not successful. The results reveal the sensitivity of the spectrophotometric measurement to the components present in the slurry. Therefore, the implementation of this method in a full-scale FGDs with a more complex matrix of slurry is not feasible.
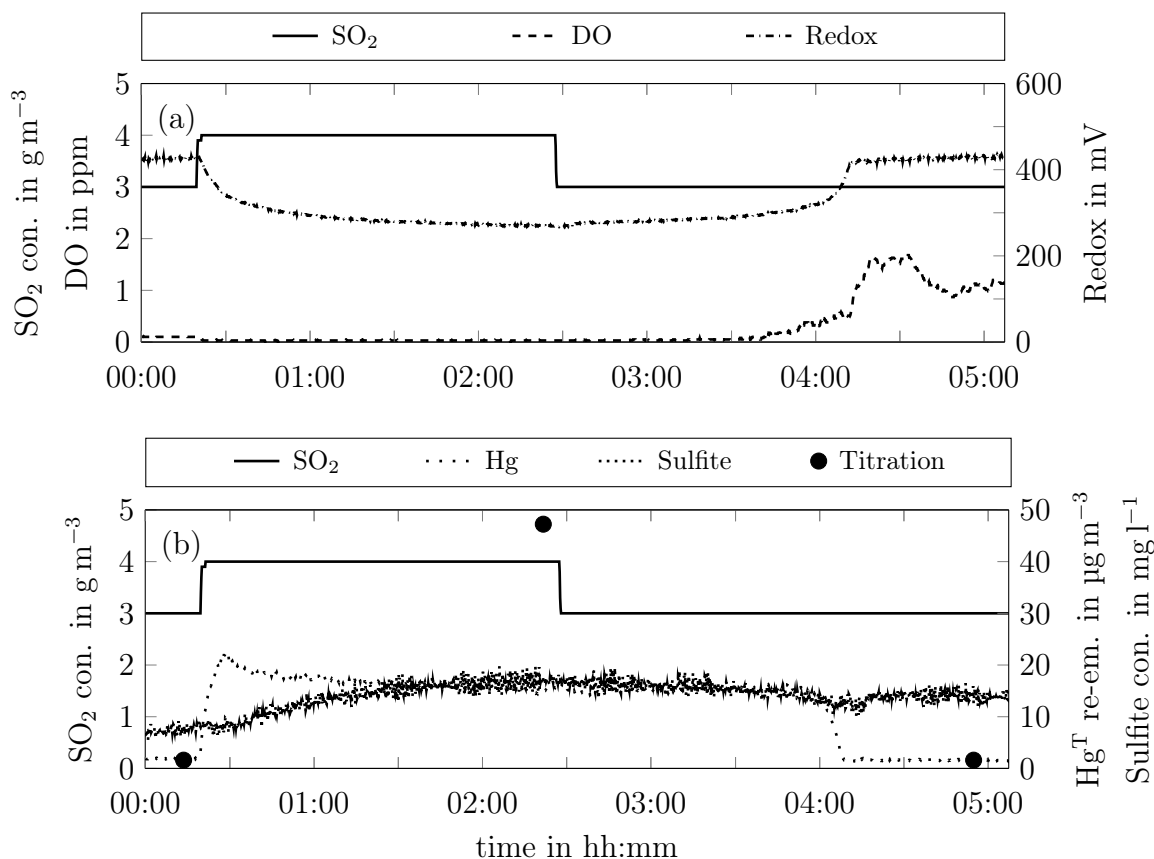
Figure 4.25: Online measurement results of the slurry containing 15 $\mathrm{g\,l^{-1}}$ chloride when changing the SO_2 concentration of flue gas (a) operating parameters (b) Hg^T re-emission and sulfite concentration.

4.2.2 Dissolved SO_2 measurement using a gas sensor

As the sulfite measurement using a spectrophotometer showed high sensitivity to chloride as the main existing halide in the slurry, a different approach needs to be introduced, with no influence from other components of the slurry. Taking the equilibrium reaction of S(IV) in aqueous solutions and pH dependency of this reaction as shown in figure 2.4 into account, acidic environment shifts the equilibrium to the side of dissolved SO_2 gas. Thus, SO_2 can be stripped from the solution and measured subsequently using a gas sensor. The concentration of dissolved S(IV) can be calculated according to the SO_2 gas concentration and is presented as sulfite concentration.

The setup consists of a peristaltic pump, a gas pump, a stripping reactor, a cooler and a SO_2 gas sensor as shown in figure 3.3. Sulfuric acid (H_2SO_4) was used to provide the acidic environment. After removing the solid fractions by filtration, the sample was mixed with H_2SO_4 and pumped in a reactor, in which the dissolved SO_2 is stripped

using air. Afterwards, the SO_2 containing air flow was introduced to a vessel, where the concentration of SO_2 was measured using a membrane SO_2 gas sensor, which was then re-calculated as sulfite concentration in the aqueous solution. The setup was used to measure sulfite concentration in the slurry of the lab-scale FGD. The delay time of the signal was less than one minute; however, lower delay time leads to faster sample extraction and higher required sample volume, which made the sampling time limited. It was shown that re-dosing of a fresh slurry to the sump in order to keep the slurry volume constant leads to some changes in the system. Thus, it was decided to use only the existing slurry. Consequently, the measurement period was limited, and sulfite was measured semi-continuously in different intervals. It must be mentioned that the goal of this study is to prove the measurement concept and the feasibility of the principle to be used in full scale FGDs, in which the problem of limited sample is not an issue. Before starting the measurement, the setup was calibrated using solutions with different concentrations of Na_2SO_3, which were measured in advance using iodometric titration. To check the interference of other slurry components as previously seen in the spectrophotometer tests, chloride and mercury containing solutions with the same concentrations as occurring in the synthetic slurry were tested in the new set-up and the selectivity of the sulfite measurement was proven.

The measurement procedure was identical to the one explained in chapter 4.1.8. The synthetic flue gas was injected into the FGD with a wet flow of 4.3 $l\,min^{-1}$ and the rest of the parameters were adjusted as mentioned in chapter 3.1. The increase in SO_2 concentration was carried out only in one step from 3 to 5 $g\,m^{-3}$ and after a period of time, the reverse change was done. Redox potential, dissolved oxygen and the concentration of Hg re-emission were measured continuously. In addition, sulfite concentration was measured semi-continuously. That is why the measurement data of sulfite concentration are shown in points. However, a continuous curve can be derived from the measurement points. Due to the selectivity of the sulfite measurement in this set-up, additional sulfite measurement using iodometric titration was not carried out during the tests.

The first measurement, shown in figure 4.26, was carried out using a slurry without halides, as the behavior of Hg can be traced back to the influence of solely sulfite. To prove the feasibility of the measurement method in the presence of different halides, the measurement was repeated using different synthetic slurries each containing one of the halides with the concentrations of 10 $g\,l^{-1}$ chloride (figure 4.27), 1 $g\,l^{-1}$ bromide (figure 4.28) and 0.1 $g\,l^{-1}$ iodide (figure 4.29). For each measurement, figure (a) shows

the dynamic measurement of redox potential and dissolved oxygen according to the change in SO_2 concentration and figure (b) reveals the continuous Hg^T re-emission and its correlation with the measured sulfite concentration. As the behavior of the system has already been explained in detail in chapter 4.1.8, the focus of this chapter is on the sulfite measurement.

For all the slurries the redox potential and dissolved oxygen fall several minutes after increasing the SO_2 concentration and increased again after decreasing the SO_2 concentration; however, for dissolved oxygen the rise started with a considerable delay. This behavior can be directly linked to the measured sulfite concentration. In all the cases the redox potential started to rise as soon as the sulfite concentration started to fall and when sulfite concentration reached low values, dissolved oxygen started to increase from zero. It must be noted that due to the extraction of the samples and subsequent reduction of the slurry's volume, the change of SO_2 back to $3\ \mathrm{g\,m^{-3}}$ did not bring the system to a similar steady state condition as at the start of the measurement. However, the goal of this chapter is to prove the sulfite measurement concept.

Checking the sulfite concentration for all slurries shows the amount of less than $10\ \mathrm{mg\,l^{-1}}$ at the steady state having $3\ \mathrm{g\,m^{-3}}$ SO_2 in the flue gas. By changing the SO_2 concentration to $5\ \mathrm{g\,m^{-3}}$, the sulfite concentration started to rise. The increase in sulfite concentration was stopped as soon as the SO_2 concentration was changed back to $3\ \mathrm{g\,m^{-3}}$, and after a short time the accumulated S(IV) in the slurry started to be oxidized and thus, a decrease in sulfite concentration could be observed. The maximum concentration of sulfite depends on the duration of flue gas injection containing $5\ \mathrm{g\,m^{-3}}$ SO_2 and by keeping the system in this condition longer, a larger amount of sulfite is accumulated. For all measurements the system was running with the high SO_2 concentration for 40 to 60 minutes and the maximum sulfite concentration was measured in the range of 115 to 130 $\mathrm{mg\,l^{-1}}$ for all slurries except the iodide containing slurry, which reached 70 $\mathrm{mg\,l^{-1}}$ sulfite after 40 minutes of measurement.

At the beginning of the measurement and at the steady state of the system Hg^T re-emission was 70, 14, 6 and 11 $\mathrm{\mu g\,m^{-3}}$ for slurries containing no halides, chloride, bromide and iodide, respectively. The difference of Hg^T re-emission for various slurries can be explained with the formation of mercury complexes and has already been discussed in detail in chapter 4.1.7. For all slurries the peak in Hg^T re-emission was observed as soon as the concentration of sulfite rose. Depending on the existing halides in the slurry and the formation of halidomercurate complexes, the maximum height of the peak differed.
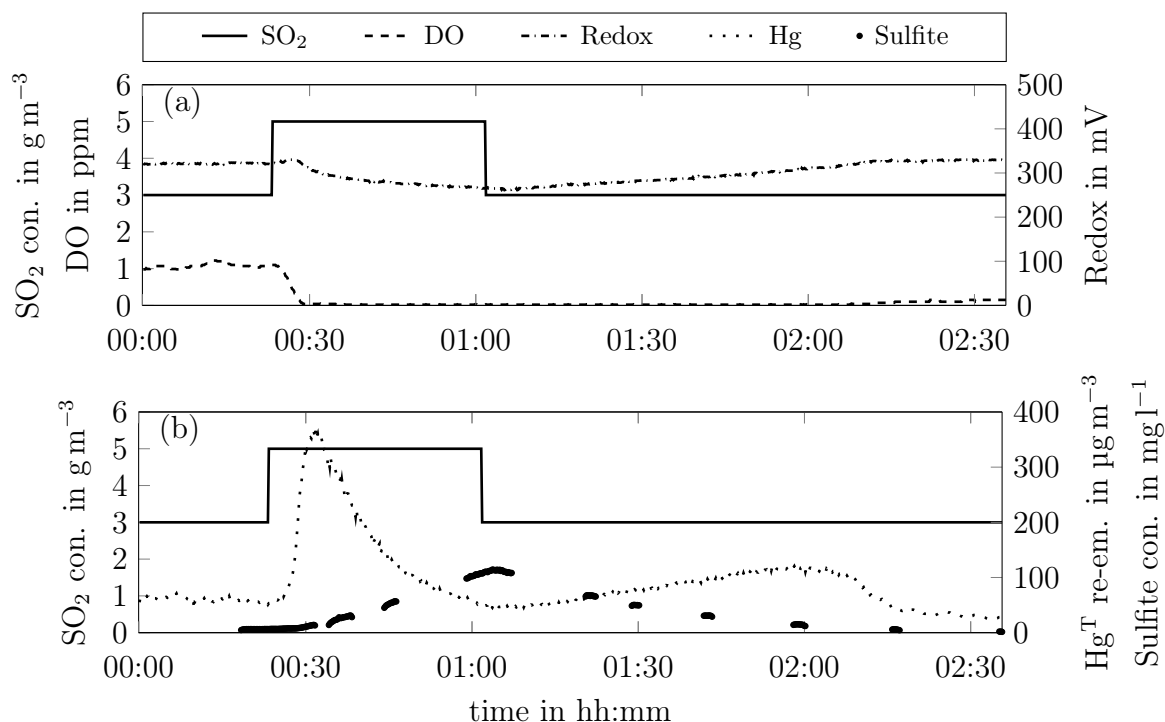
Figure 4.26: Online measurement results of the slurry containing no halides (a) operating parameters (b) Hg^T re-emission and sulfite concentration.

After reaching the peak of Hg^T re-emission and the simultaneous increase of sulfite concentration, Hg^T re-emission started to decrease. The latter was clearly visible for the slurry without halides as sulfite is an important ligand for Hg and thus its increase resulted in the formation of $Hg(SO_3)_2^{2-}$ complexes. It could be seen that the minimum amount of Hg^T re-emission at 5 $g\,m^{-3}$ SO_2 concentration was reached, when sulfite reached its maximum concentration, which reveals the importance of mercury disulfite complex formation in the slurry containing no halides. As halides are suitable ligands for Hg as well, the increase of sulfite concentration did not show a significant effect on Hg complexation after the peak. As shown in figure 4.27, for the chloride containing slurry sulfite played a role in complex formation as the Hg^T re-emission decreased slightly at a higher sulfite concentration. However, this effect could not be observed for slurries containing bromide and iodide.

The slurry without halides revealed a second peak when sulfite concentration was around 13 $mg\,l^{-1}$, which is almost the same range of concentration when the first Hg^T re-emission peak occurred. It can be concluded that at this sulfite concentration for this system, the formation of $HgSO_3$ is favoured and due to its fast decomposition, Hg^{2+} is easily reduced.
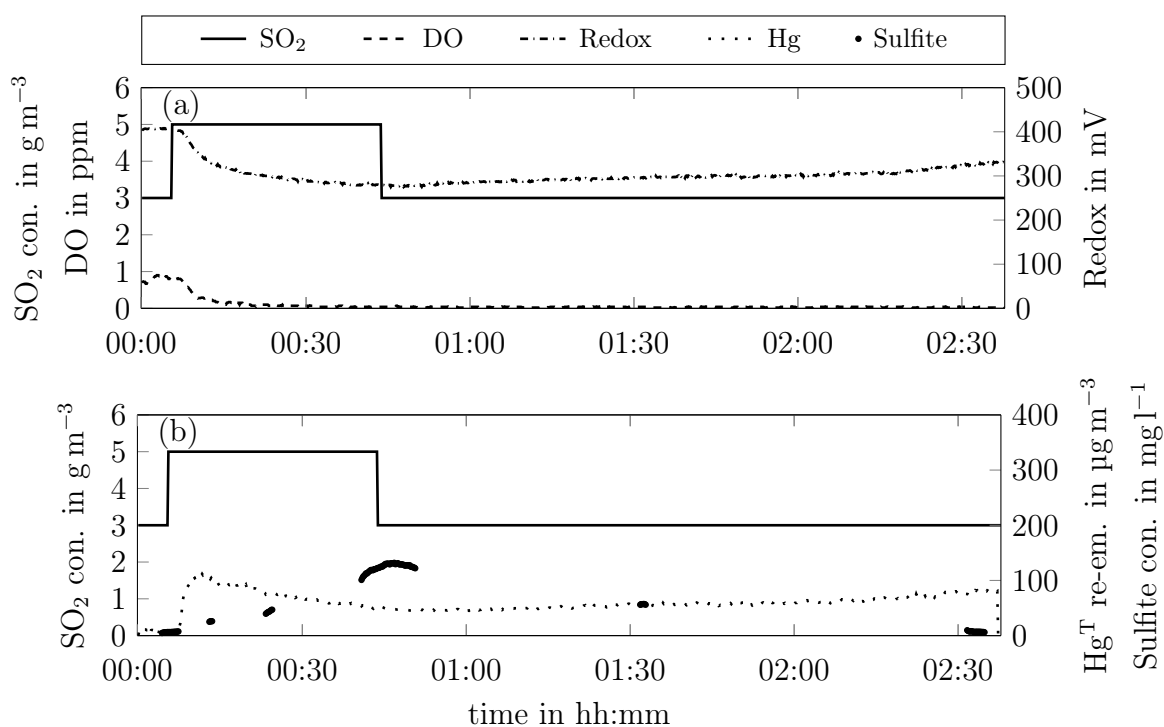
Figure 4.27: Online measurement results of the slurry containing 10 g l^{-1} chloride (a) operating parameters (b) Hg^{T} re-emission and sulfite concentration.
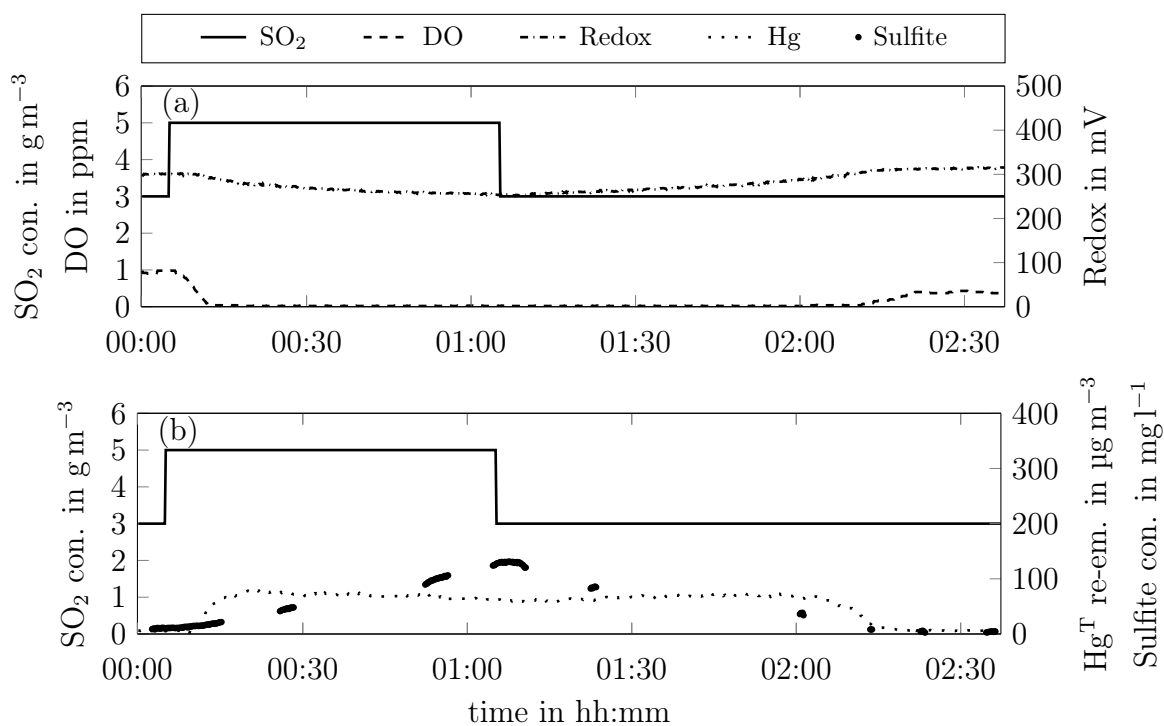

Figure 4.28: Online measurement results of the slurry containing 1 g l^{-1} bromide (a) operating parameters (b) Hg^{T} re-emission and sulfite concentration.
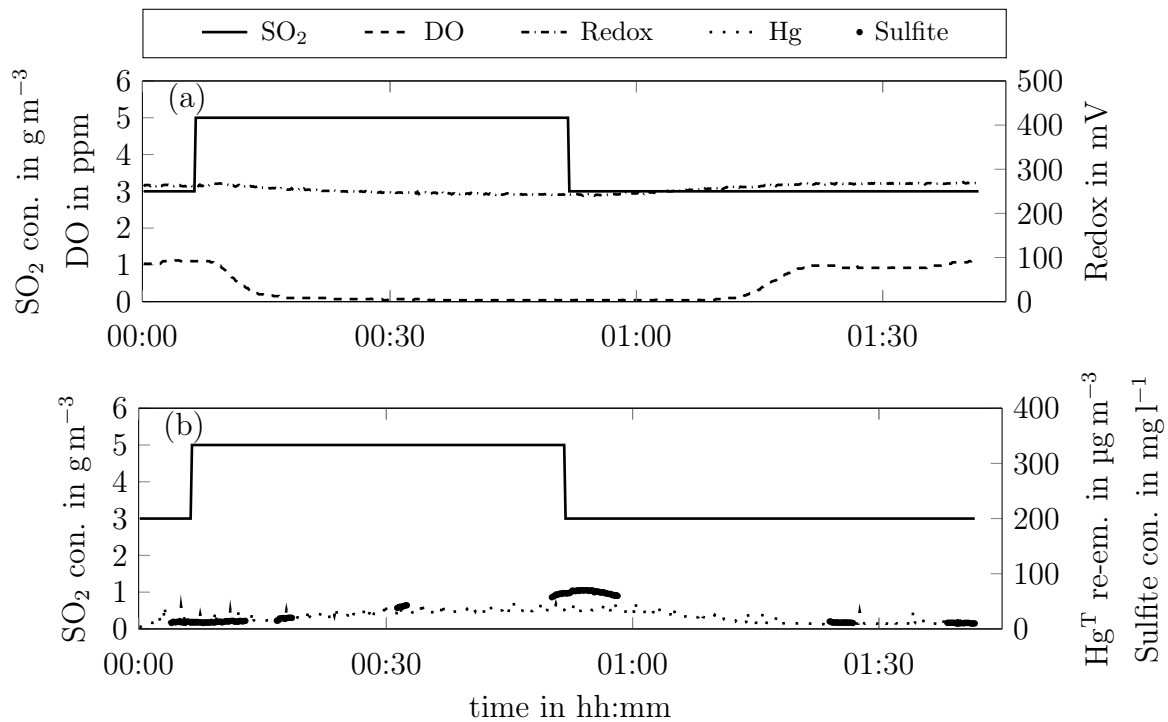
Figure 4.29: Online measurement results of the slurry containing 0.1 g l^{-1} iodide (a) operating parameters (b) Hg$^{\mathrm{T}}$ re-emission and sulfite concentration.

Concluding from all the results, the amount of sulfite in the slurry has to be kept in the range of less than 10 mg l^{-1} to prevent high Hg$^{\mathrm{T}}$ re-emission, regardless of the slurry composition. However, this value is only valid for the studied lab-scale FGD and has to be determined for each full scale FGD according to its operating parameters and slurry composition. The concentration of sulfite in the slurry can be adjusted to a desired value by injecting the required amount of oxidation air to prevent sudden peaks of Hg$^{\mathrm{T}}$ re-emission due to unexpected changes in the FGDs' parameters.

The results of this chapter prove that the used principle is a promising method to measure S(IV) continuously especially in full scale FGDs, in which the amount of required sample is not a problem and the measurement can be done continuously.

4.3   Utilization of additives for preventing Hg re-emission

To reduce the amount of re-emitted Hg from the slurry, it is important to keep Hg^{2+} in a stable form and decrease the possibility of its reduction. Using additives in the

slurry can help to stabilize Hg and prevent the reduction reaction. In this chapter the utilization of two types of additives in different synthetic slurries has been studied to investigate their effect on preventing Hg re-emission and their performance in the presence of different halides.

The first group of studied additives are the sulfur containing precipitating agents, whose results are discussed in chapter 4.3.1. They form poorly water-soluble HgS bonds and thus, precipitate as solid substances. The second group, which is discussed in chapter 4.3.2, are the activated carbon based sorbents, which adsorb Hg^{2+}-compounds according to their physical and chemical characteristics and due to their adsorption equilibria.

Both groups of additives were tested in the presence of different halides and their results are compared with the results of slurries containing the same amount of halides without the addition of additives, which were previously discussed in chapter 4.1.7. The influence of all additives on Hg partitioning in the wet FGD as well as their effect on SO_2 removal efficiency at the steady state of the system are investigated.

Furthermore, in chapter 4.3.3 the role of additives in preventing sudden peaks of Hg re-emission, due to a sudden change in the SO_2 concentration of flue gas is investigated and compared with the results of chapter 4.1.8, when the same slurries in the absence of additives were tested. It has to be mentioned that in each run, the additives were added when the synthetic slurry was prepared, as an injection later on might trigger changes that would not reflect the real behavior of a slurry containing this additive. All the experiments were carried out using a wet flue gas flow of 4.3 $l min^{-1}$.

4.3.1   Precipitating agents

In this chapter 2,4,6-trimercaptotiazine, trisodium salt (TMT) and sodium sulfide (Na_2S) are tested as sulfur containing precipitating agents using different slurries in order to examine their behavior in the presence of different halides and draw conclusions for the involved reactions. Unlike most commercially available precipitating agents, the chemical formulas of TMT and Na_2S are known. Therefore, the dosing concentration can be calculated instead of being based on the manufacturer's recommendation. For both precipitating agents, ten times of the required stoichiometric concentration is added to the slurries. After revealing the influence of these two additives on Hg in the presence of different halides, the results of TMT as a commonly used organic precipitating agent for Hg removal from aqueous solutions are compared with another two

commercially used inorganic cross linked polysulfide precipitating agents Diplexin AM-550 and NETfloc SMF-1 in a chloride containing slurry. These precipitating agents are purchased from Färber & Schmid GmbH and NET GmbH, respectively. As the chemical formula for this precipitating agents are unknown, the dosing values were chosen the same as the one for TMT for easier comparison. Table 4.1 shows the concentration of the investigated additives. It has to be mentioned that TMT is commercially available as a 15 wt.-% aqueous solution (TMT 15) from Evonik Industries AG, however, the concentration in table 4.1 refers to the concentration of pure TMT.

Table 4.1: Concentration of investigated precipitating agents in $\mathrm{mg\,l^{-1}}$.

Precipitating agent	Formula	Concentration
2,4,6-trimercaptotiazine, trisodium salt (TMT)	$Na_3S_3C_3N_3$	2.4
Sodium sulfide	Na_2S	1.2
Diplexin AM-550	$HO_3S\text{-}S_n\text{-}SO_3H$	2.4
NETfloc SMF-1	$[O_3S\text{-}S_n\text{-}SO_3]^{2\text{-}}$	2.4

The sulfur concentration of the used precipitating agents was measured in the laboratory and showed the values of 5.9 %, 16.6 % and 15.8 % for TMT 15, Diplexin and NETfloc, respectively. However, these values does not reveal the concentration of active sulfur, which participate in the reaction with mercury. As shown in the reaction between TMT and Hg (recation 2.26), not all of the present sulfur reacts with mercury. Thus, the concentration of sulfur in each case is not the only factor for predicting the behavior of the precipitating agents and the stoichiometry and kinetic of the reactions as well as the stability of the products are important factors as well.

In the following, the results of TMT and Na_2S addition to the same slurries as in chapter 4.1.7 are shown. Figure 4.30 illustrates the SO_2 removal efficiency of the absorber without using additives in the presence of different halides, and with the addition of the additives to the system. It can be seen that neither of additives affects the SO_2 removal efficiency in a pronounced way. Thus, the same removal of around 60 % is observed in the presence of these additives.

After reaching steady state in each run, concentrations of Hg^T and Hg^0 were measured in the external sump. Figure 4.31 shows the mass flow of total re-emitted Hg from the external sump in all cases. For an easier comparison especially in the case of values lower than $1\,\mathrm{\mu g\,h^{-1}}$, the exact values are presented in table 4.2 as well.

Table 4.2: Hg^T re-emission in $\mu g\,h^{-1}$ of slurries containing different halides and precipitating agents.

precipitating agent	No halides	Cl^-	Br^-	I^-
No additive	6.4	1.1	0.5	1.5
TMT	0.9	0.2	0.0	0.6
Na_2S	7.8	0.2	0.1	0.4
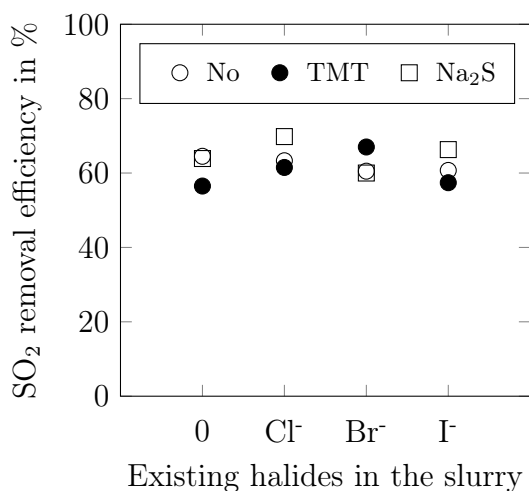
Figure 4.30: Effect of different precipitating agents on SO_2 removal efficiency.
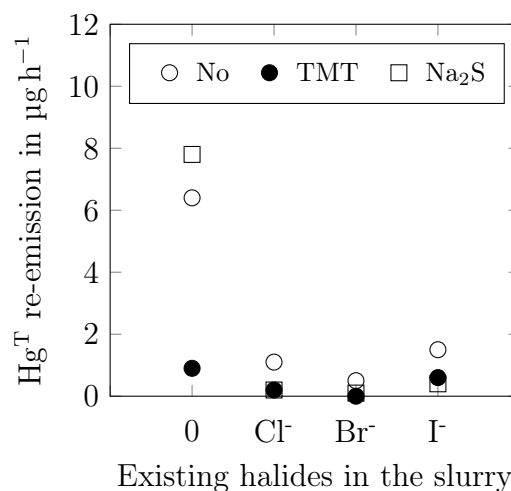
Figure 4.31: Effect of different precipitating agents on Hg^T re-emission.

The influence of halides on Hg re-emission and its speciation measurement has already been discussed in detail in chapter 4.1.7. Thus, at this point the influence of additives is explained. In all cases when TMT was added to the slurry, total Hg loss was less than 1.5 % of the initial Hg inventory of the slurry. The bromide-containing slurry achieved almost zero Hg re-emission. In the presence of iodide, total Hg re-emission decreased by about 60 %. Figure 4.32 shows the distribution of Hg^{2+} and Hg^0 in the case of using TMT and can be compared with figure 4.18, when no additive was used. As depicted in figure 4.32, in contrast to suppressed Hg^0 re-emission, Hg^{2+} re-emission was not inhibited completely. As mentioned before, TMT is a sulfidic precipitating agent. It bonds with Hg^{2+} in the slurry and forms macromolecular organo-metallic compounds, which removes dissolved Hg^{2+} from the aqueous phase and therefore, prevents its reduction to Hg^0 and subsequently its re-emission. However, TMT and halides compete for the Hg^{2+} inventory of the slurry. Due to the large formation constants of Hg^{2+}-complexes
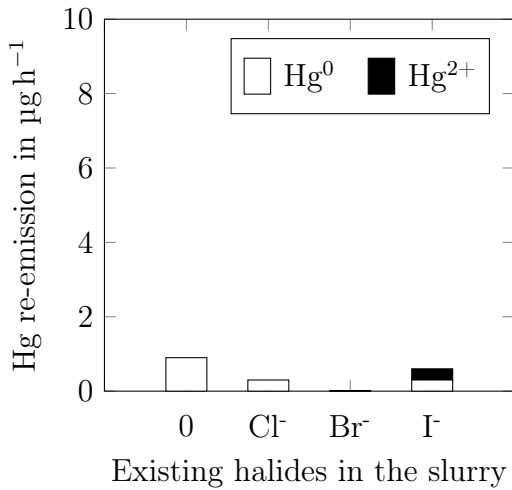
Figure 4.32: Effect of TMT on Hg re-emission at presence of different halides.
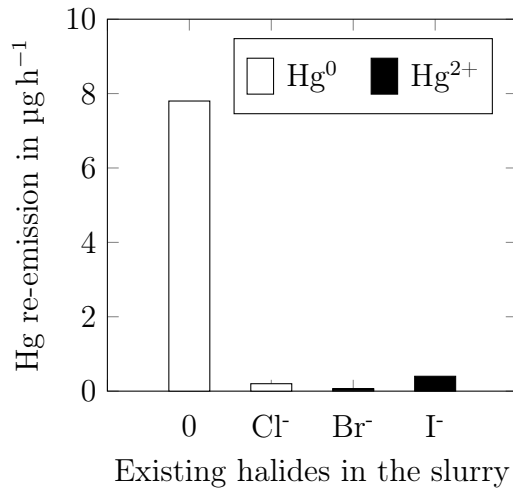
Figure 4.33: Effect of Na_2S on Hg re-emission at presence of different halides.

with iodide ligands, a fraction of Hg^{2+} remains inaccessible for a reaction with TMT. This leads to ongoing low re-emission levels of Hg^0 and HgI_2 in the presence of both TMT and iodide.

The addition of Na_2S to slurries containing halides decreased the Hg loss to less than 0.5 % of the initial Hg inventory of the slurry. Figure 4.33 shows the same effect on Hg re-emission for addition of Na_2S as TMT, except for the slurry containing no halides. It seems that the presence of Na_2S alone and without halides is not enough to prevent the re-emission of Hg. However, in the case of TMT the re-emission was decreased significantly compared to the absence of additives. This could be due to the different stability of the HgS bond formed comparing both TMT and Na_2S [54, 96]. Speciation measurement of Hg re-emission in the presence of Na_2S revealed 100 % Hg^0 re-emission in the absence of halides and only Hg^{2+} re-emission when the slurry contained iodide.

The data shown in figure 4.31 reveals that the addition of Na_2S to the slurry without halides resulted in higher Hg^T re-emission than the slurry containing any additives. The results can be explained by checking the total Hg present in the slurry in each case. To have a better understanding of the behavior of the additives and their effect on the reactions involving Hg, two samples were taken from the slurry at two different times. The first sample was taken from the slurry after mixing all the components and heating them up to 60 °C, without running the FGD and without the influence of flue gas and oxidation air. The second sample was taken after the system reached steady state, which included the influence of meeting the flue gas and specifically the
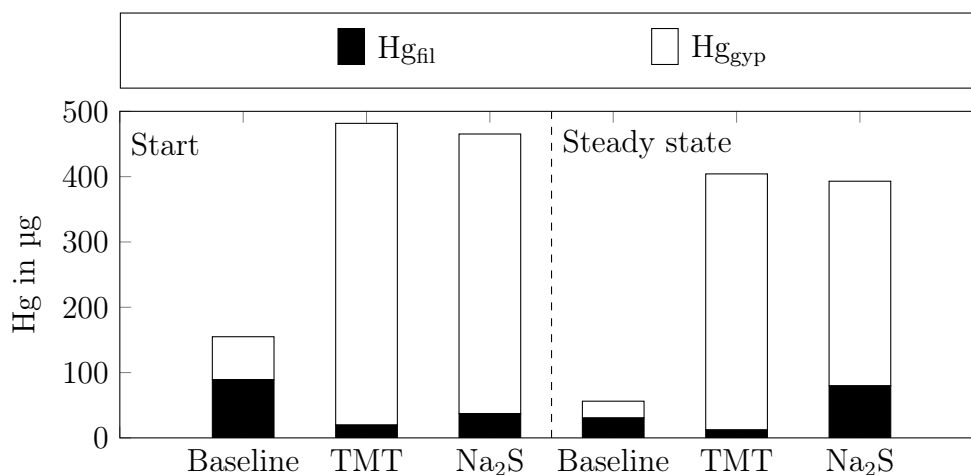
Figure 4.34: Hg partitioning in the slurry containing no halides at start and after steady state at baseline and by addition of TMT and Na$_2$S.

presence of S(IV). Comparing these two samples and the initial Hg inventory of the slurry, which was around 480 µg, reveals if the loss and re-emission of Hg was due to the heating step and therefore, changing the solubility or due to the reduction reaction with sulfite. Figure 4.34 shows the Hg partitioning of both samples between solid and aqueous phase of the slurry. The results belong to the slurry containing no halides and are shown at the absence of additives, by addition of TMT or Na$_2$S. Comparing the results of the first samples with the initial Hg inventory of the slurry, represents the loss of around 67 % of the Hg for the baseline case only due to the heating step. However, both Na$_2$S and TMT were able to effectively prevent evaporation of Hg to the gas phase and due to the HgS bonds formed in these cases, most of the share of Hg ended up in the solid fraction of the slurry.

For the steady state samples, the highest Hg concentration in the aqueous phase belonged to the slurry with Na$_2$S. It can be concluded that HgS bonds formed due to the presence of Na$_2$S were not as stable as the macromolecular organo-metallic compounds formed when TMT was used. Hence, the presence of sulfite in the slurry, changed the equilibrium and resulted in the higher Hg concentration in the aqueous phase. The stability of HgS bonds using different precipitating agents has already been studied in [54, 96], which is in accordance to the results in this study. Comparing the Hg content of the aqueous phase for the slurry without additives and the slurry containing Na$_2$S, the higher mass flow of Hg^T re-emission at the presence of Na$_2$S can be explained. Due to the higher Hg inventory of the aqueous phase, the rate of the reduction reaction was higher and thus, the slurry containing Na$_2$S re-emitted more Hg at the steady state.
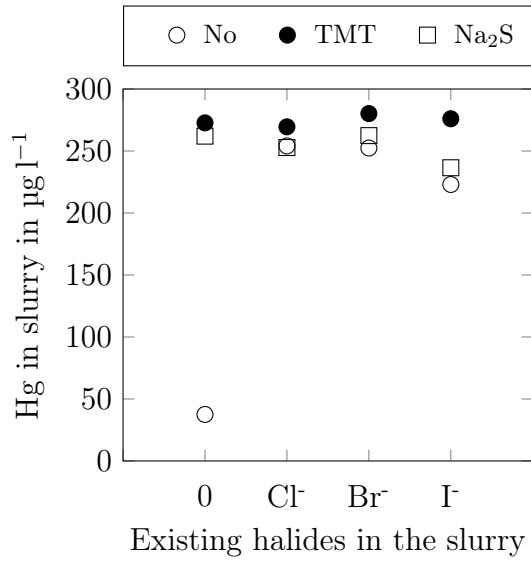
Figure 4.35: Effect of different precipitating agents on concentration of Hg in the slurry.
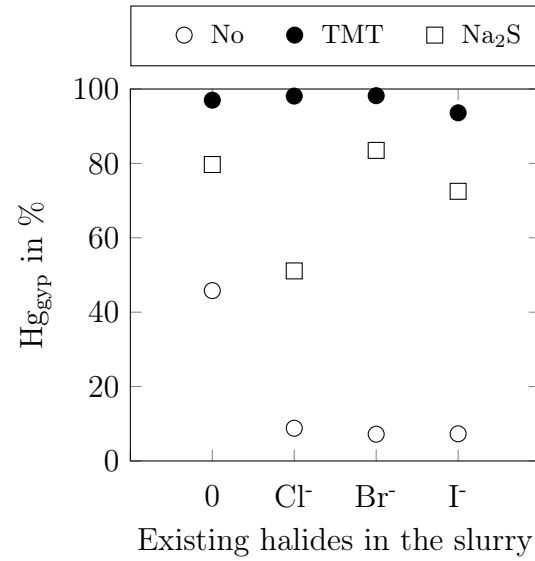
Figure 4.36: Effect of different precipitating agents on share of Hg in gypsum.

It has to be mentioned that the Hg difference between the first and the second sample in each case shows the amount of re-emitted Hg in the start-up phase until the system reached steady state as well as the absorbed amount of Hg in the absorber during the test, which was not significant. The decrease in Hg content of the slurry related to the inventory after heating the slurry was equal to 64 %, 15 % and 16 % for the baseline, Na_2S and TMT, respectively. Thus, the higher Hg^T re-emission at steady state for Na_2S containing slurry does not conclude a negative influence on the amount of Hg^T re-emission during the whole experiment, as in total the re-emission in the absence of additives was the highest.

Figure 4.35 shows the total Hg concentration of the slurry for steady-state operation of the system, considering the measured Hg concentration in gypsum and filtrate. Low Hg content in the slurry indicates high transient Hg re-emission from the slurry in the whole process until reaching steady state and cannot be directly compared to the Hg^T re-emission mass flow at steady state. It can be seen that the addition of TMT to the slurry improved the ability of the slurry to retain its Hg inventory and suppressed the re-emission of Hg to an extent and it did not significantly depend on the specific composition of the slurry. The presence of Na_2S in the slurry improved the Hg retention as well; however, in the presence of iodide the retention effect of TMT is more pronounced compared to Na_2S. In the absence of halides as explained previously, Na_2S
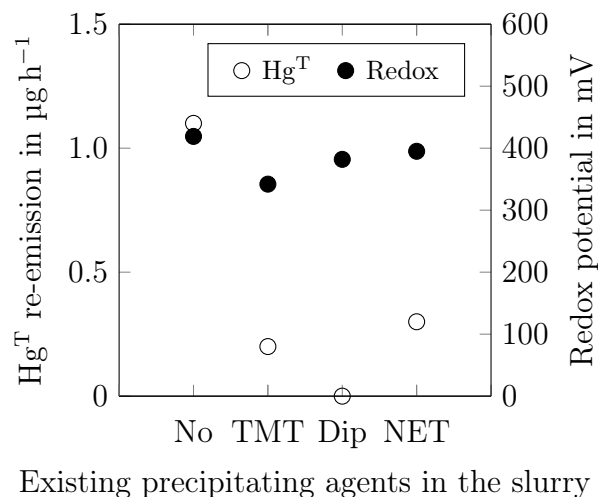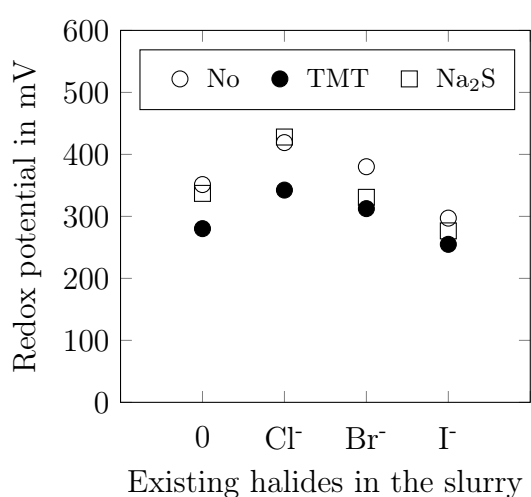
Figure 4.37: Effect of different precipitating agents on redox potential of the slurry.

Figure 4.38: Effect of precipitating agents on Hg^T re-emission and redox potential of the slurry.

could retain high amounts of Hg in the slurry despite high Hg^T re-emission measured at steady state.

The share of Hg in the solid phase of slurries with different halide contents and with the use of additives is shown in figure 4.36. Comparing the results of the additives with the slurry containing no additives reveals the shift of Hg partitioning to the solid fraction. Using TMT resulted in a shift of partitioning to almost 100 % of Hg in the solid fraction for all halide-containing slurries. For the slurries containing Na_2S, Hg in the solid fraction increased as well. However, the extent of increase was less distinct for Na_2S, when compared to the slurry containing TMT. This observation is in line with the corresponding redox potential data of the experiments shown in figure 4.37. For all slurries, there was a correlation between redox potential and the share of Hg in the aqueous phase. Since adding Na_2S caused a less distinct decrease in redox potential, the share of Hg content of the solid fraction in the slurry was also less pronounced. It has to be mentioned that using Na_2S in the chloride containing slurry resulted in almost 50 % Hg share in the solid fraction, which was much lower than in the other cases. However, this can be explained due to the comparably higher redox potential of the slurry which leads to the low share of Hg in its solid fraction.

It has to be stressed that the separation process of the solid and aqueous fraction of the slurry was conducted by filtration through a paper filter. Therefore, the solid residue contained the entire particle content of the slurry, including the very small particle size

fractions. Hence, these results may not be transferred to predict gypsum properties produced by full-scale FGD plants. Full scale FGDs in power plants use hydro cyclones to separate the gypsum from the slurry. The separation process of hydro cyclones is much more dependent on particle size than that of the cake filtration process. Hydro cyclones are designed to remove the coarse particle fraction for gypsum production. The fine particles with the highest surface area, containing most of the adsorbed Hg, are fed back to the FGD or subsequently to the waste water treatment plant. To investigate actual gypsum Hg content using additives, the separation process has to be carried out using hydro cyclones.

At this point, the results of adding TMT in a chloride containing slurry are compared with the other two precipitating agents, Diplexin and NETfloc. For a better comparison of the additives' performance, the results of the chloride containing slurry without additives are plotted as well. Both Diplexin and NETfloc were added to the slurries with a concentration of $2.4 \text{ mg} \, l^{-1}$. As the chemical formulas of these additives are unknown, the same concentration as in the TMT test was chosen for the comparison measurements. As mentioned before, this concentration is related to pure TMT.

Figure 4.38 presents the mass flow of Hg^T re-emission as well as the redox potential of the slurry for the experimented cases at steady state. Comparing the Hg^T re-emission mass flows show the best performance for Diplexin followed by TMT and NETfloc. Using Diplexin with the mentioned concentration in the slurry of the lab-scale FGD, resulted in almost zero re-emission at the steady state condition of the system. It must be noted that these results are only related to the experimented conditions in the lab-scale FGD and do not reveal the suitable dosing value for a full-scale FGD. All additives caused a slight decrease in redox potential of the slurry. The reduction in redox potential for the additives was around 24 mV, 37 mV and 76 mV for NETfloc, Diplexin and TMT, respectively. Slurries with low redox potentials did not automatically show lower Hg re-emissions, which is a sign for the formation of stable Hg complexes, which cannot be reduced easily.

The Hg distribution in the slurry at the start up and steady state in the presence of NETfloc and Diplexin are shown in figure 4.39 and are compared with the addition of TMT and the baseline measurement in the presence of chloride. At the beginning of the measurement and after heating up the slurry, no significant loss of Hg could be observed for Diplexin and NETfloc, however, in the presence of TMT almost the same amount of Hg loss was measured as in the baseline case. For the baseline measurement most of the Hg was present in the filtrate and only a small fraction was found in the
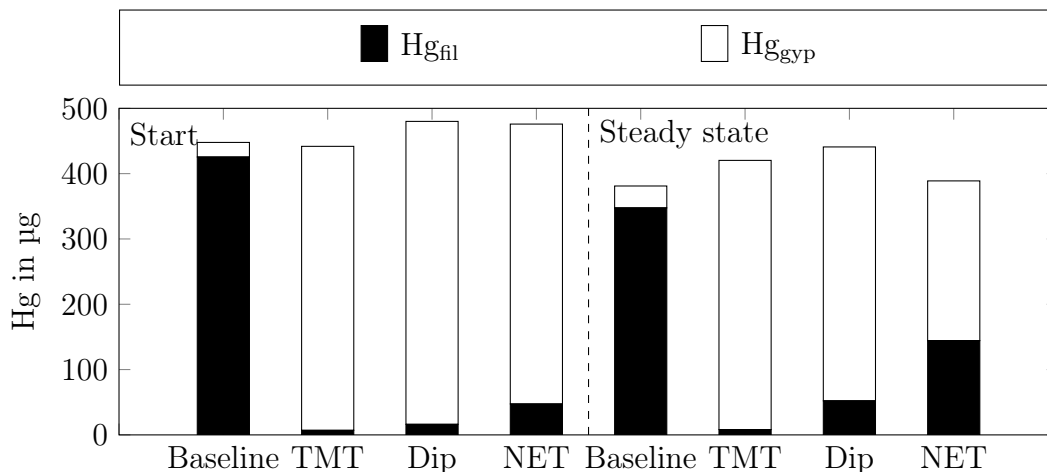
Figure 4.39: Hg partitioning in slurries containing 10 g l^{-1} chloride at the start and after steady state of the baseline and by addition of precipitating agents.

gypsum, however, utilization of any of the tested additives resulted in an excessive shift of Hg from filtrate to gypsum. NETfloc showed the highest share of Hg in the filtrate compared to the other two precipitating agents.

By comparing the results of both samples of start and steady state of the system, it can be seen that after introducing SO$_2$ to the system, the highest Hg loss belonged to NETfloc followed with Diplexin and TMT with 18 %, 8 % and 5 %, respectively. A shift in Hg share to the filtrate was observed for all additives, however, the shift was not as significant in the case of TMT. Between the four results of the start sample, TMT showed the highest Hg loss and despite this highest Hg loss, which occurred during heating for the slurry containing TMT, the presence of SO$_2$ resulted in the lowest Hg loss. The highest share of Hg in the filtrate at steady state was measured using NETfloc with 37 %, followed by Diplexin with 12 % and the lowest for TMT with 2 %. The latter could be the reason for higher Hg re-emission in the presence of NETfloc, as a higher share of Hg is present in the filtrate, which can be reduced and re-emitted. Diplexin showed the best performance due to its lowest Hg loss during the transition time as well as lowest Hg re-emission at steady state.

4.3.2   Activated carbon-based sorbents

Activated carbon acts as a sorbent for Hg and SO$_2$ due to its high porosity and surface area. In this chapter three different activated carbons are tested regarding their effect on SO$_2$ removal efficiency and Hg partitioning in the lab-scale FGD. The chosen

activated carbons are produced using different base materials, which are activated bituminous coal (ABC), activated lignite (AL) and activated coconut shells (ACS). They have different characteristics according to their origin, which is shown in table 4.3. It has to be mentioned that both ACS and ABC were in powdered form and the AL was provided in a slurry form containing 19.4 wt.-% sorbents mixed with water.

Table 4.3: Properties of experimented sorbents.

Sorbents	Material	d_{50} in µm	Surface area in m^2 g^{-1}	Imp.	Con. in mg l^{-1}
ABC	Bituminous coal	25	684.8	2 % Sulfur	200
AL	Lignite	8	291.9	-	200
ACS	Coconut shell	25	1121.5	-	200

As mentioned previously in chapter 2.3.6, depending on the utilized raw material, the pore distribution of activated carbons can vary. However, the activation process also has a significant impact. Thus, the pore distribution of the tested activated carbons were calculated using the data provided from the isotherm BET, t-plot method and BJH adsorption method analyses. Table 4.4 represents the pore distribution of the three samples. It can be seen that the largest share of the surface area of ACS is related to the micropores with a diameter < 2 nm, which is around 1006.7 m^2 g^{-1}. ABC contains 495.3 m^2 g^{-1} microporous surface area and AL 133.7 m^2 g^{-1}. Regarding the surface area of mesopores, ABC contains the largest surface area with 78.8 m^2 g^{-1} and ACS with 37.1 m^2 g^{-1} the lowest. The largest area of macropores belongs to ABC and the lowest to ACS. Thus, it has to be considered that even though ACS has the highest surface area in comparison to the other activated carbons, its meso- and macropore areas are smaller, which can be important depending on the size of the adsorptives.

Table 4.4: Distribution of pore areas of the tested sorbents in m^2 g^{-1}.

Sorbents	Micropores	Mesopores	Macropores
ABC	495.3	78.8	110.7
AL	133.7	65.4	92.7
ACS	1006.7	37.1	77.6

To compare the sorptive behavior of each of the sorbents, simple pre-tests have been carried out, in which the adsorption capacity of the activated carbons in gas and aqueous phase was tested. The gas phase tests were carried out, using the gas preparation part of the experimental system to prepare the required synthetic gas, which was compressed air containing 50 µg m^{-3} Hg. With the help of a SCR catalyst and 10 mg m^{-3} HCl dosing, the share of Hg^{2+} to Hg^0 was adjusted to 50 %. 20 mg of the sorbents were installed in a glass reactor as a fixed bed and a flow of around 4 l min^{-1} was sucked through it using a gas pump. The sorbent reactor as well as the gas preparation zone were heated to 200 °C using heating bands, simulating the condition of a sorbent injection into the gas phase before an ESP. The concentration of Hg leaving the sorbents was measured using a Hg gas analyzer. The measurements were carried out until the breakthrough curve was reached and the inlet and outlet Hg concentration of the sorbent were equal. The amount of adsorbed Hg could be calculated using the breakthrough curves as well as analyzes of the tested sorbents in the laboratory.

In addition, the sorbents were tested in an aqueous phase using only water and 300 µg l^{-1} Hg^{2+}, which was given in the form of a Hg(NO$_3$)$_2$ solution and the concentration of sorbents in the solution was 200 mg l^{-1}. The solution was heated to 60 °C to have the same temperature as the slurry in the FGD. The sorbents were added to the solution which was then heated up and continuously stirred. After one hour, the solution was filtrated using filter papers. The sorbents were dried the same way as the gypsum samples and their Hg content was analyzed in the laboratory.

Figure 4.40 shows the concentration of Hg in the sorbents in both sets of measurements. It has to be mentioned that the absolute value of the Hg concentration in the two measurement sets cannot be compared directly. However, the order of sorbents performance can be. It can be seen that in the gas phase the best sorbent with the highest adsorbed Hg was ACS followed by ABC and AL. However, in the aqueous phase AL had the best performance while ACS adsorbed the least amount of Hg.

The performance of the sorbents can be influenced by different parameters. One is the pore size distribution, which plays an important role depending on the size of the adsorptive. Comparing the sorbents in the gas phase test shows the best performance for ACS. It is important to mention that the gas phase test contained 50 % Hg^0, and the Hg^{2+} in the form of HgCl$_2$. The size of a Hg^0 atom is 0.1 nm [107] and HgCl$_2$ has the size of around 1 nm [13, 107], which categorize them in the range of micro-pores. Therefore, ACS with the highest surface area of micropores showed the best adsorption capacity in the gas phase. However, in the aqueous phase measurement bigger molecules may
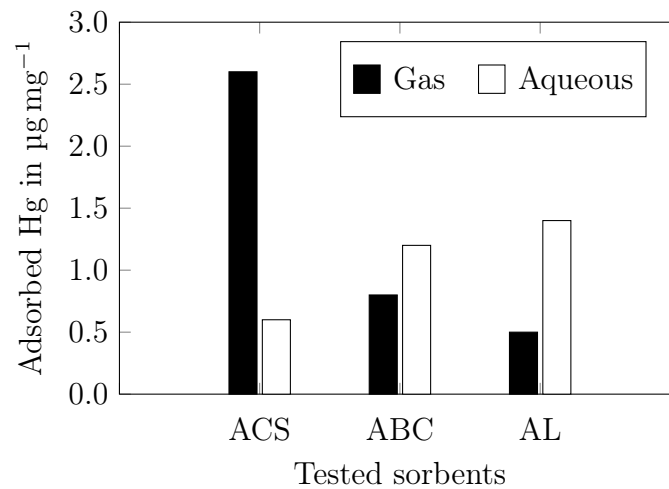
Figure 4.40: The sorbents' adsorption performance in the gas and aqueous phase.

exist, which do not fit in the micropores and thus, a decrease in the performance of ACS could be observed. It can be concluded that the Hg adsorption in the gas phase was directly related to the area of micropores in the sorbents, whereas, in the aqueous phase the sorbents with higher meso- and macropores area showed better performance. The adsorbed amount of Hg on ABC and AL did not differ significantly and were 1.2 and 1.4 $\mu g\,mg^{-1}$, respectively, as they have similar surface areas regarding their meso- and marcopores. In addition, other factors such as hydrophobicity of the sorbent and their surface energy may play an important role in the adsorption process in aqueous phases, which are not discussed in this work.

The influence of all three activated carbons on SO_2 and Hg behavior in the FGD was investigated first in the slurry without halides. Afterwards the effect of halides on the reactions and effectiveness of the sorbents were studied using the synthetic slurries containing chloride, bromide or iodide with the same concentrations as described in the previous chapters. In the case of ACS only the chloride containing slurry was tested. The results are compared with the results of chapter 4.1.7, when no sorbent was present in the slurry.

Figure 4.41 represents the SO_2 removal efficiency of the FGD of all cases. In general, the presence of the sorbents increased the removal efficiency of SO_2 from the flue gas. The increase varied between 10 % to more than 30 % and the best performance was observed for the AL in all of the cases, despite its lowest active surface area. For all investigated halide concentrations and in the presence of AL, the FGD showed a SO_2 removal of around 90 %. Generally, the presence of halides for the investigated
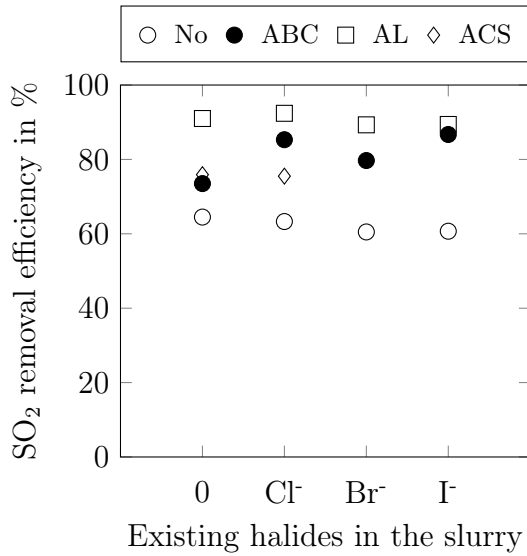
Figure 4.41: Effect of different sorbents on SO$_2$ removal efficiency.
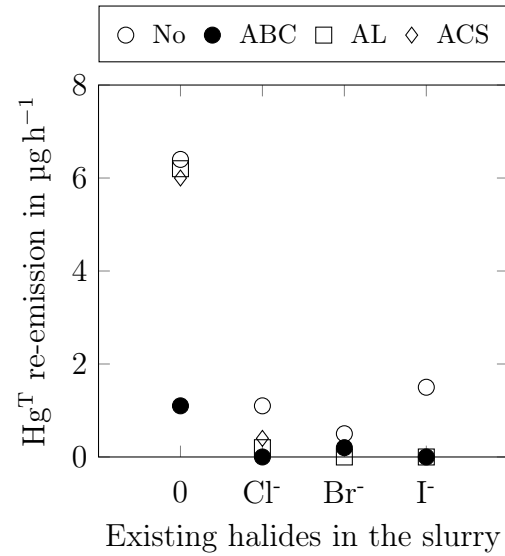
Figure 4.42: Effect of different sorbents on Hg^T re-emission.

concentrations showed no significant impact on SO$_2$ removal efficiency. Only in the case of ABC in the slurry containing no halides, the increase in SO$_2$ removal efficiency was lower than slurries containing halides. ACS showed the same increase in SO$_2$ removal efficiency as ABC in the absence of halides and for the chloride containing slurry the lowest impact belonged to ACS. It has to be emphasized, that the significant increase in SO$_2$ removal efficiency may not be transferred to full-scale plants without caution. In contrast to full-scale FGDs, the baseline operating conditions of the lab-scale test-rig are not optimized for SO$_2$ removal efficiency. In a full-scale FGD, the increase may be less pronounced as the efficiency of the plant is already over 90 %.

Table 4.5: Hg^T re-emission in µg h^{-1} from slurries containing different halides and sorbents.

Sorbent	No halides	Cl$^-$	Br$^-$	I$^-$
No additive	6.4	1.1	0.5	1.5
ABC	1.1	0.0	0.2	0.0
AL	6.2	0.2	0.0	0.0
ACS	6.0	0.4	-	-

The mass flow of Hg^T re-emission for all of the experimented cases is shown in figure 4.42. The measurement was done after the system reached steady state and for a bet-

ter comparison, the exact values are shown in table 4.5. The lowest Hg^T re-emission belonged to the slurries containing ABC regardless of the existing halides. AL performance was almost the same as ABC, except for the case in which the slurry did not contain any halides. The addition of ACS did not show any significant impact on Hg^T re-emission in the absence of halides as well. Despite having the highest surface area, ACS showed the poorest performance of all sorbents in the chloride containing slurry. However, as it was seen in the pre-test measurements, ACS revealed the worst adsorption performance in the aqueous solution due to its lowest meso- and macropores surface area. In order to explain the results and have a comprehensive understanding on the impact of each of the sorbents, slurry samples were taken at the start-up and steady state of the FGD and their Hg partitioning between aqueous and solid phase for all the cases are compared in figures 4.43 (a)-(d).

The results of the slurries without halides in figure 4.43 (a) show the positive effect of additives on keeping the Hg in the slurry and preventing its re-emission. Comparing the start up samples, which show Hg partitioning in the slurry after heating it up to 60 °C, with the initial Hg inventory of the slurry (480 µg), reveals a high Hg loss of around 67 % when no additives were present. Due to the adsorption of Hg on the sorbents, the loss of Hg during the heating of the slurry decreased significantly. The lowest Hg loss in this case belonged to ABC with 11 % of the initial Hg inventory, followed by AL with 13 % and ACS with 30 %. The Hg content in the solid fraction was the highest for ABC with around 85 % of the total Hg in the slurry. Due to the sulfur content of the ABC, the adsorption of Hg on its active surface was followed by the formation of HgS bonds, which made the adsorption more stable.

After starting the FGD, flue gas was introduced and the slurry started to absorb SO_2. It took some time until the system reached steady state and the second sample was taken. The difference between the results of the first and second sample shows the Hg loss during this transition phase as a result of either the presence of sulfite or the stripping of bivalent Hg compounds and a small amount of absorbed Hg in the absorber. It can be seen that for all cases the amount of Hg in the slurry and aqueous phase decreased due to the re-emission of Hg. As there were no halides in the slurry, the adsorption of Hg on AL and ACS was a physical adsorption. The loss of Hg from the aqueous phase caused a shift in the equilibrium and the desorption of Hg from the solid fraction in the case of AL and ACS. It can be seen that the aqueous Hg concentration after steady state was almost the same as in the first sample, however, the Hg content of the solid fraction decreased. This was not the case for ABC, as the HgS bond formation made it

difficult for Hg to be desorbed back to the aqueous phase, which resulted in a lower Hg concentration in the aqueous phase at steady state. The Hg loss of the slurries during the transition state, which can be seen comparing the Hg content of start and steady state samples, was the highest for ACS with 64 %, even higher than for the baseline as it had more inventory after heating up. ABC lost the least amount of Hg with around 17 %. In total after reaching the steady state, the baseline slurry lost 88 % of its initial Hg inventory (480 µg) followed by ACS with 75 %, AL with 40 % and ABC with 26 %. Hg^T re-emission of AL and ACS shown in figure 4.42 were as high as the slurry without any sorbents. The reason for this can be found when comparing the Hg concentration of the aqueous phase of the AL, ACS and baseline tests. The Hg, which was adsorbed on the sorbents, was measured in the solid fraction, therefore, Hg content of the aqueous fraction was able to be reduced and re-emitted to the gas phase. High aqueous concentration of Hg at steady state for AL and ACS resulted in a high Hg re-emission. If Hg^T re-emission at steady state is calculated related to the inventory of the slurry at steady state, the absence of additives resulted in 75 % re-emission. However, presence of ACS decreased this value to 33 % and in the case of the addition of AL to almost 14 %, which shows the positive influence of additives on Hg retention in the slurry.

It can be concluded that even though ACS had the highest BET among the sorbents, its performance regarding Hg adsorption was the worst, which can be due to its lowest surface area of meso- and macropores. ABC showed the best performance due to its sulfur content which resulted in chemisorption of Hg on its active sites. Ultimately, the BET seems to have no significant influence on the adsorption process of Hg while other factors such as the pore distribution of the sorbents and their chemical impregnation play a more important role.

The presence of halides in the slurry changed the partitioning of Hg and its retention in the slurry depending on the existing halides. The results of the first sample in the absence of sorbents showed the positive effect of halides on Hg retention due to the complex formation. It can be seen that the Hg concentration in the aqueous phase increased significantly for all the halides and the Hg loss due to the heating was mostly related to the bivalent Hg as no sulfite had been introduced to the system yet. Thus, the highest Hg content in the slurry of first sample belonged to the chloride containing slurry followed by bromide and iodide containing slurries with the values of 448 µg, 397 µg and 360 µg, respectively. This is in accordance with Henry's law and the respective vapor pressure of the bivalent Hg compounds and it has been already discussed previously.
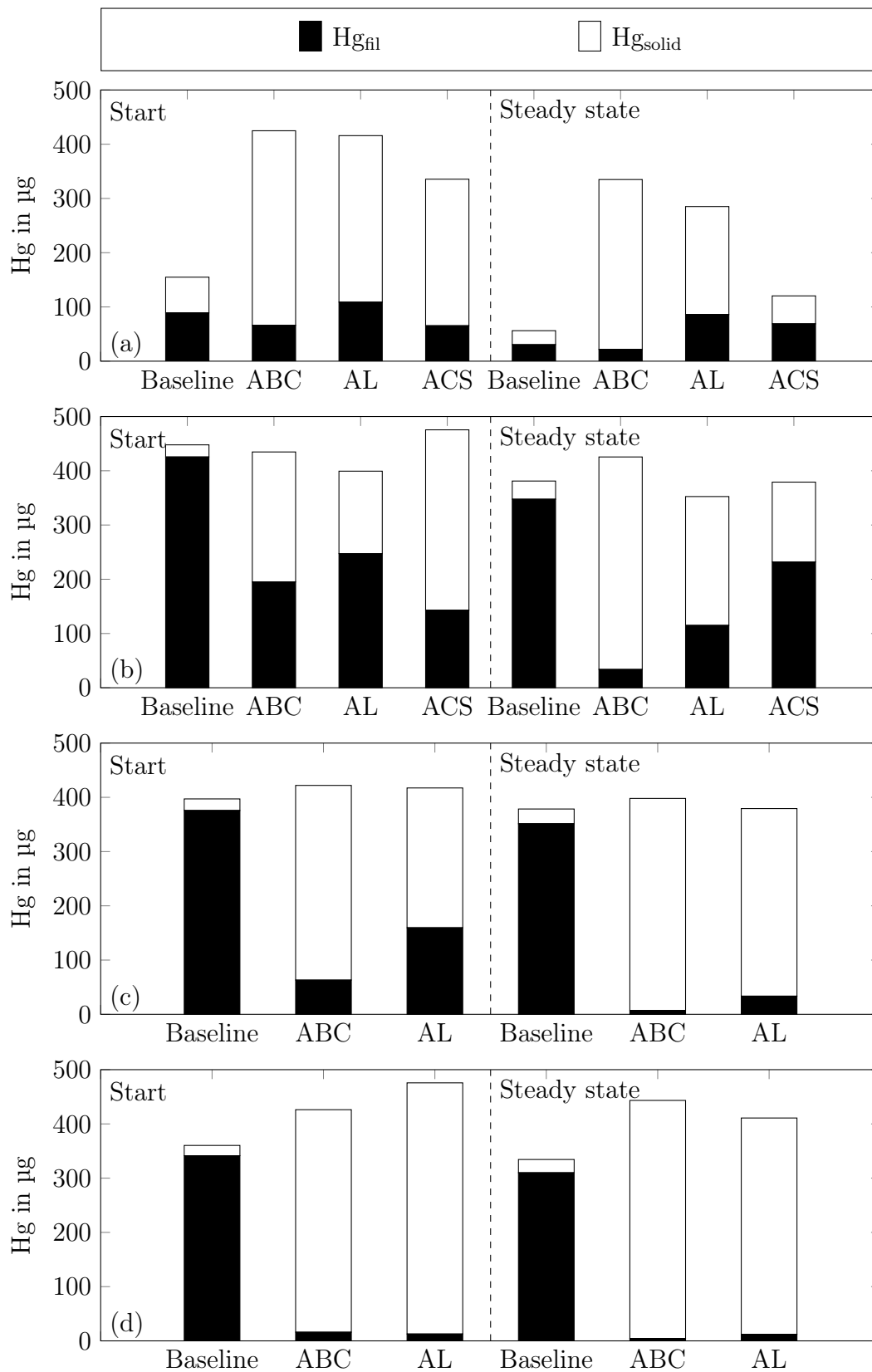
Figure 4.43: Hg partitioning at the start and at steady state of the baseline and by addition of different sorbents in slurries containing (a) no halides (b) $10 \mathrm{~g\,l^{-1}}$ chloride (c) $1 \mathrm{~g\,l^{-1}}$ bromide (d) $0.1 \mathrm{~g\,l^{-1}}$ iodide.

The total amount of Hg in first sample in the presence of AL and ABC was almost the same regardless of the type of halides or even without any halide. However, the partitioning of Hg between the solid and aqueous phase was different in each case. For both sorbents, the highest share of Hg in the solid fraction between the halide containing slurries was in the iodide containing slurry followed by bromide and the lowest for chloride. Presence of halides on the one hand resulted in the formation of Hg complexes in the aqueous phase and on the other hand increased the adsorption of Hg compounds on the active surface of sorbents. Depending on the type of halide and the existing concentrations one of the mentioned factors showed a stronger influence. It can be concluded from the results that the presence of iodide significantly leads to the adsorption of Hg compounds on the solid fractions, while chloride results in a higher Hg concentration in the aqueous phase.

The second sample taken at steady state revealed a Hg loss due to the reduction of Hg with sulfite and for the slurries containing AL and ABC an increase in Hg share in the solid fraction. It can be concluded that in the presence of halides, sulfite can increase the share of Hg in the solid fraction. The increase in Hg adsorption can be observed for both the gypsum and sorbents, with the sorbents having a higher share. The share of Hg in the solid fraction for slurries containing no additives also increased slightly after introducing sulfite to the system. As discussed previously in chapter 4.1.8, increasing the S(IV) concentration in the slurry leads to the formation of HgS according to reactions 2.24 and 2.25 and consequently, increases the concentration of Hg in the solid fraction. It could be seen that in the absence of halides, this effect was not as significant due to the high Hg loss of the slurry. The loss of Hg during the transition phase for halides containing slurries was much lower compared to the slurries without halides. The presence of halides leads to either complexation of Hg in the aqueous phase or higher adsorption of it on the active surface of sorbents, which both result in lower Hg reduction. Due to the same reason, the Hg re-emission at the steady state was quite small as shown in figure 4.42.

ABC and AL containing slurries in the presence of halides resulted in very low Hg^T re-emission at steady state as shown in figure 4.42. The measurement of the ACS containing slurry was only carried out in the presence of chloride. The results reveal higher Hg retention for the first sample due to the complex formation. In contrast to the results gained from other cases, the presence of S(IV) resulted in a lower Hg share in the solid fraction when ACS was added to the slurry. This can be attributed to the low surface area regarding meso- and macropores and the bigger size of Hg complexes
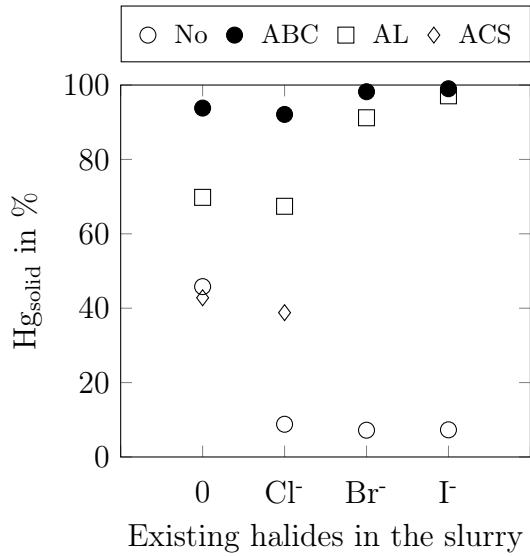
Figure 4.44: Effect of different sorbents on Hg content of the solid fraction.
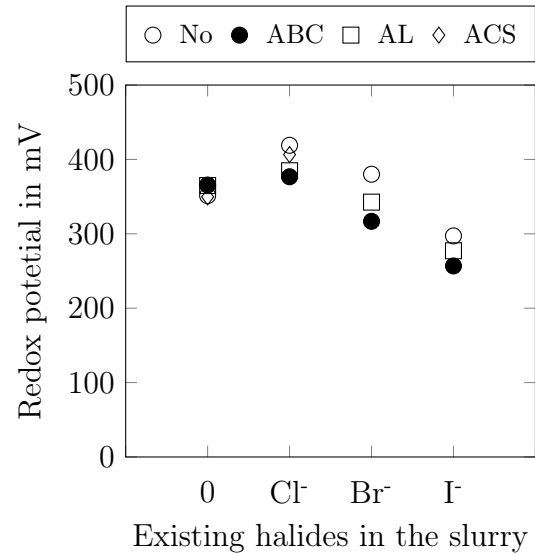
Figure 4.45: Effect of different sorbents on redox potential of the slurry.

associated with S(IV). In nearly all cases the highest total Hg loss belonged to the baseline and the lowest to the slurries containing ABC.

Figure 4.44 shows the summary of the Hg share in the solid fraction for all the experimented cases. It can be seen that ABC resulted in the highest share of Hg in the solid fraction and the lowest share belonged to the slurries containing ACS. Apart from the previously mentioned characteristics such as sulfur content and pore distribution, the redox potential of the slurries can also lead to the same conclusions. Figure 4.45 shows the redox potential of all the slurries at steady state conditions. In the presence of halides, the slurries containing ABC had the lowest redox potential, which shifted the sorption equilibria of Hg-compounds towards the adsorbed species. Stable adsorbed Hg^{2+}-species are hardly available for redox reactions, hence, the more reducing environment in the presence of the additives investigated in this study does not promote the reduction of Hg^{2+} to Hg^0. It is important to stress that redox potential may only be used as an indicator for Hg^{2+} reduction for comparable slurry compositions. This is especially relevant for processes involving adsorption equilibria.

It has to be mentioned that the separation process of solid and aqueous fractions of gypsum was carried out using filter papers, which leads to different results than using hydro cyclones as applied in full scale FGDs. Activated carbons have a lower density than gypsum. Therefore, they are mainly separated with the aqueous fraction including the fine particles in the hydro cyclone. In contrast, particle density is of negligible

importance for the cake filtration conducted in this study. Hence, the derived results provide an insight into sorption equilibria, but may not be used for the prediction of gypsum quality parameters.

4.3.3 Effect of additives on Hg re-emission by dynamic change of SO_2 concentration

This chapter focuses on the effect of additive utilization in the slurry of the FGD on Hg re-emission, when a sudden change in SO_2 concentration in the raw gas entering the absorber occurs. As previously discussed in chapter 4.1.8, the sudden change in SO_2 concentration influences the sulfite concentration in the slurry and subsequently the amount of re-emitted Hg depending on the properties of the slurry. This change in sulfite concentration has been measured in chapter 4.2 and the role of sulfite on the reactions involving Hg has already been discussed. In this chapter the same procedure is followed using different additives in slurries containing the same halide concentrations as in the previous chapters to check the potential of the used additives on preventing Hg re-emission peaks.

It could be observed that using additives in the slurry mostly resulted in lower Hg re-emission peaks and regarding different halides the trend of measured Hg re-emission was almost the same as when no additives were added. Therefore, only one set of data is shown in the following. The dynamic change in SO_2 and its influence on Hg re-emission by utilization of activated lignite in the slurry is shown in figures 4.46 (a)-(d), which are related to a slurry without halides and slurries containing 10 $g\,l^{-1}$ chloride, 1 $g\,l^{-1}$ bromide or 0.1 $g\,l^{-1}$ iodide. The dynamic measurement of redox potential and dissolved oxygen is also plotted in each diagram.

By comparing the results with the results of chapter 4.1.8, it can be seen that in the slurry containing no halides, the same trend can be observed. The increase in SO_2 resulted in a peak in Hg^T re-emission and the counter change to 3 $g\,m^{-3}$ triggered the system to have a second smaller peak in Hg^T re-emission. The ambivalent role of sulfite could be also observed in the slurry using AL. The Hg^T re-emission at the steady state at the beginning of the measurement was the same as in the system without AL; however, using AL diminished the maximum Hg^T re-emission peaks. The results reveals a Hg^T re-emission peak already at SO_2 concentration of 4 $g\,m^{-3}$, due to a faster decrease of dissolved oxygen. However, the significant change in redox potential started after changing the SO_2 concentration to 5 $g\,m^{-3}$. It has to be considered that as mentioned

previously in chapter 4.3.2, AL adsorbes SO_2 as well, which increases the SO_2 removal efficiency. Thus, it influences the amount of dissolved sulfite in the system as well, which makes the direct comparison of Hg^T re-emission behavior challenging. It has to be noted that the absolute amount of re-emitted Hg depends strongly on the duration of the change and cannot be compared directly between different measurements.

Adding AL in the slurries containing halides resulted in significantly lower Hg^T re-emission peak. In the cases of chloride and bromide containing slurries, despite low redox potential and no dissolved oxygen in the system, the Hg^T re-emission peaks were as low as 17 and 7 $\mu g\,m^{-3}$, respectively. In the slurry containing iodide, no change in redox potential was measured and the amount of dissolved oxygen never went down to zero as it started with a higher value. In this case no Hg^T re-emission peak was measured. The results can be explained by comparing the Hg partitioning between aqueous and solid fraction of the slurry after steady state as shown in chapter 4.3.2, in which the role of halides in increasing the Hg adsorption and its stability is described.

For an easy comparison of the influence of different additives in four slurries containing different halide concentrations, the value of Hg^T re-emission peaks are shown in figure 4.47 and the exact values are listed in table 4.6. For the case of ABC and ACS the tests with halides were only carried out for the chloride containing slurries. The highest Hg^T re-emission peak after a sudden change in SO_2 concentration was recorded for the slurry containing Na_2S with 445 $\mu g\,m^{-3}$. This is an even higher value than measured in the slurry without any additives at all, 248 $\mu g\,m^{-3}$. The reason for this behavior can be found when looking at the Hg content of the slurry at steady state before the change of the SO_2 concentration, as shown in figure 4.34. Due to the high Hg loss from the slurry without additives, the Hg content of the slurry at steady state was quite low at around 56 μg, with 30 μg in the aqueous phase. However, adding Na_2S to the slurry prevented the Hg loss due to heating as well as SO_2 addition significantly. The slurry contained 393 μg Hg at steady state, with 80 μg Hg in the aqueous phase. After the sudden change in SO_2 concentration, the slurry containing a higher Hg content in the aqueous phase resulted in a higher Hg re-emission peak as there were also no halides present to prevent Hg^{2+} reduction. It can be also concluded that in the presence of Na_2S as an additive, the formed HgS was quite unstable and could be easily solved back to the aqueous solution in unfavorable conditions.

Among the activated carbon based sorbents, AL showed the highest Hg^T re-emission peak in the slurry without halides. The results in figure 4.43 (a) in the absence of halides, shows that ABC had the highest Hg content in the slurry. However, 94 % of it
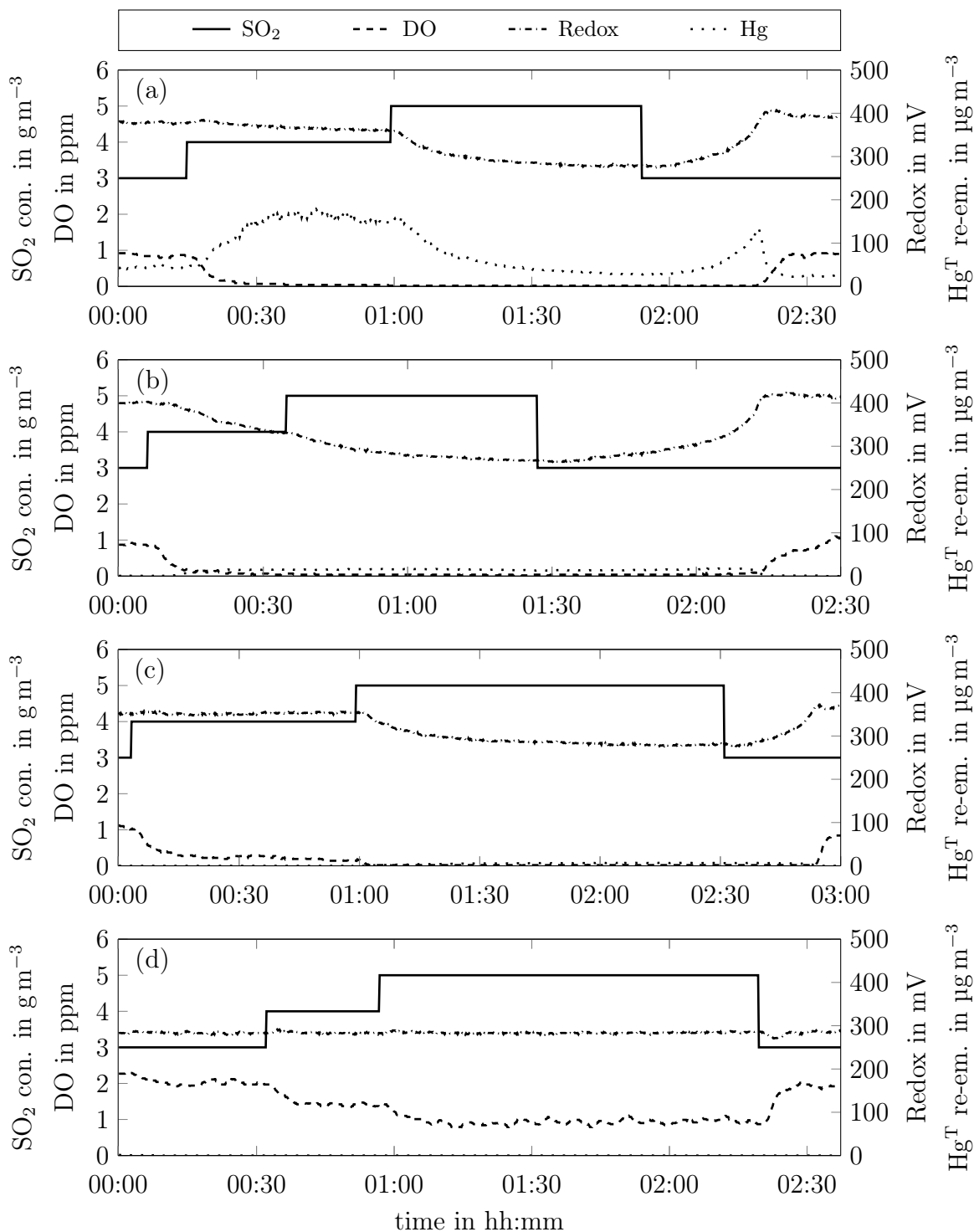
Figure 4.46: Effect of AL on operating parameters and Hg^T re-emission when changing the SO_2 concentration of flue gas of slurries containing (a) no halides (b) 10 $g\,l^{-1}$ chloride (c) 1 $g\,l^{-1}$ bromide and (d) 0.1 $g\,l^{-1}$ iodide.
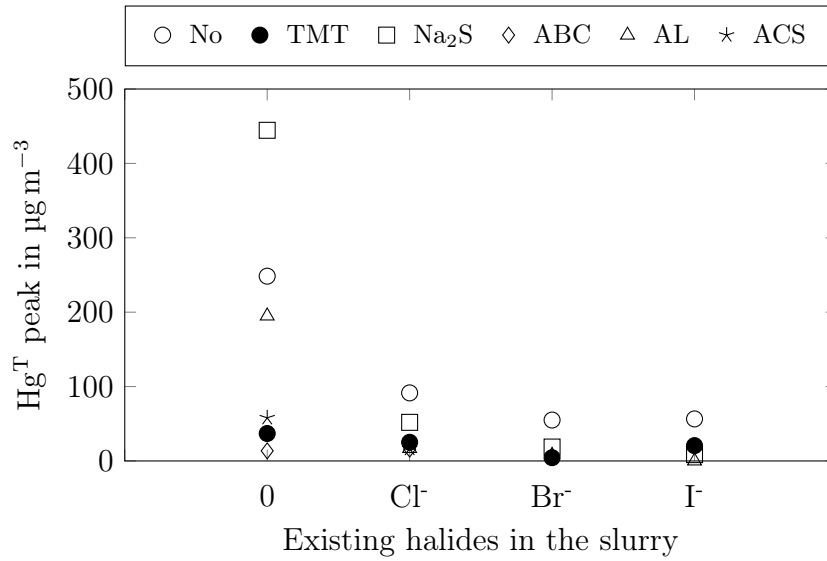
Figure 4.47: Effect of different additives on Hg re-emission peak by sudden change of SO_2 concentration of the flue gas.

was adsorbed on the solid fraction. Comparing AL and ACS shows a higher Hg content of the slurry with AL with 285 µg, followed by ACS with 120 µg. As Hg adsorption in the case of AL and ACS was not chemisorptions like ABC, the higher inventory resulted in higher Hg^T re-emission after the sudden change in SO_2 concentration. It can be seen that the presence of halides in the slurries decreased the Hg^T re-emission peaks considerably. The best performance belonged to ABC, even when no halides were present, which shows the stability of HgS bonds on the activated surface of the sorbent.

Table 4.6: Hg^T peak in $\mu g\,m^{-3}$ caused after the change in SO_2 concentration of the flue gas in slurries containing different halides when using additives.

Sorbent	No halides	Cl⁻	Br⁻	I⁻
No additive	248	92	55	57
TMT	37	25	4	21
Na₂S	445	52	19	9
ABC	14	16	-	-
AL	195	17	7	0
ACS	58	17	-	-

In general, it can be concluded that the utilization of additives in combination with

the proper concentration of halides in the slurry inhibits the Hg inventory loss of the slurry and helps to decrease total Hg re-emission. This is also valid in the case of a sudden change in S(IV) concentration of the slurry, which results in a peak in Hg^T re-emission. The proper choice of additive depends on the slurry composition in each plant. However, in the case of the lab-scale FGD, ABC proved to be the best sorbent due to its pore distribution and the sulfur impregnation. Regarding the precipitating agents, the best performance for reducing Hg re-emission was observed by using Diplexin. However, due to the different characteristic and unknown chemical formulas, more research has to be conducted to find the suitable injection amount and the effect on the gypsum quality.

Chapter 5

Summary and conclusion

The increase in renewable energy production requires a more flexible operation of the conventional power plants for providing the stable base energy production and compensate the fluctuations. This will be the role of conventional power plants in the next years, in which the transition from fossil fuels to the renewable energy production is taking place. Hence, the flue gas cleaning of fossil fired power plants will remain an important topic for the coming years; especially the influence of a flexible operation on the performance of pollution control devices needs to be better understood. Flue gas desulfurization is the main sink for Hg from the flue gas, and the change in its operating conditions influences the chemical reactions regarding Hg and thus, its removal efficiency. In this study, the phase partitioning of Hg in the slurry of the FGD and the parameters influencing its re-emission were investigated to gain further knowledge on its behavior and the possible measures to prevent its re-emission.

The experiments were carried out in a lab-scale FGD using a synthetic slurry and flue gas. At first the influence of different operating parameters and slurry compositions were tested. The temperature dependency of the gas solubility was demonstrated by the SO_2 removal efficiency, which decreased with increasing temperature of the slurry. In addition, Hg^T re-emission increased exponentially with increasing temperature due to the lower solubility of Hg as well as the higher kinetic of the Hg^{2+} reduction reaction. The Hg partitioning in the slurry showed the exothermic characteristic of an adsorption reaction. However at 80 °C, the Hg concentration in the gypsum increased, which could be due to the higher rate of sulfite disproportionation and formation of HgS.

The improvement of SO_2 removal efficiency was observed by increasing the pH of the slurry. Hg^T re-emission increased by increasing the pH as the presence of SO_3^{2-} at higher pH is more favored and the equilibrium of the reduction reaction is shifted

towards Hg^0. At lower pH, HSO_3^- is the favored S(IV) species, which results in the formation of $Ca(HSO_3)_2$ with a higher solubility than $CaSO_3$ and a higher oxidation rate. This can explain the decrease in dissolved oxygen concentration at pH of 4.2.

The direct correlation of the kinetic of the reduction reaction to Hg^{2+} concentration in the slurry was shown to be limited to a specific Hg^{2+} inventory. However, at higher concentrations the reduction reaction's kinetic depended not only on the Hg^{2+} concentration but also on other factors such as S(IV) concentration or Hg^0 diffusion into the gas phase. Adsorption isotherm behavior has been shown by checking Hg concentration in the gypsum at different Hg^{2+} inventories in the slurry.

Increasing the SO_2 concentration of the flue gas resulted in higher absorbed S(IV) and therefore a higher demand of dissolved oxygen for oxidation. The ambivalent influence of S(IV) concentration on Hg^{2+} reduction was observed. At low concentrations of SO_2, the presence of S(IV) led to Hg complex formation and therefore, lower Hg^T re-emission. However, at higher concentrations of SO_2 and subsequently S(IV), there was a sharp increase in Hg^T re-emission due to reduction reactions. The concentration of Hg in the slurry was measured low in the experiments with high Hg^T re-emission due to the loss of Hg to the gas phase.

In general, the presence of NH_3 can have two different effects on the behavior of SO_2 and Hg in the FGD depending on its concentration. NH_3 in the slurry could improve the SO_2 removal efficiency due to accelerating the dissolution rate of limestone. However, higher concentrations of NH_3 affected the pH and fresh $CaCO_3$ dosing drastically, which led to a decrease in SO_2 removal efficiency. At lower NH_4^+ concentrations of up to $500\,mg\,l^{-1}$ in the slurry, Hg^T re-emission increased and at higher concentrations a decrease in Hg^T re-emission was observed. This behavior could be due to the change in S(IV) concentration or Hg complex formation with NH_3, which resulted in a decrease in Hg^T re-emission. The concentration of Hg in the gypsum depended on the concentration of NH_3, as the Hg amine complexes have different solubilities and at higher NH_3 concentration, the more soluble complexes are formed.

Testing synthetic slurries containing different halides revealed no significant impact on SO_2 removal efficiency. However, the presence of halides decreased Hg^T re-emission. The slurry containing iodide showed the highest value of Hg^{2+} re-emission due to the highest vapor pressure of HgI_2. The limiting adsorption capacity of the solid particle content of the slurry could be observed, as all of the slurries had the same absolute amount of Hg in their gypsum regardless of the Hg inventory of the slurry.

The effect of a sudden change in S(IV) concentration on Hg re-emission was studied

in different slurries by sudden changes of the SO_2 concentration in the flue gas. The experiment with the slurry without halides clearly revealed the ambivalent influence of S(IV) in reactions involving Hg. As the increase of S(IV) concentration, caused a high Hg^T re-emission peak at first, which started to decrease slowly. This showed the role of S(IV) in Hg-complex formation. As the decomposition rate of $Hg(SO_3)_2^{2-}$ is much lower than $Hg(SO_3)$, a higher concentration of S(IV) led to less Hg^{2+} reduction in this case. The same trend was observed for slurries containing halides; however, the values were quite different. The peak of Hg^T re-emission decreased depending on the existing halides in the slurry. The role of S(IV) was less significant, when halides were present. S(IV) increased the Hg concentration in the gypsum for the slurries containing halides due to the formation of HgS. In the slurry without halides, the presence of S(IV) resulted in high Hg inventory loss due to Hg re-emission and therefore, lower Hg concentration was measured in the gypsum in the presence of S(IV).

Two different measurement principles were introduced and tested for a continuous measurement of S(IV) in the slurry of the FGD. For the first method, a UV/VIS spectrophotometer was used to measure the absorbance of light at the characteristic wavelength of sulfite. Measuring sulfite in the slurry without any halides was successfully tested. However, adding chloride did not show promising results. In the second method, all the dissolved S(IV) species were converted to SO_2 and measured by a SO_2 gas sensor. The measurement was proven to be selective regarding dissolved SO_2 in the presence of all tested halides. The interaction of sulfite and Hg could be observed best in the slurry without halides, in which the ambiguous role of sulfite as a reducing agent and complexation partner was obvious. The role of sulfite was seen to be more dependent on its concentration and the possibility of either $HgSO_3$ or $Hg(SO_3)_2^{2-}$ formation with different decomposition rates. In all tests with halides containing slurries, a correlation between sulfite concentration and Hg behavior was less pronounced as halides are strong partners for complex formation, which compete with sulfite and eliminates its effect on Hg behavior. The results proved the second method as a promising way to measure sulfite especially in full-scale FGDs.

Additives can be used in the FGD to prevent Hg re-emission and thus, increase the removal efficiency. In this work various sulfidic precipitating agents and activated carbon based sorbents were tested. The utilization of TMT and Na_2S in different slurries did not show any influence on SO_2 removal efficiency. When TMT was present in the slurry, Hg^T re-emission decreased in all slurries. The bromide-containing slurry showed zero re-emission, however, in the presence of iodide Hg^{2+} re-emission was not inhibited

completely. The addition of Na_2S decreased the Hg^T re-emission in the presence of halides as well. However, in the absence of halides, adding Na_2S showed higher Hg^T re-emission at steady state compared to the slurry without Na_2S. This is due to the higher Hg inventory of the slurry, which shows the positive effect of using Na_2S on reducing total Hg loss from the slurry. In general, using additives shifted the Hg partitioning to the solid fraction of the slurry. It was proved that in the presence of TMT the more stable macromolecular organo-metallic compounds were formed compared to HgS bonds formed due to the reaction of Hg^{2+} with Na_2S. The utilization of NETfloc and Diplexin showed a decrease in Hg^T re-emission as well.

Bituminous coal, lignite and coconut shell were the base materials for the tested activated carbon based sorbents. They had different surface areas and pore distributions. It was shown that the gas phase Hg adsorption was more favored on ACS due to the small size of adsorptives in the gas phase and the highest micropore area of ACS. However, ACS had the worst adsorption in the aqueous phase due to the larger size of Hg-compounds. ABC and AL showed a better performance in this case. Thus, the pore distribution plays a more important role than the total surface area, as depending on the environment and other existing components, the size of Hg-compounds changes.

In general, using all of the sorbents resulted in a higher SO_2 removal efficiency of the absorber, with AL having the highest increase. The lowest Hg^T re-emission belonged to the ABC containing slurry regardless of the existing halides, which can be explained with its sulfur content and pore distribution. In the absence of halides, both AL and ACS did not show a significant decrease in Hg^T re-emission, which can be explained according to the results of Hg^T of the slurry. The adsorption of Hg on ACS and AL in the absence of halides was a physical adsorption. Depending on the adsorption equilibrium and the amount of Hg in the slurry the concentration of Hg in the solid and aqueous phase could change. On ABC however, Hg could be adsorbed chemically to its surface due to its sulfur content and therefore did not desorb to the aqueous phase easily. Depending on the type of halides and their concentration either the formation of Hg complexes in the aqueous phase would increase or the adsorption of them on the active surface of the sorbents. The lowest Hg loss from the slurries belonged to ABC containing slurries and the highest to the baseline. Among the sorbents, the slurry containing ABC resulted in the highest share of Hg in solid fraction and ACS had the lowest share. Redox potential measurement of all cases showed the lowest redox potential for slurries containing ABC, which is in line with the highest Hg adsorption on the solid fraction of these slurries.

The effect of additives on preventing Hg re-emission peaks at the sudden change in SO_2 concentration was investigated in different slurries. In general, the presence of additives eliminated the sudden peak in Hg^T re-emission in all cases, except in the presence of Na_2S in the slurry without halides. In the cases of sorbents, the chemisorption of Hg on ABC even in the absence of halides led to the lowest Hg^T re-emission peak after the change.

The complex chemistry of Hg and its dependency on all operating parameters as well as on composition of the slurry was shown in this study. It was concluded that S(IV) plays an important role in reactions involving Hg and a suitable measurement principle was introduced. In addition, the utilization of additives was shown to reduce Hg re-emission especially by sudden changes in the chemistry of the slurry. Further investigation using the slurry of a full scale FGD with a much more complex composition could help to better understand the behavior of Hg in coal combustion derived slurries. In addition, sulfite measurements in pilot and full scale plants should be conducted to prove the results obtained in the lab-scale FGD. The influence of additives on the gypsum's quality and the final Hg concentration in the gypsum using a hydro cyclone in the separation process needs to be further investigated. By transferring the knowledge gained in this study and continuous measurement of sulfite, suitable measures for reducing Hg re-emission from the slurry could be implemented.

Bibliography

[1] ABDEL-LATIF, M. S.: New Spectrophotometric Method for Sulfite Determination. *Analytical Letters* 27 (13), P. 2601–2614, 1994. DOI: http://dx.doi.org/10.1080/00032719408002664

[2] APPELO, P. A.; LASLO, D. J.: Sulfite control to reduce mercury re-emission, Patent: US 8,828,341 B1

[3] BATHEN, D.; BREITBACH, M.: Adsorptionstechnik. Springer, 2001. ISBN: 978-3-642-18235-8

[4] BETTINELLI, M.; SPEZIA, S.; MINOIA, C.; RONCHI, A.: Determination of chlorine, fluorine, bromine, and iodine in coals with ICP-MS and IC. *Atomic Spectroscopy* 23 (4), P. 105–110, 2002

[5] BITTIG, M.: Zum Einfluss unterschiedlicher Liganden auf die Quecksilberabscheidung in absorptiven Abgasreinigungsstufen. Doktorarbeit, Universität Duisburg-Essen, 2010

[6] BLYTHE, G.: Mercury Capture in Wet Flue Gas Desulfurization Systems. In: GRANITE, E. J.; PENNLINE, H. W.; SENIOR, C. L.: Mercury control for coal-drived gas stream. Wiely-VCH GmbH & Co KGaA, 2015. ISBN: 978-3-527-32949-6

[7] BLYTHE, G. M.: Investigation of mercury control by wet FGD systems. In: Air Quality VIII, 2011, Arlington

[8] BLYTHE, G. M.; CURRIE, J.; DEBERRY, D. W.: Bench-scale Kinetics Study of Mercury Reactions in FGD Liquors: Final Report. United Research Services (URS) Corporation, Austin, Texas, 2008

[9] BLYTHE, G. M.; OWENS, M.: Field Testing of a Wet FGD Additive for Enhanced Mercury Control: Final Report. United Research Services (URS) Corporation, Austin, Texas, 2008

[10] BOSCH, H.; JANSSEN, F.: Catalytic reduction of nitrogen oxides: a review on the fundamentals and technology. *Catalysis Today* 2 (4), P. 369–531, 1988. DOI: http://dx.doi.org/10.1002/chin.198831346

[11] BRUTTEL, S.: Investigation of the dynamic behaviour of sulphite and its effect on Hg re-emission in wet limestone FGD. Master Thesis, University of Stuttgart, 2018

[12] BUECKER, B.; DYER, P.: Flue gas desulfurization systems for the future. *Power Plant Chemistry* 5 (7), P. 435–439, 2003

[13] CASTRO, L.; DOMMERGUE, A.; RENARD, A.; FERRARI, C.; RAMIREZ-SOLISC, A.; MARON, L.: Theoretical study of the solvation of $HgCl_2$, $HgClOH$, $Hg(OH)_2$ and $HgCl_3^-$: a density functional theory cluster approach. *Physical chemistry chemical physics* 13 (37), P. 16772–16779, 2011

[14] CENTI, G.; PERATHONER, S.: Chapter 1 Introduction: State of the art in the development of catalytic processes for the selective catalytic reduction of NO_x into N_2. In: GRANGER, P.; PÂRVULESCU, V. I.: Studies in Surface Science and Catalysis : Past and Present in DeNOx Catalysis. Elsevier, 2007. ISBN: 0167-2991. http://www.sciencedirect.com/science/article/pii/S0167299107802023 (Access on 28.09.2020)

[15] CHANG, L.; ZHAO, Y.; LI, H.; TIAN, C.; ZHANG, Y.; YU, X.; ZHANG, J.: Effect of sulfite on divalent mercury reduction and re-emission in a simulated desulfurization aqueous solution. *Fuel Processing Technology* 165, P. 138–144, 2017. DOI: http://dx.doi.org/10.1016/j.fuproc.2017.05.016

[16] CHENG, T.; ZHENG, C.; YANG, L.; WU, H.; FAN, H.: Effect of selective catalytic reduction denitrification on fine particulate matter emission characteristics. *Fuel* 238, P. 18–25, 2019. DOI: http://dx.doi.org/10.1016/j.fuel.2018.10.086

[17] CLARKSON, T. W.; MAGOS, L.: The toxicology of mercury and its chemical compounds. *Critical Reviews in Toxicology* 36 (8), P. 609–662, 2006. DOI: http://dx.doi.org/10.1080/10408440600845619

[18] CLEVER, H. L.; JOHNSON, S. A.; DERRICK, M. E.: The solubility of mercury and some sparingly soluble mercury salts in water and aqueous electrolyte solutions. *Journal of physical and chemical reference data* 14 (3), P. 631–680, 1985. DOI: http://dx.doi.org/10.1063/1.555732

[19] COASNE, B.; ALBA-SIMIONESCO, C.; AUDONNET, F.; DOSSEH, G.; GUBBINS, K.: Adsorption, structure and dynamics of benzene in ordered and disordered porous carbons. *Physical chemistry chemical physics* 13 (9), P. 3748–3757, 2011. DOI: http://dx.doi.org/10.1039/c0cp02205e

[20] CÓRDOBA, P.: Status of Flue Gas Desulphurisation (FGD) systems from coal-fired power plants: Overview of the physic-chemical control processes of wet limestone FGDs. *Fuel* 144, P. 274–286, 2015. DOI: http://dx.doi.org/10.1016/j.fuel.2014.12.065

[21] DEUTSCHE INSTITUT FÜR NORMUNG E.V. EN ISO 10304-3: Bestimmung der gelösten Anionen mittels Ionenchromatographie Teil 3: Bestimmung von Chromat, Iodid, Sulfit, Thiocyanat und Thiosulfat, Norm, 1997.

[22] DRAGO, R. S.; VOGEL, G. C.; NEEDHAM, T. E.: Four-parameter equation for predicting enthalpies of adduct formation. *Journal of the American Chemical Society* 93 (23), P. 6014–6026, 1971. DOI: http://dx.doi.org/10.1021/ja00752a010

[23] DRAGO, R. S.; WAYLAND, B. B.: A Double-Scale Equation for Correlating Enthalpies of Lewis Acid-Base Interactions. *Journal of the American Chemical Society* 87 (16), P. 3571–3577, 1965. DOI: http://dx.doi.org/10.1021/ja01094a008

[24] DRANGA, B. A.; LAZAR, L.; KOESER, H.: Oxidation Catalysts for Elemental Mercury in Flue Gases: A Review. *Catalysts* 2 (1), P. 139–170, 2012. DOI: http://dx.doi.org/10.3390/catal2010139

[25] DRISCOLL, C. T.; MASON, R. P.; CHAN, H. M.; JACOB, D. J.; PIRRONE, N.: Mercury as a Global Pollutant: Sources, Pathways, and Effects. *Environmental Science & Technology* 47 (10), P. 4967–4983, 2013. DOI: http://dx.doi.org/10.1021/es305071v

[26] EBINGHAUS, R.; TRIPATHI, R. M.; WALLSCHLÄGER, D.; LINDBERG, S. E.: Natural and Anthropogenic Mercury Sources and Their Impact on the Air-Surface Exchange of Mercury on Regional and Global Scales. In: EBINGHAUS,

R.; TURNER, R. R.; LACERDA, L. D.; VASILIEV, O.; SALOMONS, W.: Mercury Contaminated Sites: Characterization, Risk Assessment and Remediation. Springer, 1999. ISBN: 978-3-662-03754-6

[27] EVANGELOU, V. P.: Environmental Soil and Water Chemistry: Principles and Applications. John Wiley & Sons, 1998. ISBN: 978-0-471-16515-6

[28] FÖRSTNER, U.; KÖSTER, S.: Umweltschutztechnik. Springer, 2018. ISBN: 978-3-662-55163-9

[29] FORZATTI, P.; LIETTI, L.; TRONCONI, E.: Nitrogen Oxides Removal: Industrial. In: HORVÁTH, I. T.: Encyclopedia of Catalysis. John Wiley & Sons, 2002. ISBN: 978-0-471-24183-6

[30] FRANÇA, Í. W. L.; CARTAXO, S. J. M.; BASTOS-NETO, M.; GONÇALVES, L. R. B.; FERNANDES, F. A. N.: Effect of Additives to Improve Calcium-Based Sorbents in Semi-Dry Flue Gas Desulphurization. *Emission Control Science and Technology* 6, P. 105–112, 2020. DOI: http://dx.doi.org/10.1007/s40825-020-00156-0

[31] GHANTY, T. K.; GHOSH, S. K.: Correlation between hardness, polarizability, and size of atoms, molecules, and clusters. *The Journal of Physical Chemistry* 97 (19), P. 4951–4953, 1993. DOI: http://dx.doi.org/10.1021/j100121a015

[32] GOLDING, R. M.: Ultraviolet absorption studies of the bisulphite-pyrosulphite equilibrium. *Journal of the Chemical Society*, P. 3711–3716, 1960. DOI: http://dx.doi.org/10.1039/JR9600003711

[33] GRANITE, E. J.; PENNLINE, H. W.; HARGIS, R. A.: Novel Sorbents for Mercury Removal from Flue Gas. *Industrial & Engineering Chemistry Research* 39 (4), P. 1020–1029, 2000. DOI: http://dx.doi.org/10.1021/ie990758v

[34] GRIFFITHS, T. R.; ANDERSON, R. A.: The electronic spectra of the mixed mercury dihalides. Part 1. Computational procedures for calculating spectra, for a new route to equilibrium and formation constants, and the resolved spectra. *Journal of the Chemical Society, Dalton Transactions* (2), P. 205–208, 1980. DOI: http://dx.doi.org/10.1039/DT9800000205

[35] GRIFFITHS, T. R.; ANDERSON, R. A.: The electronic spectra of the mixed mercury dihalides. Part 2. Identification, equilibrium and formation constants, and

assignment of transitions. *Journal of the Chemical Society, Dalton Transactions* (2), P. 209–215, 1980. DOI: http://dx.doi.org/10.1039/DT9800000209

[36] GUFFEY, F.; BLAND, A.: Thermal pretreatment of low-ranked coal for control of mercury emissions. *Fuel Processing Technology* 85 (6), P. 521–531, 2004. DOI: http://dx.doi.org/10.1016/j.fuproc.2003.11.006

[37] GUSTIN, M. S.; LINDBERG, S. E.; AUSTIN, K.; COOLBAUGH, M.; VETTE, A.; ZHANG, H.: Assessing the contribution of natural sources to regional atmospheric mercury budgets. *Science of The Total Environment* 259, P. 61–71, 2000

[38] GUSTIN, M. S.; LINDBERG, S. E.; WEISBERG, P. J.: An update on the natural sources and sinks of atmospheric mercury. *Applied Geochemistry* 23, P. 482–493, 2008

[39] GUTBERLET, H.; NEUHAUS, S.; LUTAT, A.: Einfluss der Brennstoffqualität und verfahrenstechnischer Parameter auf Nebenreaktionen der Sulfitoxidation in Rauchgasentschwefelungsanlagen. *VGB Kraftwerkstechnik* 80 (8), P. 75–80, 2000

[40] GUTBERLET, H.; SPIESBERGER, A.: Zum Verhalten des Spurelementes Quecksilber in Steinkohlefeuerungen mit Rauchgasreinigungsanlagen. *VGB Kraftwerkstechnik* 72 (7), P. 636–641, 1992

[41] HACHIYA, N.: The History and the Present of Minamata Disease: Entering the second half a century. *Japan Medical Association Journal* 49 (3), P. 112–118, 2006

[42] HAMM, H.; HULLER, R.; KERSTEN, H. J.: 25 years experience gained in the European gypsum industry with the use of FGD gypsum. In: the 8th international science and technology conference and short course, 20.- 22.06.2004, Toronto, Canada. https://www.osti.gov/etdeweb/biblio/20543301 (Access on 28.09.2020)

[43] HAYNES, W. M.: CRC Handbook of Chemistry and Physics. CRC Press, 2014. http://www.hbcpnetbase.com (Access on 02.01.2019)

[44] HE, S.; ZHOU, J.; ZHU, Y.; LUO, Z.; NI, M.; CEN, K.: Mercury Oxidation over a Vanadia-based Selective Catalytic Reduction Catalyst. *Energy & Fuels* 23 (1), P. 253–259, 2009. DOI: http://dx.doi.org/10.1021/ef800730f

[45] HEIDEL, B.: Wechselwirkungen bei der Abscheidung von Schwefel-dioxid und Quecksilber durch nasse Rauchgasentschwefelungsanlagen. Doktorar-beit, Stuttgart Universität, 2015. https://elib.uni-stuttgart.de/bitstream/11682/2421/1/Dissertation_Barna_Heidel.pdf (Access on 28.09.2020)

[46] HEIDEL, B.; HILBER, M.; SCHEFFKNECHT, G.: Impact of additives for enhanced sulfur dioxide removal on re-emissions of mercury in wet flue gas desulfuriza-tion. *Applied Energy* 114, P. 485–491, 2014. DOI: http://dx.doi.org/10.1016/j.apenergy.2013.09.059

[47] HEIDEL, B.; KLEIN, B.: Reemission of elemental mercury and mercury halides in wet flue gas desulfurization. *International Journal of Coal Geology* 170, P. 28–34, 2017. DOI: http://dx.doi.org/10.1016/j.coal.2016.09.003

[48] HEIDEL, B.; THORWARTH, H.; SCHEFFKNECHT, G.: Spektralfotometrische Be-stimmung der Sulfitkonzentration in Suspensionen von nassen Rauchgasentschwe-felungsanlagen. In: VGB Chemie im Kraftwerk, 24.10.2012, Hamburg

[49] HO, T.-L.: Hard soft acids bases (HSAB) principle and organic chemistry. *Chem-ical Reviews* 75 (1), P. 1–20, 1975

[50] HOLLEMAN, A. F.; WIBERG, E.; WIBERG, N.: Lehrbuch der Anorganischen Chemie. Walter de Gruyter, 1995. ISBN: 978-3-11-017770-1

[51] HOWER, J. C.; SENIOR, C. L.; SUUBERG, E. M.; HURT, R. H.; WILCOX, J. L.; OLSON, E. S.: Mercury capture by native fly ash carbons in coal-fired power plants. *Progress in Energy and Combustion Science* 36 (4), P. 510–529, 2010. DOI: http://dx.doi.org/10.1016/j.pecs.2009.12.003

[52] HUHEEY, J.; KEITER, E.; KEITER, R.: Anorganische Chemie Prinzipien von Struktur und Reaktivität. Walter de Gruyter, 2014

[53] ITO, S.; YOKOYAMA, T.; ASAKURA, K.: Emissions of mercury and other trace elements from coal-fired power plants in Japan. *Science of The Total Environment* 368 (1), P. 397–402, 2006. DOI: http://dx.doi.org/10.1016/j.scitotenv.2005.09.044

[54] JIANG, J. G.; WANG, W.; ZHAO, X. L.; NA, C. Z.: Study on the applica-tion of heavy metal chelating agent in wastewater treatment. *Chinese Journal of Environmental Science* 20, P. 65–67, 1999

[55] KAMATA, H.; UENO, S.-i.; NAITO, T.; YUKIMURA, A.: Mercury Oxidation over the $V_2O_5(WO_3)/TiO_2$ Commercial SCR Catalyst. *Industrial & Engineering Chemistry Research* 47 (21), P. 8136–8141, 2008. DOI: http://dx.doi.org/10.1021/ie800363g

[56] KAMATA, H.; UENO, S.-i.; SATO, N.; NAITO, T.: Mercury oxidation by hydrochloric acid over TiO_2 supported metal oxide catalysts in coal combustion flue gas. *Fuel Processing Technology* 90, P. 947–951, 2009. DOI: http://dx.doi.org/10.1016/j.fuproc.2009.04.010

[57] KATHER, A.: Quecksilberemissionen aus deutschen Braunkohlekraftwerken im Vergleich zu US-Grenzwerten. In: VDI Wissensforum, Messung und Minderung von Quecksilberemissionen, 13.04.2016, Düsseldorf

[58] KITTO, J. B.; STULTZ, S. C.: Steam: its generation and use. The Babcock & Wilcox Company, 2005. ISBN: 0-9634570-1-2. https://www.academia.edu/12075401/Steam_its_generation_and_use_Edition_41 (Access on 28.09.2020)

[59] KOLKER, A.; QUICK, J. C.: Mercury and Halogens in Coal. In: GRANITE, E. J.; PENNLINE, H. W.; SENIOR, C. L.: Mercury control for coal-drived gas stream. Wiely-VCH GmbH & Co KGaA, 2015. ISBN: 978-3-527-32949-6

[60] KORPIEL, J. A.; VIDIC, R. D.: Effect of Sulfur Impregnation Method on Activated Carbon Uptake of Gas-Phase Mercury. *Environmental Science & Technology* 31 (8), P. 2319–2325, 1997. DOI: http://dx.doi.org/10.1021/es9609260

[61] LALLY, J.; GEC, B.; PELDSZUS, R.: Mercury Separation from Flue Gas Scrub Water with TMT 15. In: International Water Conference, 22. - 26.10.2006, Pittsburgh

[62] LARSSON, M.; BROGAARD, F. J.; WINQUIST, F.: Sulphite sensor and method for measuring sulphite concentration in a substance, Patent: EP 2,579,032 A1

[63] LASKOWSKI, J. S.: Chapter 1 Coal preparation: Developments in Mineral Processing: Coal Flotation and Fine Coal Utilization. Elsevier, 2001. ISBN: 0167-4528

[64] LASLO, D. J.: Oxidation control for improved flue gas desulfurization performance, Patent: US 9,321,006 B2

[65] LECOMTE, T.; FERRERÍA DE LA FUENTE, J. F.; NEUWAHL, F.; CANOVA, M.;
     PINASSEAU, A.; JANKOV, I.; BRINKMANN, T.; ROUDIER, S.; DELGADO SAN-
     CHO, L.: Best Available Techniques (BAT) Reference Document for Large Com-
     bustion Plants: EUR 28836 EN.

[66] LI, H.; LI, Y.; WU, C.-Y.; ZHANG, J.: Oxidation and capture of elemental
     mercury over SiO_2–TiO_2–V_2O_5 catalysts in simulated low-rank coal combustion
     flue gas. *Chemical Engineering Journal* 169 (1), P. 186–193, 2011. DOI: http:
     //dx.doi.org/10.1016/j.cej.2011.03.003

[67] LIDIN, R. A.; ANDREYEVA, L. L.; MOLOCHKO, V. A.: Constant of inorganic
     substances: A handbook Revised and Augmented Edition. Begell House, 1995.
     ISBN: 978-1-56700-041-2

[68] LIN, C.-J.; PEHKONEN, S. O.: Aqueous phase reactions of mercury with free rad-
     icals and chlorine Implications for atmospheric mercury chemistry. *Chemosphere*
     38 (6), P. 1253–1263, 1999. DOI: http://dx.doi.org/10.1016/S0045-6535(98)
     00526-8

[69] LIU, X.; WANG, S.; ZHANG, L.; WU, Y.; DUAN, L.; HAO, J.: Speciation of
     mercury in FGD gypsum and mercury emission during the wallboard production
     in China. *Fuel* 111, P. 621–627, 2013. DOI: http://dx.doi.org/10.1016/j.fuel.
     2013.03.052

[70] MASOOMI, I.: Effect of various precipitating agents at different operating param-
     eters on Hg removal in the wet limestone FGD. In: Multi-Pollutant Emissions
     from Coal Workshop, 03.03.2017, Mpumalanga, South Africa

[71] MASOOMI, I.: Investigation of different measures to reduce Hg emission from
     wet flue gas desulfurization. In: VGB Mercury Control, 05.12.2019, Berlin

[72] MASOOMI, I.: Effect of various precipitating agents at different operating pa-
     rameters on Hg removal in the wet limestone FGD. In: VGB Mercury Control,
     08.06.2017

[73] MASOOMI, I.: Investigation of different measures to reduce Hg emission from
     wet flue gas desulfurization. In: Multi-Pollutant Emissions from Coal Work-
     shop, 29.10.2019, Hanoi, Vietnam. https://www.iea-coal.org/our-events/mec/
     programme-mec-14/ (Access on 28.09.2020)

[74] MASOOMI, I.; BRUTTEL, S.; SCHMID, M. O.; SCHEFFKNECHT, G.: Sulphite measurement and its influence on Hg behaviour in wet-limestone flue-gas desulphurization. *Clean Energy* 4 (4), P. 360–371, 2020. DOI: http://dx.doi.org/10.1093/ce/zkaa016

[75] MASOOMI, I.; HEIDEL, B.; SCHMID, M. O.; SCHEFFKNECHT, G.: Effect of additives on mercury partitioning in wet-limestone flue-gas desulfurization. *Clean Energy* 4 (2), P. 132–141, 2020. DOI: http://dx.doi.org/10.1093/ce/zkaa005

[76] MASOOMI, I.; KAMATA, H.; YUKIMURA, A.; OHTSUBO, K.; SCHMID, M. O.; SCHEFFKNECHT, G.: Investigation on the behavior of mercury across the flue gas treatment of coal combustion power plants using a lab-scale firing system. *Fuel Processing Technology* 201, P. 106340, 2020. DOI: http://dx.doi.org/10.1016/j.fuproc.2020.106340

[77] MASOOMI, I.; MAZDEYASNA, S.; KLEIN, B.; SCHEFFKNECHT, G.: Effect of precipitating agents Na₂S and TMT15 on Hg re-emission at different operating parameters in wet limestone flue gas desulphurisation. *VGB PowerTech Journal* (3), P. 53–58, 2018

[78] MAZDEYASNA, S.: Investigation of the behaviour of mercury regarding different precipitating agents in the wet limestone FGD. Student research project, University of Stuttgart, 2017

[79] MEIER, J.; KEISER, B.; HIGGINS, B. S.: Fuel and Flue-Gas Additives. In: GRANITE, E. J.; PENNLINE, H. W.; SENIOR, C. L.: Mercury control for coal-drived gas stream. Wiely-VCH GmbH & Co KGaA, 2015. ISBN: 978-3-527-32949-6

[80] METROHM: Application Bulletin Nr. 225/2 d. http://products.metrohm.com (Access on 02.04.2020)

[81] MORTIMER, C. E.; MÜLLER, U.: Das Basiswissen der Chemie. Thieme, 2003. ISBN: 3134843080

[82] MÜNCH, P.: Untersuchung des Minderungspotentials von Quecksilberemission in der nassen Rauchgasentschwefelungsanlage. Masterarbeit, Stuttgart Universität, 2020

[83] MUNTHE, J.; XIAO, Z. F.; LINDQVIST, O.: The aqueous reduction of divalent mercury by sulfite. *Water Air & Soil Pollution* 56 (1), P. 621–630, 1991. DOI: http://dx.doi.org/10.1007/BF00342304

[84] NATIONAL RESEARCH COUNCIL (US) COMMITTEE ON THE TOXICOLOGICAL EFFECTS OF METHYLMERCURY: Toxicological Effects of Methylmercury. Washington (DC): National Academies Press (US), 2000. https://www.nap.edu/read/9899/chapter/1 (Access on 28.09.2020)

[85] NIKSA, S.; FUJIWARA, N.: A Predictive Mechanism for Mercury Oxidation on Selective Catalytic Reduction Catalysts under Coal-Derived Flue Gas. *Journal of the Air & Waste Management Association* 55 (12), P. 1866–1875, 2005. DOI: http://dx.doi.org/10.1080/10473289.2005.10464779

[86] NOVA, I.; BERETTA, A.; GROPPI, G.; LIETTI, L.; TRONCONI, E.; FORZATTI, P.: Monolithic catalysts for NO_x removal from stationary sources. In: CYBULSKI, A.; MOULIJN, J. A.: Structured Catalysts and Reactors. Taylor & Francis, 2006. ISBN: 0-8247-2343-0. http://citeseerx.ist.psu.edu/viewdoc/download?doi=10.1.1.575.9724&rep=rep1&type=pdf (Access on 28.09.2020)

[87] NRIAGU, J. O.: The Biogeochemistry of mercury in the environment. Elsevier/North-Holland Biomedical Press, 1979

[88] OMINE, N.; ROMERO, C. E.; KIKKAWA, H.; WU, S.; ESWARAN, S.: Study of elemental mercury re-emission in a simulated wet scrubber. *Fuel* 91 (1), P. 93–101, 2012. DOI: http://dx.doi.org/10.1016/j.fuel.2011.06.018

[89] OURA, K.; LIFSHITS, V. G.; SARANIN, A.; ZOTOV, A. V.; KATAYAMA, M.: Surface Science: An Introduction. Springer, 2003. ISBN: 978-3-662-05179-5

[90] PALMER, C. A.; MROCZKOWSKI, S. J.; FINKELMAN, R. B.; CROWLEY, S. S.; BULLOCK, J. H. JR.: The use of sequential leaching to quantify the modes of occurrence of elements in coal. In: Fifteenth annual international Pittsburgh coal conference, 14.-18.09.1998, Pittsburgh, PA (United States)

[91] POWELL, K. J.; BROWN, P. L.; BYRNE, R. H.; TAMÁS, G.; GLENN, H.; STAFFAN, S.; HANS, W.: Chemical speciation of environmentally significant heavy metals with inorganic ligands. Part 1: The Hg^{2+} - Cl^-, OH^-, CO_3^{2-}, SO_4^{2-},

and PO$_4$$^{3-}$ aqueous systems. *Pure and Applied Chemistry* 77 (4), P. 739–800, 2005. DOI: http://dx.doi.org/10.1351/pac200577040739

[92] PRESTO, A. A.; GRANITE, E. J.: Survey of Catalysts for Oxidation of Mercury in Flue Gas. *Environmental Science & Technology* 40 (18), P. 5601–5609, 2006. DOI: http://dx.doi.org/10.1021/es060504i

[93] RENTZ, O.; MARTEL, C.: Analyse der Schwermetallströme in Steinkohlefeuerungen: Einfluß der Kohlesorte und des Lastzustandes. Karlsruhe, Juni 1998. https://www.yumpu.com/de/document/read/10739467/analyse-der-schwermetallstrome-in-steinkohlefeuerungen-baden- (Access on 28.09.2020)

[94] RIEDEL, E.; ALSFASSER, R.; JANIAK, C.; KLAPÖTKE, T. M.; MEYER, H.-J.: Moderne Anorganische Chemie. Walter de Gruyter, 2007

[95] RITTMAIER, E. K.: Investigation of mercury adsorption on different sorbents. Bachelor Thesis, University of Stuttgart, 2020

[96] SCHÜTZE, J.: Quecksilberabscheidung in der nassen Rauchgasentschwefelung von Kohlekraftwerken. Doktorarbeit, Martin-Luther-Universität Halle-Wittenberg, 2013

[97] SCHÜTZE, J.; SCHILLING, U.; HILBERT, L.; STRAUSS, J. H.; HÖRTINGER, T.: Quecksilber-Abscheidung am Beispiel des Kraftwerkes Lippendorf. *VGB PowerTech* 12, P. 81–87, 2015

[98] SCHWAEMMLE, T.; HEIDEL, B.; BRECHTEL, K.; SCHEFFKNECHT, G.: Study of the effect of newly developed mercury oxidation catalysts on the DeNOx-activity and SO$_2$–SO$_3$-conversion. *Fuel* 101, P. 179–186, 2012. DOI: http://dx.doi.org/10.1016/j.fuel.2010.11.043

[99] SCHWÄMMLE, T.; BERTSCHE, F.; HARTUNG, A.; BRANDENSTEIN, J.; HEIDEL, B.; SCHEFFKNECHT, G.: Influence of geometrical parameters of honeycomb commercial SCR-DeNOx-catalysts on DeNOx-activity, mercury oxidation and SO$_2$/SO$_3$-conversion. *Chemical Engineering Journal* 222, P. 274–281, 2013. DOI: http://dx.doi.org/10.1016/j.cej.2013.02.057

[100] SCHWÄMMLE, T.; BRECHTEL, K.; SALVATI, M.; DI BLASI, M.; HARTUNG, A.; BRANDENSTEIN, J.; TEMBRINK, J.; HILBER, M.; THORWARTH, H.; HAN,

X.; Risio, B.; Senior, C.:   Optimisation of SCR-DeNOx catalyst per-
formance related to deactivation and mercury oxidation (Denopt). European
Commission, Luxembourg, 2013. https://op.europa.eu/de/publication-detail/-/
publication/c2dd018a-a7fc-46f2-b105-8e5b1e27f2d2 (Access on 28.09.2020)

[101] Senior, C.:   Mercury Behavior in Coal Combustion Systems. In: Granite,
E. J.; Pennline, H. W.; Senior, C. L.: Mercury control for coal-drived gas
stream. Wiely-VCH GmbH & Co KGaA, 2015. ISBN: 978-3-527-32949-6

[102] Senior, C. L.; Johnson, S. A.: Impact of Carbon-in-Ash on Mercury Removal
across Particulate Control Devices in Coal-Fired Power Plants. *Energy & Fuels*
19 (3), P. 859–863, 2005. DOI: http://dx.doi.org/10.1021/ef049861

[103] Senior, C. L.; Sarofim, A. F.; Zeng, T.; Helble, J. J.; Mamani-Paco,
R.: Gas-phase transformations of mercury in coal-fired power plants. *Fuel Pro-
cessing Technology* 63 (2), P. 197–213, 2000. DOI: http://dx.doi.org/10.1016/
S0378-3820(99)00097-1

[104] Sing, K.; Everett, D. H.; Haul, R. A.; Moscou, L.; Pierotti, R. A.; Rou-
querol, J.; Siemieniewska, T.: Reporting Physisorption Data for Gas/Solid
Systems with Special Reference to the Determination of Surface Area and Poros-
ity. *Pure and Applied Chemistry* 57 (4), P. 603–619, 1985

[105] Sing, K. S. W.; Everett, D. H.; Haul, R. A. W.; Moscou, L.; Pierotti,
R. A.; Rouquérol, J.; Siemieniewska, T.:   IUPAC Standards Online. De
Gruyter, 2016

[106] Singla, M.; Singh, M.; Walia, M. S.; Singla, S.; Mahapatra, P.:   An
optoelectronic instrument for the determination of sulphite in beverages. *Food
Chemistry* 97, P. 737–741, 2006. DOI: http://dx.doi.org/10.1016/j.foodchem.
2005.06.009

[107] Slater, J. C.: Atomic Radii in Crystals. *Journal of Chemical Physics* 41 (10),
P. 3199–3205, 1964. DOI: http://dx.doi.org/10.1063/1.1725697

[108] Slemr, F.; Schuster, G.; Seiler, W.: Distribution, speciation, and budget
of atmospheric mercury. *Journal of Atmospheric Chemistry* 3 (4), P. 407–434,
1985. DOI: http://dx.doi.org/10.1007/BF00053870

[109] Stein, E. D.; Cohen, Y.; Winer, A. M.: Environmental distribution and transformation of mercury compounds. *Critical Reviews in Environmental Science and Technology* 26 (1), P. 1–43, 1996. DOI: http://dx.doi.org/10.1080/10643389609388485

[110] Stumm, W.; Morgan, J. J.: Aquatic Chemistry: Chemical Equilibria and Rates in Natural Waters. John Wiley & Sons, 1995. ISBN: 978-0-471-51185-4

[111] Sui, Z.; Zhang, Y.; Li, W.; Orndorff, W.; Cao, Y.; Pan, W.-p.: Partitioning effect of mercury content and speciation in gypsum slurry as a function of time. *Journal of Thermal Analysis and Calorimetry* 119 (3), P. 1611–1618, 2015. DOI: http://dx.doi.org/10.1007/s10973-015-4403-9

[112] Sun, M.; Hou, J.; Cheng, G.; Baig, S. A.; Tan, L.; Xu, X.: The relationship between speciation and release ability of mercury in flue gas desulfurization (FGD) gypsum. *Fuel* 125, P. 66–72, 2014. DOI: http://dx.doi.org/10.1016/j.fuel.2014.02.012

[113] Sun, M.; Hou, J.; Tang, T.; Lu, R.; Cheng, L.; Xu, X.: Stabilization of mercury in flue gas desulfurization gypsum from coal-fired electric power plants with additives. *Fuel Processing Technology* 104, P. 160–166, 2012. DOI: http://dx.doi.org/10.1016/j.fuproc.2012.05.008

[114] Takashina, T.; Honjo, S.; Ukawa, N.; Iwashita, K.: Effect of Ammonium Concentration on SO_2 Absorption in a Wet Limestone Gypsum FGD Process. *Journal of Chemical Engineering of Japan* 35, P. 197–204, 2002. DOI: http://dx.doi.org/10.1252/jcej.35.197

[115] Takeshita, M.; Soud, H. N.: FGD performance and experience on coal-fired plants, EACR/58. IEA Coal Research, 1993

[116] Tang, T.; Xu, J.; Lu, R.; Wo, J.; Xu, X.: Enhanced Hg^{2+} removal and Hg^0 re-emission control from wet fuel gas desulfurization liquors with additives. *Fuel* 89 (12), P. 3613–3617, 2010. DOI: http://dx.doi.org/10.1016/j.fuel.2010.07.045

[117] Ullrich, S. M.; Tanton, T. W.; Abdrashitova, S. A.: Mercury in the aquatic environment: a review of factors affecting methylation. *Critical Reviews in Environmental Science and Technology* 31 (3), P. 241–293, 2001

[118] UN Environment: Global Mercury Assessment 2013: Sources, Emissions, Releases and Environmental Transport. UNEP Chemical Branch, Geneva, Switzerland, 2013. https://www.amap.no/documents/doc/global-mercury-assessment-2013-sources-emissions-releases-and-environmental/transport/847 (Access on 28.09.2020)

[119] UN Environment: Global Mercury Assessment 2018. UNEP Chemical Branch, Geneva, Switzerland, 2019. https://www.unenvironment.org/resources/publication/global-mercury-assessment-2018 (Access on 28.09.2020)

[120] United State Environmental Protection Agency: Mercury Study Report to Congress, EPA-452/R-97-009. Office of Air Quality and Standards and Office of Research and Development, Washington (DC), 1997. https://www3.epa.gov/airtoxics/112nmerc/volume1.pdf (Access on 28.09.2020)

[121] United State Environmental Protection Agency: Technical Bulletin, Nitrogen oxides (NO_x), Why and How they are controlled, EPA 456/F-99-006R. Office of Air Quality and Standards, North Carolina, 1999. https://www3.epa.gov/ttncatc1/dir1/fnoxdoc.pdf (Access on 28.09.2020)

[122] van Loon, L.; Mader, E.; Scott, S. L.: Reduction of the Aqueous Mercuric Ion by Sulfite: UV Spectrum of $HgSO_3$ and Its Intramolecular Redox Reaction. *The Journal of Physical Chemistry A* 104, P. 1621–1626, 2000

[123] van Otten, B.; Buitrago, P. A.; Senior, C. L.; Silcox, G. D.: Gas-Phase Oxidation of Mercury by Bromine and Chlorine in Flue Gas. *Energy & Fuels* 25 (8), P. 3530–3536, 2011. DOI: http://dx.doi.org/10.1021/ef200840c

[124] VGB PowerTech e. V.: VGB-TW 710: Vom Rauchgasentschwefelungsrückstand zum Qualitätsrohstoff REA-Gips. VGB PowerTech Service GmbH Verlag Techn.-Wiss. Schr., Essen, 2005

[125] VGB PowerTech e. V.: VGB Merkblatt M 701: Analyse von REA-Gips. VGB PowerTech Service GmbH Verlag Techn.-Wiss. Schr., Essen, 2008. https://www.vgb.org/shop/m701-ebook.html

[126] VGB PowerTech e. V.: VGB M 419: Merkblatt Fuer Bauart, Betrieb und Wartung von Rauchgasentschwefelungsanlagen (REA). VGB PowerTech Ser-

vice GmbH Verlag Techn.-Wiss. Schr., Essen, 2009. https://www.vgb.org/shop/technicalrules/merkblatter/m419ebook.html (Access on 28.09.2020)

[127] VOSTEEN, B.; HERMANN, W.; BERRY, M. S.: Native halogens in coals from USA, China and elsewhere: Low chlorine coals need bromide addition for enhanced mercury capture. In: Messung und Minderung von Quecksilber-Emissionen, 29.-30.09.2010, Mannheim. https://www.vosteen-consulting.de/fileadmin/user_upload/Publikationen/2010/2010_09_Vosteen_VDI_Technikforum_Mannheim.pdf (Access on 28.09.2020)

[128] VOSTEEN, B.; KANEFKE, R.: Bromgestützte Quecksilber-Abscheidung aus den Abgasen von Verbrennungsanlagen Studie im Auftrag des Landesumweltamts Nordrhein-Westfalen. Köln, 2003

[129] VOSTEEN, B.; KANEFKE, R.; KÖSER, H.: Bromine-enhanced Mercury Abatement from Combustion Flue Gases: Recent Industrial Applications and Laboratory Research. *VGB PowerTech* 86 (3), P. 70–75, 2006

[130] WANG, J.; ANTHONY, E. J.: An analysis of the reaction rate for mercury vapor and chlorine. *Chemical Engineering and Technology* 28 (5), P. 569–573, 2005. DOI: http://dx.doi.org/10.1002/ceat.200407063

[131] WANG, J.; WANG, T.; MALLHI, H.; LIU, Y.; BAN, H.; LADWIG, K.: The role of ammonia on mercury leaching from coal fly ash. *Chemosphere* 69 (10), P. 1586–1592, 2007. DOI: http://dx.doi.org/10.1016/j.chemosphere.2007.05.053

[132] WANG, Y.-J.; DUAN, Y.-f.; YANG, L.-g.; JIANG, Y.-m.; WU, C.-j.; WANG, Q.; YANG, X.-h.: Comparison of mercury removal characteristic between fabric filter and electrostatic precipitators of coal-fired power plants. *Journal of Fuel Chemistry and Technology* 36 (1), P. 23–29, 2008. DOI: http://dx.doi.org/10.1016/S1872-5813(08)60009-2

[133] WHITE, H. J.: Entstaubung industrieller Gase mit Elektrofiltern. VEB Deutscher Verlag für Grundstoffindustrie, 1969. https://books.google.de/books?id=FACLtQEACAAJ

[134] WILCOX, J.; RUPP, E.; YING, S. C.; LIM, D.-H.; NEGREIRA, A. S.; KIRCHOFER, A.; FENG, F.; LEE, K.: Mercury adsorption and oxidation in coal combustion

and gasification processes. *International Journal of Coal Geology* 90-91, P. 4–20, 2012. DOI: http://dx.doi.org/10.1016/j.coal.2011.12.003

[135] WIRLING, J.: Implementation of Process-Integrated Waste Gas Cleaning Using Activated Lignite. In: A&WMA Specialty Conference on Hazardous Waste Combustors, 28.-30.03.2001, Kansas City

[136] WO, J.; ZHANG, M.; CHENG, X.; ZHONG, X.; XU, J.; XU, X.: Hg^{2+} reduction and re-emission from simulated wet flue gas desulfurization liquors. *Journal of Hazardous Materials* 172 (2-3), P. 1106–1110, 2009. DOI: http://dx.doi.org/10.1016/j.jhazmat.2009.07.103

[137] WONG, J.: Introduction to Carbon Sorbents for Pollution Control. In: GRANITE, E. J.; PENNLINE, H. W.; SENIOR, C. L.: Mercury control for coal-drived gas stream. Wiely-VCH GmbH & Co KGaA, 2015. ISBN: 978-3-527-32949-6

[138] WYPIÓR, T.; KRZYŻYŃSKA, R.: Influence of ammonia wet-limestone flue gas desulfurization process from coal-based power plant. *E3S Web of Conferences* 116, 2019. DOI: http://dx.doi.org/10.1051/e3sconf/201911600101

[139] XIE, Z.-Q.; SANDER, R.; PÖSCHL, U.; SLEMR, F.: Simulation of atmospheric mercury depletion events (AMDEs) during polar springtime using the MECCA box model. *Atmospheric Chemistry and Physics* 8 (23), P. 7165–7180, 2008

[140] XU, J.; BAO, J.; TANG, J.; DU, M.; LIU, H.; XIE, G.; YANG, H.: Characteristics and Inhibition of Hg^0 Re-emission in a Wet Flue Gas Desulfurization System. *Energy & Fuels* 32 (5), P. 6111–6118, 2018. DOI: http://dx.doi.org/10.1021/acs.energyfuels.8b00686

[141] YUDOVICH, Y.; KETRIS, M. P.: Chlorine in coal: A review. *International Journal of Coal Geology* 67 (1), P. 127–144, 2006. DOI: http://dx.doi.org/10.1016/j.coal.2005.09.004

[142] ZELDOVICH, J.: The oxidation of nitrogen in combustion and explosions. *European Physical Journal A. Hadrons and Nuclei* 21, P. 577–628, 1946

[143] ZHENG, L.; LIU, G.; CHOU, C.-L.: The distribution, occurrence and environmental effect of mercury in Chinese coals. *Science of The Total Environment* 384 (1), P. 374–383, 2007. DOI: http://dx.doi.org/10.1016/j.scitotenv.2007.05.037

[144] ZHU, Z.; ZHUO, Y.; FAN, Y.; WANG, Z.: Fate of mercury in flue gas desulfurization gypsum determined by Temperature Programmed Decomposition and Sequential Chemical Extraction. *Journal of Environmental Sciences* 43, P. 169–176, 2016. DOI: http://dx.doi.org/10.1016/j.jes.2015.09.011